Performance and Durability of $(LaSr)(CoFe)O_{3-\delta}$/Doped Ceria Composite Oxygen Electrodes for Reversible Solid Oxide Fuel Cells

A Doctoral Thesis presented to the Interdisciplinary Graduate School of Medicine and Engineering University of Yamanashi

March 2017

Kazuki Shimura

Contents

Chapter 1: General Introduction

Chapter 2: Introduction of Solid Oxide Cells

Chapter 1

General introduction

1.1. Background

Since the industrial revolution, a huge amount of energy has been used for the humankind to advance better living standards. The energy that humans are using principally depends on fossil fuels such as coal, oil, and natural gas. However, global warming and air pollution are major problems caused by the emission of exhaust gases by combustion of fossil fuels. Significant increases in the emission of greenhouse gases have occurred since the industrial era (see Figure 1-1) [1].

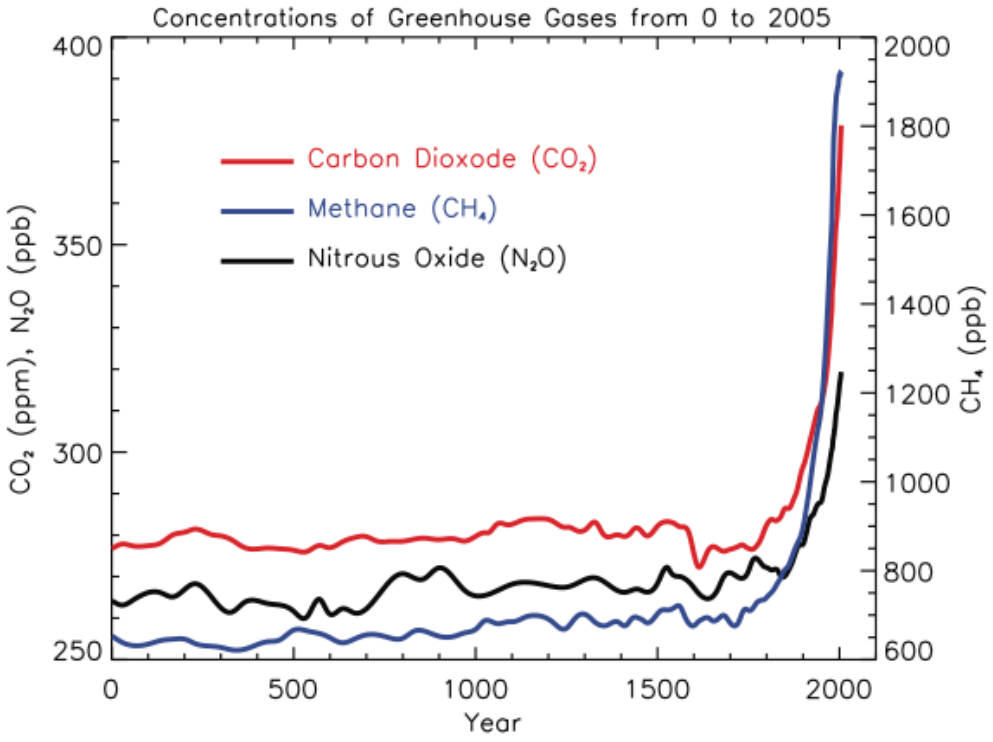

Figure 1-1. Atmospheric concentrations of important long-lived greenhouse gases over the last 2,000 years. Increases since circa 1750 are attributed to human activities in the industrial era [1].

In Japan, due to the accident of the Fukushima Daiichi Nuclear Power Station during the Great East Japan Earthquake in 2011, nuclear power generation has been stopped and once again reliance on thermal power generation is becoming important [2] (see Fig. 1-2).

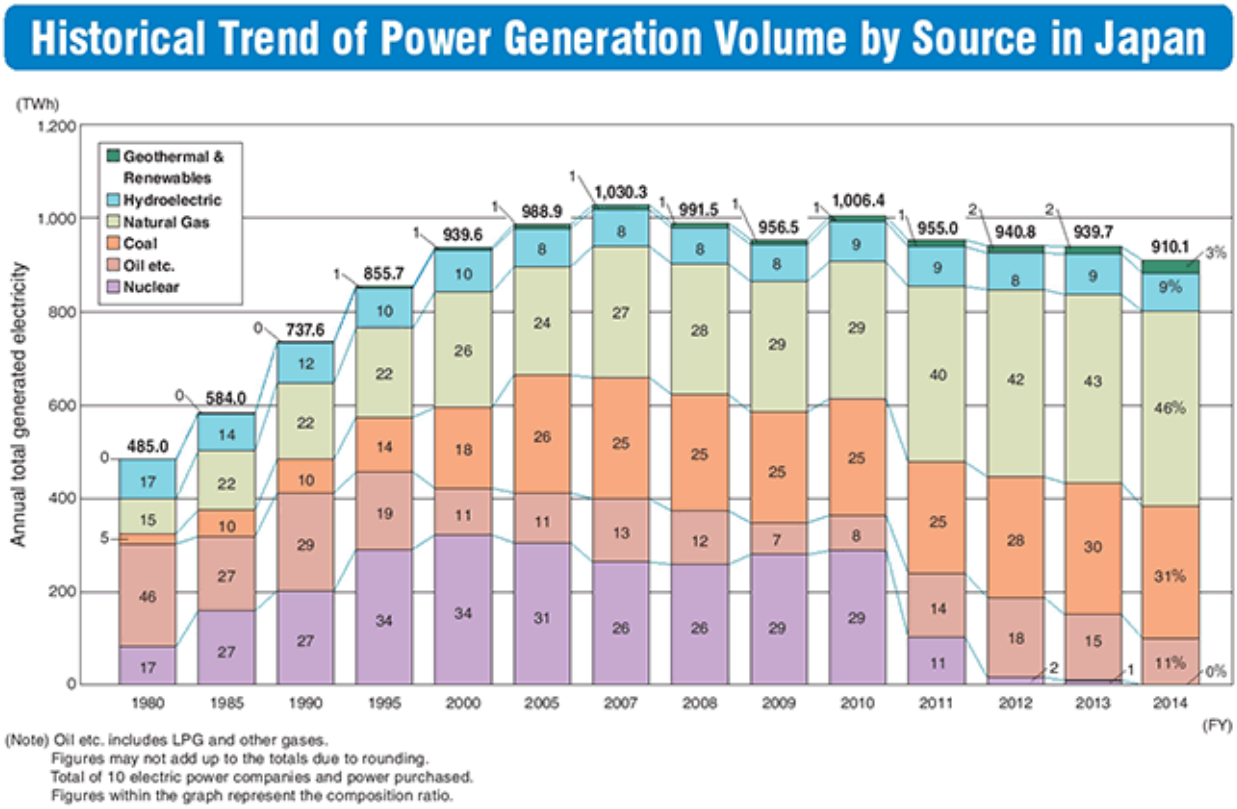

Fig. 1-2. Historical trend of power generation volume by source in Japan [3].

Therefore, as alternative to thermal power generation, new power generation methods are required and innovation in the development of earth-friendly energy is becoming an important. As an earth-friendly energy, the use of electricity generated from renewable energy sources such as solar and wind power has increased worldwide. Nonetheless, power generation from renewable energy sources (renewable electricity)

has the drawback of output fluctuation. For example, solar cells (photovoltaics) cannot generate electricity without the sun light and wind power generation (rotation rate of turbines) depends largely on the wind velocity. To match the energy supply with the demand, efficient and cost-effective storage technology is necessary to achieve effective utilization of large-scale renewable electricity. While batteries are suitable for a short-term storage of kWh to MWh-class electricity, the use of hydrogen as an energy carrier is one of the promising options for long-term and larger scale storage [4, 5].

1.2. Hydrogen production technique

Hydrogen can be produced using various techniques, i.e. steam reforming of natural gas [6, 7], biological processes [8], photochemical processes [9], water (or steam) electrolysis [10-13], and also as a by-products of industrial processes. Since the amount of by-products depends on the production volume and hydrogen produced has been already utilized as the energy within the plant, it is difficult to largely increase the production of hydrogen via industrial by-products. On the other hand, the steam reforming of natural gas can produce hydrogen at high efficiency, but hydrogen production from fossil fuels is associated with the emission of CO_2 [6, 7]. The production of hydrogen via electrolysis of water or steam is still expensive, but it is a promising technology because it can produce high purity hydrogen only with one step. When renewable electricity is supplied to the electrolyzer, hydrogen is produced without any emission of greenhouse gases.

Water electrolysis technology is generally classified according to the type of electrolyte used in the electrolysis cells. The classification includes alkaline electrolysis cells (AECs), polymer electrolyte membrane electrolysis cells (PEMECs), solid proton conducting electrolysis cells (SPCECs), and solid oxide electrolysis cells (SOECs). SOECs, operated at high temperature, provide the highest possible conversion efficiency compared with other electrolysis cells owing to the lower applied voltage required without any noble metal electrocatalysts. This is due to favorable thermodynamic and kinetics conditions at the high operating temperatures. In addition, SOECs can also provide highly efficient power generation when used as solid oxide fuel cells (SOFCs) by simply performing the reverse operation using the same electrochemical cell. Reversible solid oxide cells (R-SOCs) are, without any doubt, one of the most effective technologies that will alleviate the environmental problems that we are facing nowadays. In other to advance this technology, I have engaged in research that encompasses both fundamental and technological aspects of electrode development for R-SOCs.

1.3. Outline of the dissertation

The SOC consists of a hydrogen electrode for supplying hydrogen and an oxygen electrode for supplying oxygen to both sides of the solid electrolyte. In the oxygen electrode, it is common to insert an interlayer between the electrode and the electrolyte to prevent solid state reaction. The main degradation factor of oxygen electrode is the solid state reaction between electrode and electrolyte, and the use of doped ceria

interlayers to prevent unfavorable solid state reactions is nowadays a common feature in SOCs. I have investigated how this doped ceria interlayer greatly affects the oxygen electrode durability under R-SOC conditions and also I have given answers to whether the interlayer could also affect the cell performance. Thus, the development and evaluation of the dope ceria interlayer as an important part of the oxygen electrode is the axis of this dissertation.

In this section, I briefly describe the outline of the dissertation and briefly explain the content of chapters that follows to Chapter 1. Considering the nature of various experiments that I have carried out, instead of a chapter dedicated to "Experimentals", I have decided to include an experimental section in each of the corresponding chapters.

In Chapter 2, I will describe the SOCs: the working principle, main constituent materials specifically focusing on the oxygen electrode, some recent developments regarding performance, and the electrode degradation phenomena.

In Chapter 3, I will focus on the preparation method of the interlayer, which plays an important role of suppressing the solid state reaction(s) between the oxygen electrode and the solid electrolyte. I have succeeded in producing a dense, uniform, and thin interlayer by the spin-coating method coupled to the use of rare earth octoates as precursors.

In Chapter 4, I will describe the durability of oxygen electrodes during a long-term test. The test was carried out at 900°C and a constant current density of 0.5 A cm^{-2} for up to 5000 hours. By the use of a symmetric cell, the performances of

electrodes for the oxygen evolution reaction (anodic polarization) and oxygen reduction evaluation (cathodic polarization) were evaluated. I have shown that the newly developed oxygen electrode with a dense, uniform and thin doped ceria interlayer has stably performed under anodic and cathodic operation up to 5500 h. The post-mortem analysis clearly demonstrated differences in the degradation between anodic and cathodic operations. Thus, a new insight on degradation of the oxygen electrode was obtained that also triggered my interest on the possible effect of the interlayer on the cell performance.

In Chapter 5, I will compare the performances of the oxygen electrode using the doped ceria interlayers with different microstructures. I will demonstrate the essential role of a dense interlayer with uniform thickness in improving the performance of the oxygen electrode.

Finally, I summarize the results of all chapters, and presented the guidelines for producing durable and high performance oxygen electrode for R-SOCs in Chapter 6. Based on my results, I have made suggestions that could guide researchers in the near future to further improve the performance of the oxygen electrode.

1.4. References

[1] S. Solomon, D. Qin, M. Manning, Z. Chen, M. Marquis, K.B. Averyt, M. Tignor, H.L. Miller (eds.). Contribution of Working Group I to the Fourth Assessment Report of the Intergovernmental Panel on Climate Change, Cambridge University Press, Cambridge, United Kingdom and New York, NY, USA, 2007 p.135

[2] Outline of the FY2013 Annual Report on Energy (Energy White Paper 2014), Agency for Natural Resources and Energy:
http://www.meti.go.jp/english/report/downloadfiles/2014_outline.pdf
[3] The Federation of Electric Power Companies of Japan:
https://www.fepc.or.jp/english/nuclear/necessary/sw_necessary_02/index.html
[4] S.D. Ebbesen, S.H. Jensen, A. Hauch, M.B. Mogensen, High Temperature Electrolysis in Alkaline Cells, Solid Proton Conducting Cells, and Solid Oxide Cells, Chem. Rev. 114 (2014) 10697-10734.
[5] K. Chen, S.P. Jiang, Review—Materials Degradation of Solid Oxide Electrolysis Cells, J. Electrochem. Soc. 163 (2016) F3070-F3083.
[6] T. Rostrup-Nielsen, Manufacture of hydrogen, Catal. Today 106 (2005) 293-296.
[7] J.R. Rostrup-Nielsen, T. Rostrup-Nielsen, Large-Scale Hydrogen Production,CATTECH 6 (2002) 150-159.
[8] M. Ni, D. Y. C. Leung, M. K. H. Leung, K. Sumathy, An overview of hydrogen production from biomass, Fuel Process. Technol. 87 (2006) 461-472.
[9] A.Fujishima, K. Honda, Photolysis-decomposition of water at the surface of an irradiated semiconductor, Nature 238 (1972) 37-38.
[10] F. Barbir, PEM electrolysis for production of hydrogen from renewable energy sources, Sol. Energy 78 (2005) 661-669.
[11] S. A. Grigoriev, V. I. Porembsky, V. N. Fateev, Pure hydrogen production by PEM electrolysis for hydrogen energy, Int. J. Hydrogen Energy 31 (2006) 171-175.

[12] H. Uchida, N. Osada, M. Watanabe, High-Performance Electrode for Steam Electrolysis Mixed Conducting Ceria-Based Cathode with Highly-Dispersed Ni Electrocatalysts, Electrochem. Solid-State Lett. 7 (2004) A500-A502.

[13] A. Hauch, S. D. Ebbesen, S. H. Jensen, M. J. Mogensen, Highly efficient high temperature electrolysis, Mater. Chem. 18 (2008) 2331-2340.

Chapter 2

Introduction of Solid Oxide Cells

2.1. Solid oxide cells (SOCs)

It was already stated in chapter 1 that the SOCs are primarily used as fuel cells, SOFCs, and that the same cells can work reversibly and be used as electrolysis cells, SOECs. When the device can combine both operations, I talk about reversible solid oxide cells (R-SOCs). This dissertation is focused on the development of the oxygen electrode for such a reversible device. In this chapter, I introduce the operation principle of the SOFCs and SOECs, the typical cell construction and the materials commonly used. A short review on the degradation the oxygen electrode in these cells is included.

2.1.1. Solid oxide fuel cell (SOFC)

When hydrogen and oxygen are supplied to the SOC, electricity is generated with high conversion efficiency that including the recovery of waste heat as shown Fig. 2-1. Porous electrodes are attached to both sides of the solid oxide electrolyte, and air (oxygen) is supplied to the cathode and fuel such as hydrogen or reformate (H_2 + CO + CO_2) is supplied to the anode. When two electrodes are connected via an external circuit, oxygen molecules receive electrons at the cathode and are reduced to oxide ions (O^{2-}) and move through the electrolyte towards the anode. At the anode, the oxide ions react with hydrogen to form water vapor, and at the same time, the electrons are

emitted, whereby a current flows through an external circuit. The reaction at each electrode of the SOFC proceeds as follows:

$$\text{Cathode: } 1/2O_2 + 2\,e^- \rightarrow O^{2-}$$

$$\text{Anode: } H_2 + O^{2-} \rightarrow H_2O + 2e^-$$

$$\text{Cell reaction: } H_2 + 1/2\,O_2 \rightarrow H_2O$$

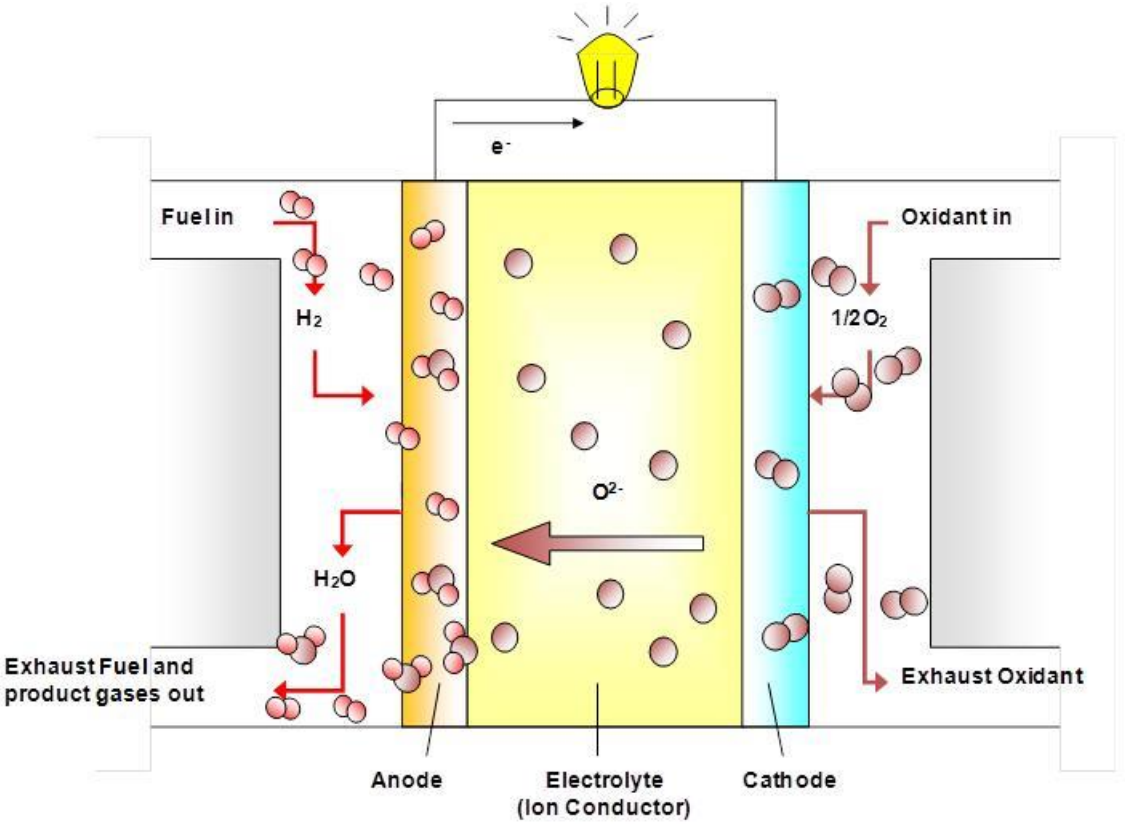

Fig.2-1. Schematic representation of a solid oxide fuel cell (SOFC).

A detailed description of the thermodynamic analysis is given, for the sake of clarity, in sections 2.1.4.

At high operating temperature of the SOFC, the electrode reaction rate is sufficiently high and the activation overpotential can be reduced without using any expensive noble metal catalyst such as Pt. Furthermore, it is possible to use a variety of fuels such as coal gas or methane gas because CO is oxidized to CO_2 without poisoning of the anode. Moreover, since all constituent materials are solid, it is also possible to reduce the resistance loss by making thinner components. Also, SOFC produces high quality heat for co-generation. Overall efficiencies for co-generation type SOFC can reach up to 95% [1]. Since 2014, in Japan, a household fuel cell system called ENE・FARM that uses state-of-the-art SOFC technology is being commercialized.

2.1.2. The SOCs typical configuration and materials

In general, the SOC is composed of an oxide ion conducting electrolyte such as yttria-stabilized zirconia (YSZ) contacted with two porous ceramic electrodes. Typical configuration of SOC with electrolyte-supported button cell is shown in Fig. 2-2 and Fig. 2-3. A perovskite-type oxide such as $La_{1-x}Sr_xMnO_3$ (LSM) or $La_{1-x}Sr_xCo_{1-y}Fe_yO_{3-\delta}$ (LSCF) are used as an oxygen electrode, while on the opposite side a cermet electrode made of nickel and YSZ is used as a fuel electrode. An interlayer is used for preventing a solid phase reaction between the oxygen electrode and the electrolyte.

In the following sections I will explain separately each component of the SOFC with emphasis on the materials commonly used. It is important to notice that basically the same types of electrodes are used in the SOECs, the operating principles of which will be explained in section 2.1.3.

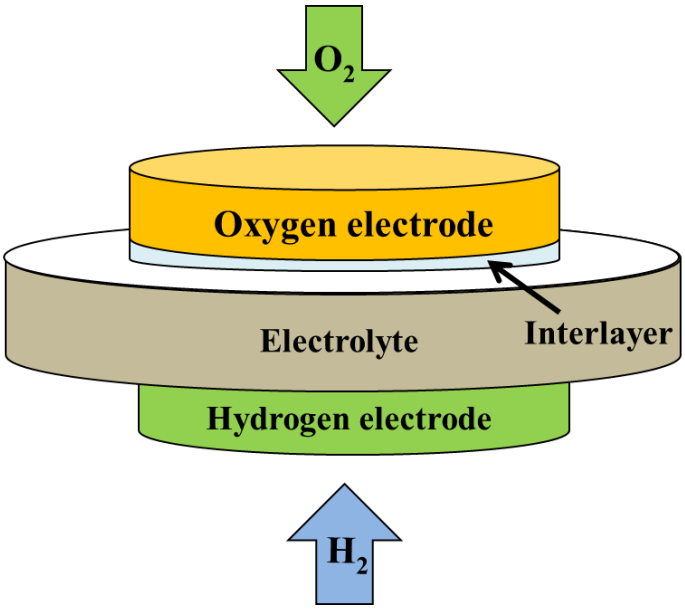

Fig. 2-2. Schematic configuration of electrolyte-supported SOC.

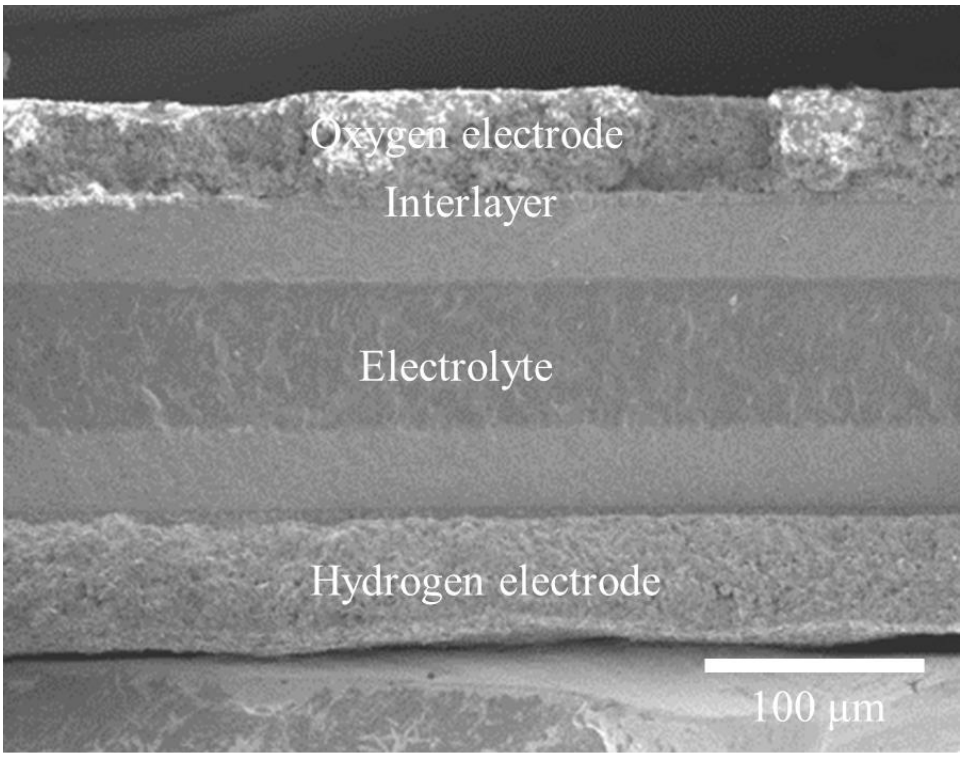

Fig. 2-3. Cross-section view of a typical electrolyte-supported SOC single cell.

2.1.2.1. Hydrogen electrode

The hydrogen electrode has to be stable in the reducing environment of the fuel, and has enough electron conductivity and sufficient porosity for the transport of gases.

The so-called Ni–YSZ cermet with a Ni content over 50 vol% has been used as the hydrogen electrode for R-SOC [2-4]. However, in general, sintering and grain growth of Ni are promoted during operation in the temperature range of 800 to 1000°C, causing a drastic reduction of the effective reaction zone (ERZ). Moreover, the inherent redox instability of the Ni–YSZ cermet during the reversible operation (under a large range of oxygen partial pressure variation) is considered also to be a major disadvantage for this material. Consequently, alternative materials as well as fabrication techniques with a focus on the judicious design of the ERZ have been proposed to improve the electrode microstructure, and with this, its performance and stability [5-9]. Our laboratory has engaged in research and development of catalyzed-reaction layers, which achieve high performance in both the anode and cathode for intermediate temperature SOFCs [5, 10]. The essential design concepts established so far are 1) the use of mixed ionic and electronic conducting oxides having high ionic conductivity (σ_{ion}) and electronic conductivity (σ_e) as the porous electrode material, 2) the control of the microstructure of the porous mixed-conducting electrode to extend the ERZ, where oxide ions, electrons, and reactant gases can have maximum contact, and 3) the activation of the reaction by highly dispersed catalysts on the electrode surface. In the hydrogen electrode, our laboratory reported that a Ni or

NiCo-dispersed samaria-doped ceria [SDC, $(CeO_2)_{0.8}(SmO_{1.5})_{0.2}$] hydrogen electrode exhibited very high performance in both SOFC and SOEC [10-15].

2.1.2.2. Electrolyte

The dense electrolyte is a oxide ion conductor and that its main role in the SOCs, however, at the same time it has as a function to separate the gases, so that the hydrogen supplied to the hydrogen electrode and oxygen or air supplied to the oxygen electrode do not mix. Hence, the dense electrolyte material requirements are:

- High oxide ion conductivity at high temperature
- No or negligible electron conductivity
- Excellent mechanical stability
- High chemical stability at high temperature under oxygen or hydrogen atmospheres.

In addition, chemical compatibility with other adjacent elements is required. Generally, yttria stabilized zirconia (YSZ) is used as an electrolyte material [16]. Especially, the YSZ with 8mol% of yttria is the most commonly used. Besides, $La_xSr_{1-x}Ga_yMg_{1-y}O_{3-\delta}$ (LSGM) [17], scandia stabilized zirconia (ScSZ) and at lower temperatures, samaria doped ceria (SDC) and gadolinia doped ceria (GDC) are also used as electrolytes.

2.1.2.3. Oxygen electrode

The oxygen electrode for R-SOC is a highly electron conductive material with high electro-catalytic activity and stable in an oxidizing atmosphere, and, of preference, chemically compatible with the electrolyte. Fig. 2-4 shows the oxygen reduction reaction (ORR) occurred at the oxygen electrode.

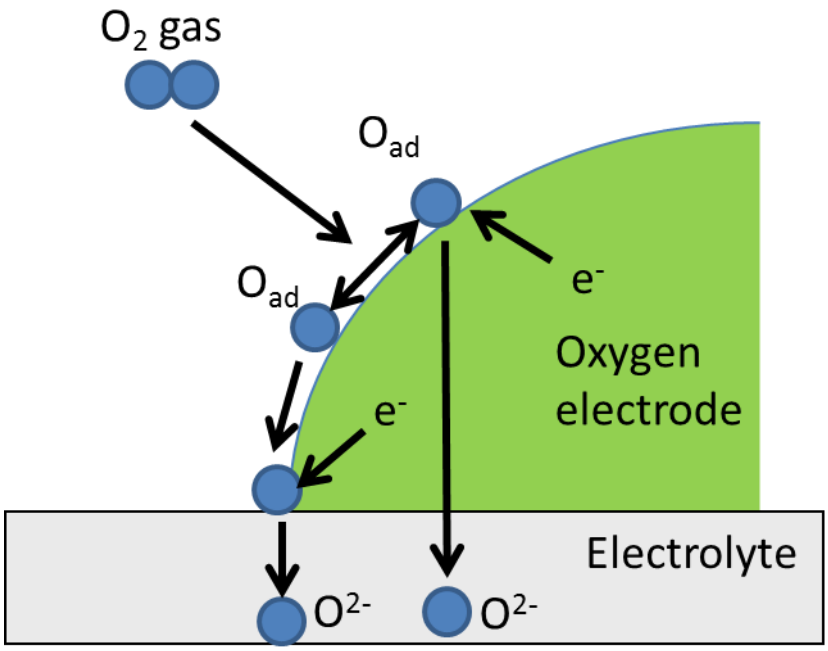

Fig.2-4. ORR Mechanism of oxygen electrode under SOFC condition.

The supplied oxygen gas (O_2 gas) adsorbs to the surface of the electrode material and becomes adsorbed oxygen (O_{ad}). After that, it moves to the electrode material surface and towards the reaction field called the triple phase boundary (TPB) where the electrode, the electrolyte and the gas phase meet. At the TPB, the adsorbed oxygen reacts with electrons supplied by the electrode, becomes oxide ion, and finally moves through the electrolyte towards the hydrogen electrode. In addition, mixed electron-ion

conductors (MIECs) with combined electronic and oxide ion conductivity are used as materials in the oxygen electrode. In this case, surface-exchange reactions are composed of basically the same sequential steps, i.e., adsorption from the gas phase, charge transfer reaction between the adsorbed species and the bulk to form oxide ions, and bulk-diffusion within the MIEC. In the case of a metal electrode, the oxygen gas is chemisorbed once on the electrode, although the adsorption field is limited. At high temperatures, the coverage of oxygen atoms O_{ad} on the electrode is usually low and the transfer (or diffusion) of O_{ad} to the TPB dominates the reaction rate. On the other hand, in the porous oxide electrode using MIECs, the oxide ion is readily produced on the surface and by bulk-diffusion reach the electrolyte. Therefore, the coverage is not so important, and charge transfer at the electrode/electrolyte interface is the rate determining step.

Various oxide materials such as $La_{1-x}Sr_xMnO_3$ (LSM) [18], $La_{1-x}Sr_xCoO_{3-\delta}$ (LSC) [19, 20], $La_{1-x}Sr_xCo_{1-y}Fe_yO_{3-\delta}$ (LSCF) [21-23], $Ba_{1-x}Sr_xCo_{1-y}Fe_yO_{3-\delta}$ (BSCF) [24] and $Sm_{1-x}Sr_xCoO_{3-\delta}$ (SSC) [25] are commonly investigated and even used in both SOFCs and SOECs.

Depending upon specific requirements of ion or electron conductivity the oxygen electrode can be made of a single phase oxide or combined with other oxides to form a composite.

2.1.2.3.1. Single phase electrode

In previous studies, LSM and LSC have been used as single electrodes. LSM was the first choice for practical SOFC cathode and it has a good performance at 1000°C. However, by lowering the operating temperature, its polarization property was not satisfactory. Some papers reported an improvement of the electrode performance at medium temperatures by means of optimization of the microstructure of LSM cathode [26]. In contrast, LSC has good performance and transport properties, but also a high thermal and chemical expansion [20].

Therefore, materials with high performance and low thermal expansion are necessary. Composite electrodes were developed to overcome these problems.

2.1.2.3.2. Composite electrode

The LSCF has lower electron conduction than LSC, but has less thermal and chemical expansion than LSC [21, 22, 27]. Hence, LSCF is a potential candidate for the oxygen electrodes, which can be operated at intermediate-temperature. To compensate for lower performance than LSC, samaria-doped ceria (SDC) or gadolinia-doped ceria (GDC) were typically used to fabricate composite-type LSCF electrodes with increased ionic conductivity, σ_{ion} [23, 28] in order to extend the active sites to the entire electrode. By mixing LSCF with high electron conductivity and SDC or GDC with high oxide ion conductivity under the oxidizing atmosphere, the composite electrode increases the triple phase boundary which is the ERZ, and the success improves.

In one of my previous studies, which it is not part of this dissertation, I have already focused on the oxygen electrode for R-SOC. I have succeeded in improving the reversible performances of the single layer LSCF–SDC composite oxygen electrode at 800 and 900°C [29], compared with those of an identical-type electrode in our laboratory's previous work [23]. A similar behavior in the anodic reaction (oxygen evolution) and the cathodic reaction (oxygen reduction) indicates a high degree of reversibility for the LSCF–SDC electrode. In this dissertation, however, I am focusing on more systematic experiments and the developing of interlayer of oxygen electrodes for R-SOC aiming at improving its performance and durability.

2.1.2.3.3. Concept of oxygen electrode

In our laboratory, a highly efficient oxygen electrode was proposed as shown in Fig.2-5 [23]. Fundamental data such a crystal structures, physical properties and characterization of raw powders of the materials of interest, LSCF and SDC, are presented in the appendix.

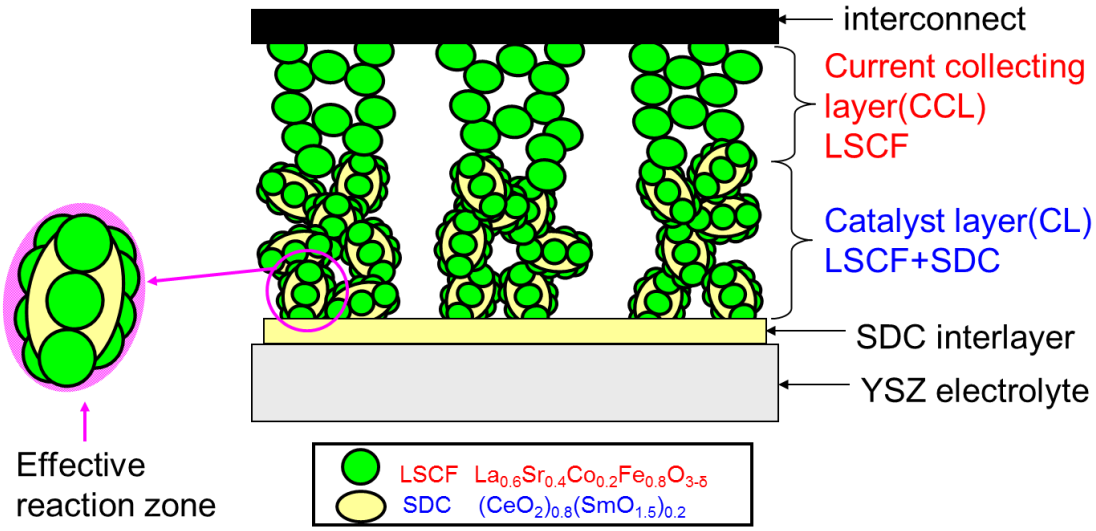

Fig.2-5. Schematic representation of an LSCF–SDC/LSCF double layer oxygen electrode for reversible SOFCs [23].

In brief, a composite electrode obtained by mixing LSCF with high electron conductivity and SDC with high oxide ion conductivity was used for certainly enlarges the ERZ. In addition, in order to keep the current collection between the electrode and the interconnector satisfactorily, LSCF with high electron conductivity was applied as the porous current collecting layer. However, the LSCF tend to react readily with YSZ electrolyte to produce highly resistive phase such as $SrZrO_3$, resulting in degradation of cell performance and durability. Therefore, in order to prevent the solid state reaction of LSCF and YSZ, an SDC interlayer was inserted [30]. It was also expected that the compatibility of the thermal expansion coefficient with the LSCF–SDC electrode will be increased by inserting the SDC interlayer [23]. In the proposed ideal oxygen electrode, the interlayer is used only as a barrier layer for preventing a solid state reaction between the electrode and the electrolyte. Therefore, in this concept the

role of the interlayer is limited to prevent unfavorable reactions or to reduce the mechanical incompatibility, thus only durability was the important factor when dealing with the interlayer. However, as we will see, when considering the interlayer as an important part of the electrode, the quality of the interlayer may have effects other than those expected for durability of the SOCs.

2.1.2.4. Interlayer

I have already stated that that the interlayer has been commonly employed as reaction barrier. In spite of avoiding the direct contact between the oxygen electrode and the YSZ electrolyte, the interlayer allows the diffusion of cations component from the electrode towards the YSZ electrolyte and/or Zr component from YSZ to the electrode during long-term operations. In general, the mass transport occurs via surface, grain boundary and bulk diffusion. it has been reported that diffusion of Sr diffuses an electrode containing Sr (LSCF or LSM) on the doped-ceria interlayer (GDC or SDC) at high temperature for a long time [31, 32]. The influence of the various factors such as the thickness, porosity and composition in interlayer on diffusion of Sr has been investigated [32-34]. Methods for prepared interlayers such as screen-printing, dip coating, magnetron sputtering have been studied and used [31, 35, 36].

2.1.3. Solid oxide electrolysis cell (SOEC)

When the electricity and water vapor are supplied to the SOC, thus operating as SOEC, hydrogen is produced with the high conversion efficiency as shown Figure 2-6.

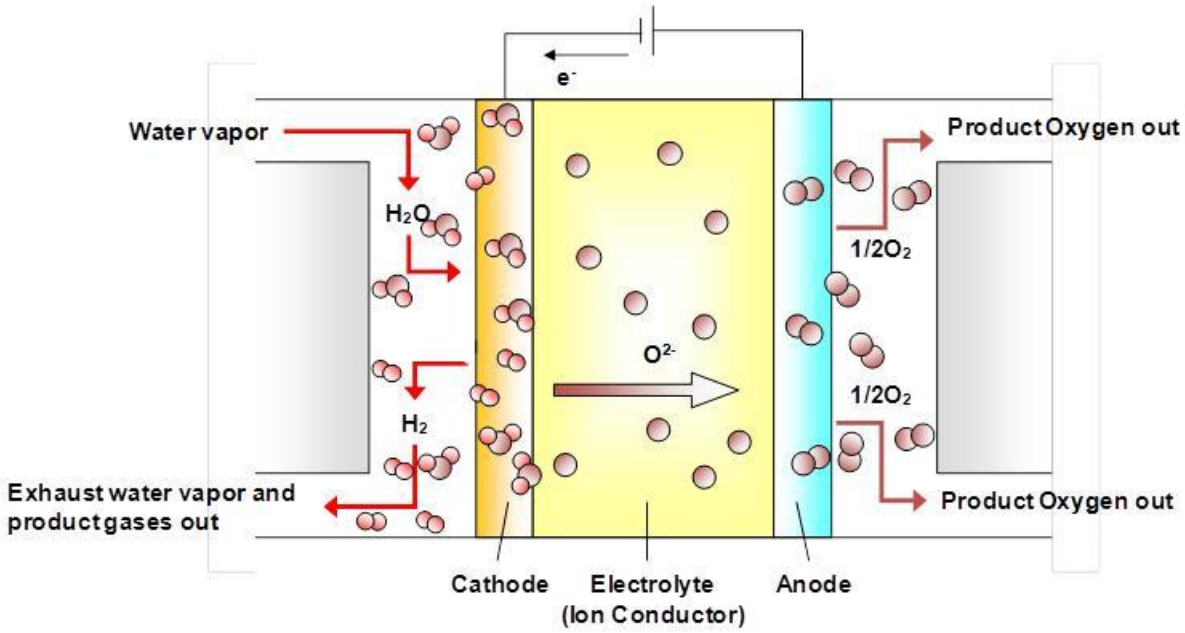

Fig.2-6. Schematic representation of a solid oxide electrolysis cell (SOEC) operated with water vapor.

Porous electrodes are attached to both sides of the solid oxide electrolyte, and water vapor is supplied to the cathode. When a voltage is applied from an external power source connected to the porous electrode, electrolysis begins. At the cathode, water vapor molecules receive electrons and are reduced, forming hydrogen molecules with oxide ions and generating hydrogen. The generated oxide ions move toward the anode in the solid oxide electrolyte. At the anode, oxide ions emit electrons and generate oxygen. The electrode reaction proceeds as follows:

Anode: $O^{2-} \rightarrow 1/2\ O_2 + 2e^-$

Cathode: $H_2O + 2e^- \rightarrow H_2 + O^{2-}$

Cell reaction: $H_2O \rightarrow 1/2\ O_2 + H_2$

The oxygen evolution reaction (OER) mechanism of the oxygen electrode is shown in Fig.2-7.

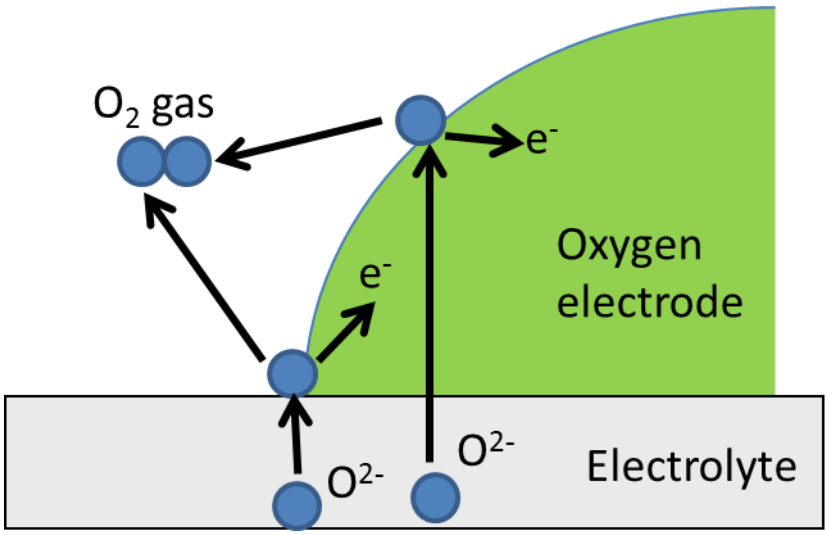

Fig.2-7. OER mechanism of oxygen electrode under SOEC condition

From the hydrogen electrode side, oxide ions are supplied to the oxygen electrode through the electrolyte, which releases electrons at the TPB or electrode surface to generate oxygen gas. The electrode reaction rate is sufficiently high even without using an expensive noble metal catalyst for high temperature operation and all the constituent materials are solid so there is no problem of leakage or dissipation of the electrolytic solution. The first-generation SOECs, resulting from the pioneering work in the late

1960s [37] and the HOT-ELLY (hot-electrolysis) project in 1980s [38], have been operated at temperatures around 1000°C because of insufficient performance of the solid oxide electrolyte and electrodes. Lowering the operating temperature from 1000°C to 600–800°C range would reduce not only degradation rate of component materials but also manufacturing and operating costs. However, two major according to the reduced operating temperature obstacles must be solved. The first is to reduce ohmic loss in the device. There has been marked progress in the use of a very thin film zirconia electrolyte in an SOEC [39]. Therefore, the development of oxygen electrode and hydrogen electrode with high performance and high durability is very important.

2.1.4 Characteristic of SOFC and SOEC

The theoretical power generation efficiency of SOFC is given by the following equation.

$$\frac{\Delta G^\circ}{\Delta H^\circ} = \frac{-2FE^\circ}{\Delta H^\circ} \quad (1)$$

where ΔG° is the standard Gibbs free energy change of the reaction, ΔH° is the standard enthalpy change of the reaction, E° is the theoretical standard electromotive force, and F is the Faraday constant. Thermodynamic values at each temperature, and E° calculated from above equation are shown in Fig. 2-8. As shown in Fig. 2-8, with increasing the operating temperature, the absolute value of ΔG decreases. Thus, at high operation temperatures E° decreases and the theoretical power generation efficiency decrease.

On the other hand, the theoretical electrolysis efficiency (ε) of SOEC is given by the following equation.

$$\varepsilon = (\frac{\Delta H^{\circ}}{2F})/\mathrm{E}^{\circ} \quad (3)$$

therefore, the standard enthalpy change ΔH° of the water decomposition reaction at 25°C is 285.8 kJ/mol in higher heat value (HHV), it can be converted as follows.

$$\varepsilon = \frac{1.48\ V}{E^{\circ}} \quad (4)$$

The standard electrolysis voltage (E°) of the above formula is given by the Nernst equation as follows.

$$\mathrm{E}^{\circ} = \frac{\Delta G^{0}}{2F} \quad (5)$$

where ΔG° is the Gibbs standard free energy change. Water electrolysis is a reverse reaction of hydrogen fuel cell reaction, absolute values of ΔH°, ΔG°, E° are the same as those shown in Fig. 2-8. Thus, in electrolysis of water by the high-temperature steam electrolysis method, the value of ΔG° decreases as the operating temperature becomes higher, so E° becomes smaller and the theoretical conversion efficiency becomes higher. For example, the standard (thermodynamic) decomposition voltage of water vapor is only 0.95 V at 900°C. Theoretically, the efficiency of SOFC is decreasing with increasing operation temperature, while the efficiency of SOEC improves on the contrary.

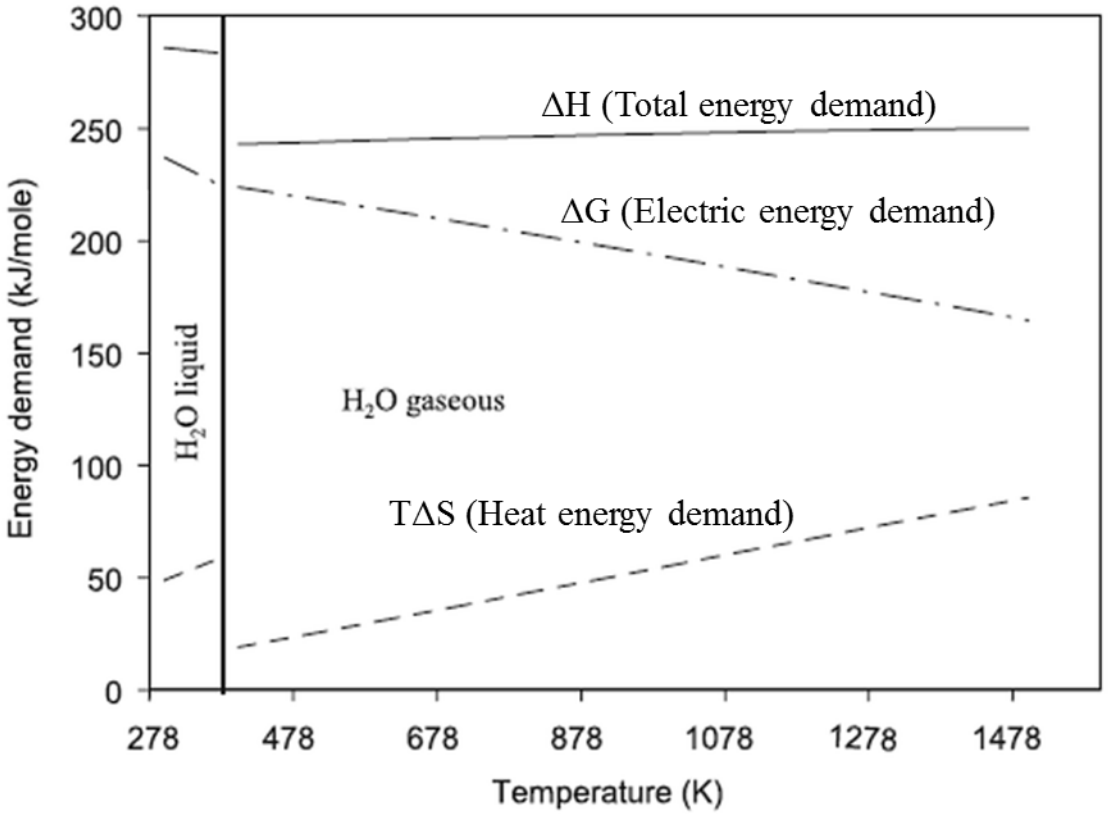

Fig.2-8. Energy demand for water electrolysis [40].

2.2. Reversible Solid Oxide Cells (R-SOCs)

Since SOFC and SOEC are opposite reactions as described above, reversible operation is possible as R-SOC using the same cell. The R-SOC technology is regarded as an efficient reciprocal direct energy convertor between hydrogen and electricity. Therefore, it is expected as a device for leveling power using renewable energy [41, 42]. The advantages of using reversible solid oxide cells operating with ideally a pure steam–hydrogen mixture can be illustrated by thermodynamic considerations of the relevant electrochemical conversion processes [43-45]. For roundtrip energy storage,

the theoretical maximum roundtrip stack efficiency is ΔG/ΔH of the electrochemical conversion in other words, the maximum electrical energy generated in fuel cell mode (ΔG) divided by the total energy required in electrolysis mode (ΔH). As it was shown in the previous section (Fig. 2-8) for a device operating with steam–hydrogen, as temperature increases, the maximum roundtrip efficiency decreases because more waste heat (TΔS) is generated during fuel cell operation. The electrical energy requirement for electrolysis is equivalent to the maximum electricity generation in fuel cell mode (ΔG), although the additional energy (TΔS) must be provided as either heat or electricity. The theoretical maximum efficiency for the steam–hydrogen falls below 80% at 625°C. As partially explained in section 2.1.3, since SOFC is an exothermic reaction and SOEC is an endothermic reaction, by using waste heat generated by SOFC for SOEC, R-SOC shows high efficiency from the viewpoint of heat utilization [46].

2.3. Degradation of the oxygen electrode

Degradation of oxygen electrode is caused by contamination of impurities, formation of resistance layer by reaction of constituent material, and delamination of electrode. Many studies have focused on elucidating degradation mechanisms and reducing degradation.

In recent years, the NEDO Project on Rapid Evaluation Method for SOFC Durability has been conducted in Japan. The goal of this project is establishment of basic technology to rapid evaluate the durability of 90,000 h [47]. As a deterioration

factor in the oxygen electrode, there is an influence by impurities (Cr or S). Degradation by sulfur is complicated in terms of temperature, concentration, etc., and can not be judged simply by only the amount of impurities. Also, considering the deterioration of several tens of thousands of hours, it is necessary to take into consideration other than the influence of simple impurities. In contrast, degradation by chromium is almost understanding of fundamental things [48, 49]. Further, by analyzing the generation behavior of $SrZrO_3$, which is a well-known degradation factor of the oxygen electrode, by FIB-SEM or 3D reconstruction, it is found that the ceria-based interlayer has a great influence on the durability. In recent years, the behavior of protons in ceria is the focus. Generally, the proton conductivity of SDC, GDC, and YSZ is sufficiently low in oxidizing atmosphere. However, in long-term tests, this slightly accumulated effect due to conduction can not be ignored. However, it is not certain at the present time how the microstructure of ceria is involved in the steam generation reaction on the air side or the volatilization reaction of the Sr component [47].

2.4. Contents of the dissertation

As I have stated above, R-SOCs surged as an attractive technology to helping solve the pressing environmental problems. However, at world scale, research on R-SOCs is just a fraction of the research efforts that have been devoted to SOECs and SOFCs as independent devices. I will explain the SOC is an electrochemical device composed of a solid electrolyte sandwiched between the so called oxygen electrode and

hydrogen electrode. Both electrodes are prone to degradation during operation due to many and often complex factors that, to date, are not well understood. The SOC technology still requires further maturation to become economically viable in the competitive market of energy technologies. In particular, the sluggish ORR, at the oxygen electrode, greatly reduces the energy efficiency of a SOC operated to produce electricity and little is still know of how the performance of the oxygen electrode would affect the efficiency of electrolysis process or the durability of the device, this is, when the OER takes place at the oxygen electrode. Therefore, the development of oxygen electrode materials and structures with high electro-catalytic activity for ORR and OER displaying an excellent durability is, needless to say, an imperative to the deployment of commercially competitive of R-SOCs.

In this dissertation, I report my findings in design, fabrication, and characterization of a novel oxygen electrode for R-SOCs with dramatically enhanced durability and cell performance.

2.5. References

[1] A. B. Stambouli, E. Traversa, Solid oxide fuel cells (SOFCs): a review of an environmentally clean and efficient source of energy, Renewable and Sustainable Energy Reviews 6 (2002) 433-455.

[2] D.W. Dees, T.D. Claar, T.E. Easler, D.C. Fee, F.C. Mrazek, Conductivity of Porous Ni / ZrO_2 - Y_2O_3 Cermets, J. Electrochem. Soc. 134 (1987) 2141-2146.

[3] Y.M. Park, G.M. Choi, Microstructure and electrical properties of YSZ–NiO composites, Solid State Ionics 120 (1999) 265-274.

[4] H. Koide, Y. Someya, T. Yoshida, T. Maruyama, Properties of Ni/YSZ cermet as anode for SOFC, Solid State Ionics 132 (2000) 253-260.

[5] M. Watanabe, H. Uchida, M. Shibata, N. Mochizuki, K. Amikura, High Performance Catalyzed‐Reaction Layer for Medium Temperature Operating Solid Oxide Fuel Cells, J. Electrochem. Soc. 141 (1994) 342-346.

[6] S. P. Jiang, S. Zhang, Y. D. Zhen, A. P. Koh, Performance of GDC-Impregnated Ni Anodes of SOFCs, Electrochem. Solid-State Lett. 7 (2004) A282-A285.

[7] J. Qiao, K. Sun, N. Q. Zhang, B. Sun, J. R. Kong, D. Zhou, Ni/YSZ and Ni–CeO2/YSZ anodes prepared by impregnation for solid oxide fuel cells, J. Power Sources 169 (2007) 253-258.

[8] T. Klemensø, K. Thyd´en, M. Chen, H. J. Wang, Stability of Ni–yttria stabilized zirconia anodes based on Ni-impregnation, J. Power Sources 195 (2010) 7295-7301.

[9] C. Yang, C. Jin, F. Chen, Micro-tubular solid oxide fuel cells fabricated by phase-inversion method, Electrochem. Commun. 12 (2010) 657-660.

[10] H. Uchida, M. Watanabe, in R.E. White, M.E. Gamboa-Aldeco (Eds.), Modern Aspects of Electrochemistry, Vol. 42, Ch. 2, Springer, New York, 2008, p. 53.

[11] H. Uchida, S. Suzuki, M. Watanabe, High Performance Electrode for Medium-Temperature Solid Oxide Fuel Cells Mixed Conducting Ceria-Based Anode with Highly Dispersed Ni Electrocatalysts, Electrochem. Solid-State Lett., 6 (2003) A174-A177.

[12] S. Suzuki, H. Uchida, M. Watanabe, Interaction of samaria-doped ceria anode with highly dispersed Ni catalysts in a medium-temperature solid oxide fuel cell during long-term operation, Solid State Ionics, 177 (2006) 359-365.

[13] H. Uchida, N. Osada, M. Watanabe, High-Performance Electrode for Steam Electrolysis Mixed Conducting Ceria-Based Cathode with Highly-Dispersed Ni Electrocatalysts, Electrochem. Solid-State Lett. 7 (2004) A500-A502.

[14] N. Osada, H. Uchida, M. Watanabe, Polarization Behavior of SDC Cathode with Highly Dispersed Ni Catalysts for Solid Oxide Electrolysis Cells, J. Electrochem. Soc. 153 (2006) A816-A820.

[15] R. Nishida, P. Puengjinda, H. Nishino, K. Kakinuma, M.E. Brito, M. Watanabe, H. Uchida, High-performance electrodes for reversible solid oxide fuel cell/solid oxide electrolysis cell: Ni–Co dispersed ceria hydrogen electrodes, RSC Adv. 4 (2014) 16260-16266.

[16] H. Uchida, M. Yoshida, M. Watanabe, Effect of Ionic Conductivities of Zirconia Electrolytes on Polarization Properties of Platinum Anodes in Solid Oxide Fuel Cells, J. phys. chem. 99 (1995) 3282-3287.

[17] T.Ishihara, H. Matsuda, Y. Takita, Doped LaGaO3 Perovskite Type Oxide as a New Oxide Ionic Conductor, J. Am. Chem. Soc. 116 (1994) 3801-3803.

[18] T. Tsai, S.A. Batnett, Effect of LSM-YSZ cathode on thin-electrolyte solid oxide fuel cell performance, Solid State Ionics 93 (1997) 207-217.

[19] O. Yamamoto, Y. Takeda, R. Kanno, M. Noda, Perovskite-type oxides as oxygen electrodes for high temperature oxide fuel cells, Solid State Ionics, 22 (1987) 241-246.

[20] J. Mizusaki, Y. Mima, S. Yamauchi , K. Fueki, H. Tagawa, Nonstoichiometry of the perovskite-type oxides $La_{1-x}Sr_xCoO_{3-\delta}$, J. Solid State Chem., 80 (1989) 102-111.

[21] L. -W. Tai, M. M. Nasrallah, H. U. Anderson, D. M. Sparlin, S. R. Sehlin, Structure and electrical properties of $La_{1-x}Sr_xCo_{1-y}Fe_yO_3$. Part 1. The system $La_{0.8}Sr_{0.2}Co_{1-y}Fe_yO_3$, Solid State Ionics, 76 (1995) 259-271.

[22] L. -W. Tai, M. M. Nasrallah, H. U. Anderson, D. M. Sparlin, S. R. Sehlin, Structure and electrical properties of $La_{1-x}Sr_xCo_{1-y}Fe_yO_3$. Part 2. The system $La_{1-x}Sr_xCo_{0.2}Fe_{0.8}O_3$, Solid State Ionics, 76 (1995) 273-283.

[23] Y. Tao, H. Nishino, S. Ashidate, H. Kokubo, M. Watanabe, H. Uchida, Polarization properties of $La_{0.6}Sr_{0.4}Co_{0.2}Fe_{0.8}O_3$-based double layer-type oxygen electrodes for reversible SOFCs, Electrochim. Acta, 54 (2009) 3309-3315.

[24] Y. Bo, Z. Wenqiang, X. Jingming, C. Jing, Microstructural characterization and electrochemical properties of $Ba_{0.5}Sr_{0.5}Co_{0.8}Fe_{0.2}O_{3-\delta}$ and its application for anode of SOEC, Int. J. Hydrogen Energy, 33 (2008) 6873-6877.

[25] T. Ishihara, M. Honda, T. Shibayama, H. Furutani, Y. Takita, Intermediate Temperature Solid Oxide Fuel Cells Using a New $LaGaO_3$ Based Oxide Ion Conductor I. Doped Formula as a New Cathode Material, J. Electrochem. Soc., 145 (1998) 3177-3183.

[26] T. Inoue, K. Hoashi, K. Eguchi, H. Arai, An effect of microstructure on the interface resistance between a perovskite-type oxide electrode and yttria-stabilized zirconia, J. Mater. Sci., 28, (1993)1532-1536.

[27] Y. Teraoka, H.-M. Zhang, S. Fukuoka, A. Yamazoe, Oxygen permeation through perovskite-type oxides, Chem. Lett. 14 (1985) 1743-1746.

[28] V. Dusastre, J. A. Kilner, Optimisation of composite cathodes for intermediate temperature SOFC applications, Solid State Ionics, 126 (1999) 163-174.

[29] H. Uchida, P. Puengjinda, K. Miyano, K. Shimura, H. Nishino, K. Kakinuma, M. E. Brito, M. Watanabe, Effect of Microstructure on Performances of Hydrogen and Oxygen Electrodes for Reversible SOEC/SOFC, ECS Trans. 68 (2015) 3307-3313.

[30] H. Uchida, S. Arisaka, M. Watanabe, High Performance Electrode for Medium‐Temperature Solid Oxide Fuel Cells La (Sr) CoO_3 Cathode with Ceria Interlayer on Zirconia Electrolyte, Electrochem. Solid-State Lett. 2 (1999) 428-430.

[31] R. Kiebach, W. -W. Zhang, W. Zhang, M. Chen, K. Norrman, H. -J. Wang, J. R. Bowen, R. Barfod, P. V. Hendriksen, Stability of $La_{0.6}Sr_{0.4}Co_{0.2}Fe_{0.8}O_3/Ce_{0.9}Gd_{0.1}O_2$ cathodes during sintering and solid oxide fuel cell operation, J. Power Sources, 283 (2015) 151-161.

[32] F. Wang, M. E. Brito, K. Yamaji, D. -H. Cho, M. Nishi, H. Kishimoto, T. Horita, H. Yokokawa, Effect of polarization on Sr and Zr diffusion behavior in LSCF/GDC/YSZ system, Solid State Ionics, 262 (2014) 454-459.

[33] T. Matsui, M. Komoto, H. Muroyama, K. Kishida, H. Inui, K. Eguchi, Degradation factors in $(La,Sr)(Co,Fe)O_{3-\delta}$cathode/$Sm_2O_3$–$CeO_2$ interlayer/Y_2O_3–ZrO_2 electrolyte system during operation of solid oxide fuel cells, J. Power Sources, 312 (2016) 80-85.

[34] M. Z. Khan, M. T. Mehran, R. -H. Song, J. -W. Lee, S. -B. Lee, T. -H. Lim, S. -J. Park, Effect of GDC interlayer thickness on durability of solid oxide fuel cell cathode, Ceramics International, 42 (2016) 6978-6984.

[35] M. Shionoa, K. Kobayashi, T. L. Nguyen, K. Hosoda, T. Kato, K. Ota, M. Dokiya, Effect of CeO_2 interlayer on ZrO_2 electrolyte/La(Sr)CoO_3 cathode for low-temperature SOFCs, Solid State Ionics 170 (2004) 1-7.

[36] N. Jordan, W. Assenmacher, S. Uhlenbruck, V.A.C. Haanappel, H.P. Buchkremer, D. Stöver, W. Mader, $Ce_{0.8}Gd_{0.2}O_{2-\delta}$ protecting layers manufactured by physical vapor deposition for IT-SOFC, Solid State Ionics 179 (2008) 919-923.

[37] H.S. Spacil, C.S. Tedmon Jr., Electrochemical dissociation of water vapor in solid oxide electrolyte cells I. Thermodynamics and cell characteristics, J. Electrochem. Soc. 116 (1969) 1618-1626.

[38] K.H. Quandt, R. Streicher, Concept and design of a 3.5 MW pilot plant for high temperature electrolysis of water vapor, Int. J. Hydrogen Energy 11 (1986) 309-315.

[39] A. Hauch, S.H. Jensen, S. Ramousse, M. Mogensen, Performance and durability of solid oxide electrolysis cells, J. Electrochem. Soc. 153 (2006) A1741-A1747.

[40] S. H. Jensen, P. H. Larsen, M. Mogensen, Hydrogen and synthetic fuel production from renewable energy sources, Int. J. Hydrogen Energy 32(15) (2007) 3253-3257.

[41] M. Mogensen, S. H. Jensen, A. Hauch, I. Chorkendorff, and T. Jacobsen, Reversible solid oxide cells, In Ceram. Eng. Sci. Proc 28 (2008) 91-101.

[42] K. Eguchi, T. Hatagishi, H. Arai, Power generation and steam electrolysis characteristics of an electrochemical cell with a zirconia- or ceria-based electrolyte, Solid State Ionics 86-88 (1996) 1245-1249.

[43] C.H. Wendel, P. Kazempoor, R. J. Braun, Novel electrical energy storage system based on reversible solid oxide cells: System design and operating conditions, J. Power Sources 276 (2015) 133–144.

[44] C. H. Wendel, Z. Gao, S. A. Barnett, R. J. Braun, Modeling and experimental performance of an intermediate temperature reversible solid oxide cell for high-efficiency, distributed-scale electrical energy storage, J. Power Sources 283 (2015) 329-342.

[45] C. H. Wendel, R. J. Braun, Design and techno-economic analysis of high efficiency reversible solid oxide cell systems for distributed energy storage, Appl. Energy 172 (2016) 118–131.

[46] S. Kasai, Hydrogen electrical energy storage by high temperature steam electrolysis for next millennium energy security, Int. J. Hydrogen Energy 39 (2014) 21358-21370.

[47] H. Yokokawa, Progress Report of NEDO Project on Rapid Evaluation Method for SOFC Durability, The 25th Symposium on Solid Oxide Fuel Cells in Japan 101A (2016).

[48] S. P. Jiang, X. Chen, Chromium deposition and poisoning of cathodes of Solid oxide fuel cells -A review, Int. J. Hydrogen Energy 39 (2014) 505-531.

[49] H. Yokokawa, T. Horita, K. Yamaji, H. Kishimoto, T. Yamamoto, M. Yoshikawa, Y. Mugikura, K. Tomida, Chromium Poisoning of $LaMnO_3$ ‐ Based Cathode within Generalized Approach, Fuel Cells, 13 (2013) 526-535.

Chapter 3

Preparation and characterization of samaria-doped ceria (SDC) interlayer

3.1. Introduction

In SOC, cell performance often deteriorates due to the solid-state reaction between the oxygen electrode and the electrolyte, resulting in formation of a high resistance layer like $SrZrO_3$ or $La_2Zr_2O_7$. It is well known that solid-state reaction can be suppressed by inserting the interlayer. In our laboratory, for the first time, an SDC interlayer was found to be effective to prevent unfavorable solid-state reaction [1]. Moreover, it was also reported that the LSCF–SDC electrode with SDC interlayer exhibited durability of 5000 h under anodic conditions [2]. However, degradation due to the formation of $SrZrO_3$ is also observed in the cell with the interlayer [3, 4]. This is due to the fact that Sr and Zr diffuse through voids and grain boundaries in the interlayer during the preparation of electrodes and interlayer or during long-term operation [3, 4]. To prevent this, a dense, thin and uniform interlayer is required.

As the preparation method of SDC interlayer, various methods such as screen-printing [3], dip coating [5], and magnetron sputtering [6] have been studied. For example, in our laboratory, a mixed solution of cerium and samarium nitrates was screen-printed on YSZ surface, followed by sintering. Such process was repeated several times to obtain the SDC interlayer. However, it is usually difficult to prepare thin and dense interlayer by screen-printing and dip coating, followed by sintering. In contrast, the magnetron sputtering method can prepare thin and dense interlayer, but it

is costly and difficult to produce the interlayer industrially. Therefore, it is important to produce a dense, thin and uniform interlayer in a scalable method. Therefore, I investigate a new method to prepare a dense, thin and uniform SDC interlayer. The spin-coating method can generally form a thin film. And metal octoate have been reported to make it possible to produce a dense and thin film with good adhesion [7, 8]. I have chosen spin-coating of metal 2-ethylhexanoate (denoted as octoate), followed by sintering.

3.2. Experimental

A process of the spin-coating method is shown in Fig.3-1. First, a precursor solution is dropped onto the YSZ electrolyte substrate. Next, by thinning out excess solution by rotating the YSZ electrolyte disk at high speed, a thin film can be formed on the electrolyte. The spin coater (ACT-220D II, Active. Japan) used in this experiment is shown in Fig.3-2.

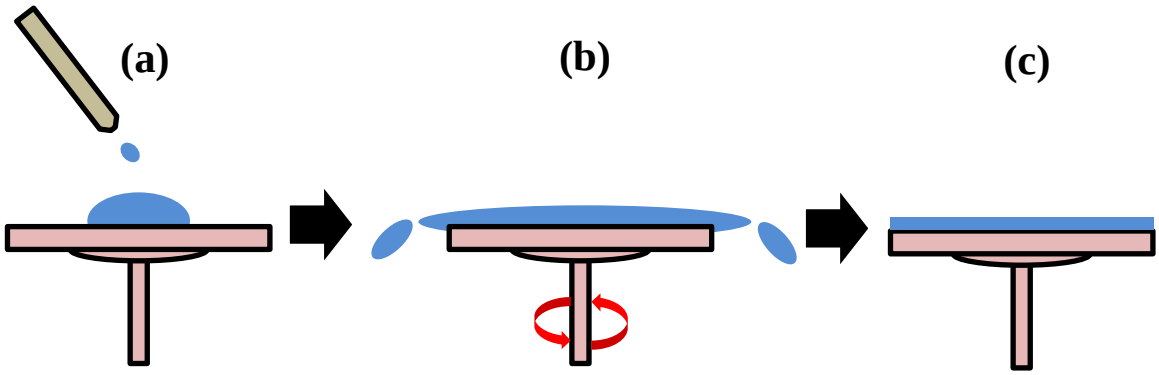

Fig. 3-1. The process of the spin-coating method (a) solution drop on onto the electrolyte, (b) rotating the electrolyte at high speed, (c) thin film formation on the electrolyte

Fig. 3-2. A picture of spin coater used in the experiment

(http://www.acti-ve.co.jp/spincoater/standard/act220d2.html)

The SDC interlayers were prepared on the YSZ electrolyte disk as follows. A mixed solution of cerium and samarium octoates (Ce: Sm = 8:2, Nihon Kagaku Sangyo Co., LTD, Japan) in toluene solvent was spin-coated on the YSZ disk surface, followed by heat-treatment at 300°C. The spin-coating and the heat-treatment were repeated several times. The YSZ with SDC interlayer was sintered at 1050°C for 2 h. This protocol was repeated three times to form SDC interlayer. The SDC interlayer thus prepared from the octoates will be denoted as o-interlayer. For comparison, a SDC interlayer was prepared by screen-printing a mixed solution of cerium and samarium nitrates with a thickener, followed by heat-treatment at 400°C [2]. The screen-printing and the heat-treatment were repeated several times, and finally the interlayer was sintered at 1150°C for 4 h. The SDC interlayer thus prepared from the nitrates will be denoted as n-interlayer. The above preparation procedure is shown in Scheme 3-1 and 3-2. The characterization of these interlayers was observed by scanning electron microscopy (SEM, S-5200, Hitachi High-Technologies Co. Japan) and X-ray diffraction (XRD, Rigaku Ultima IV, Japan).

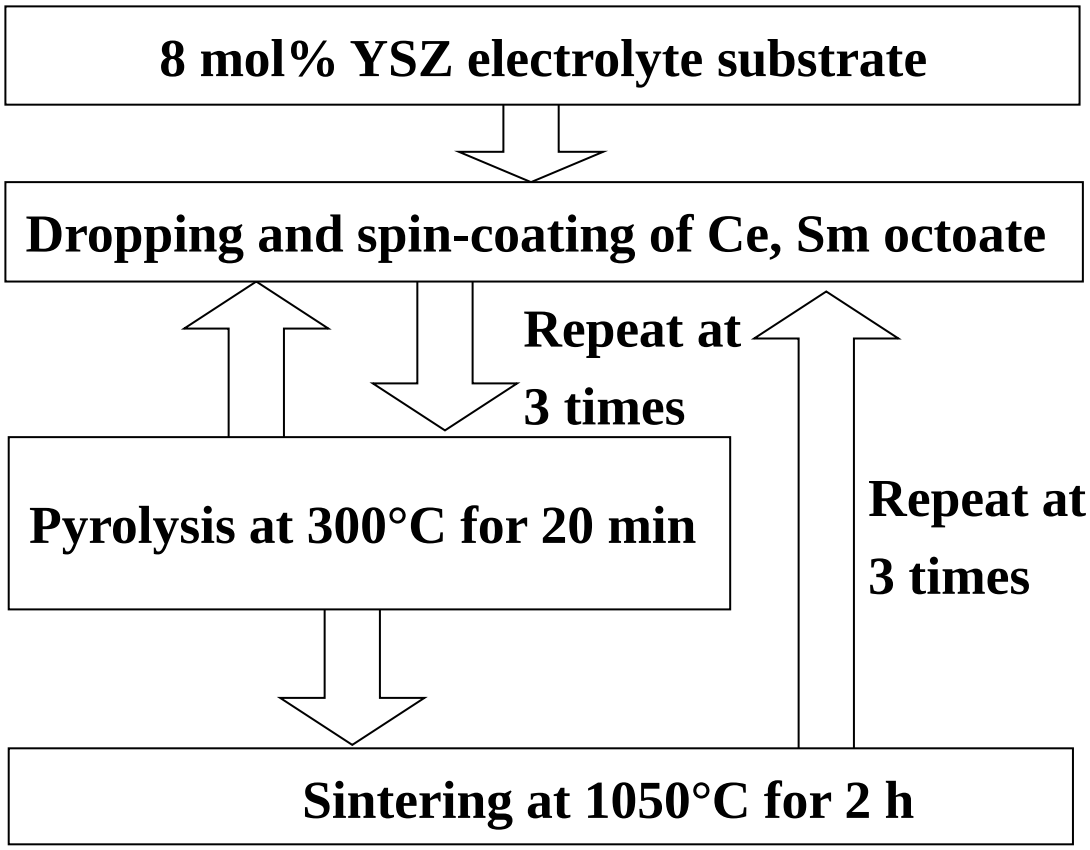

Scheme 3-1 Preparation procedure of the o-interlayer

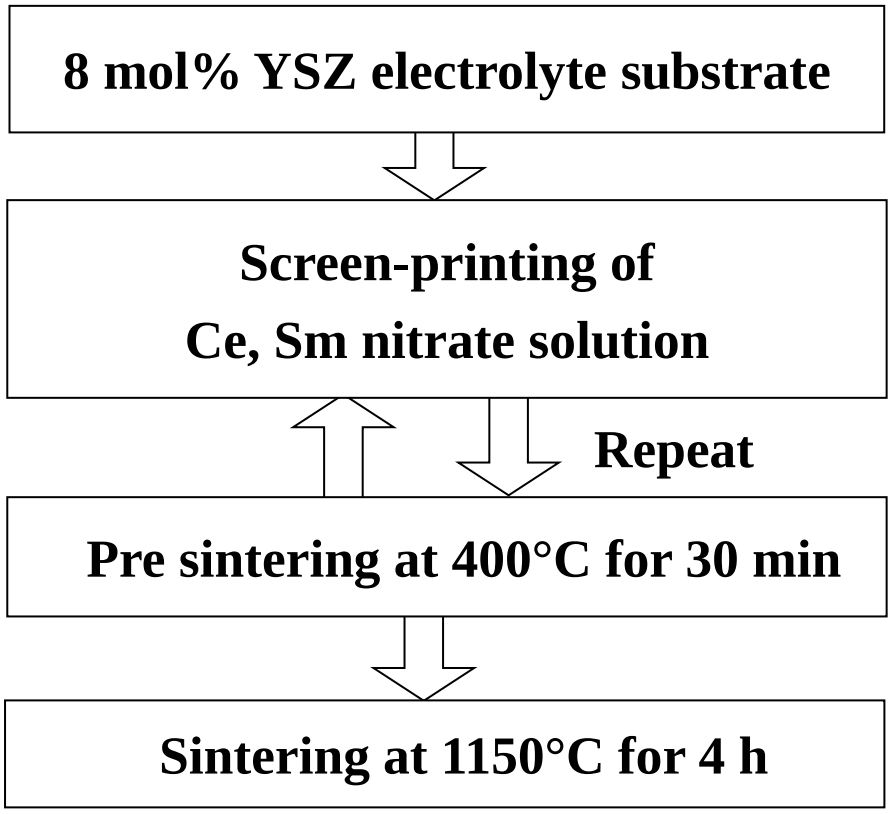

Scheme 3-2 Preparation procedure of the n-interlayer

3.3. Results and discussion

3.3.1. Characterization of o-interlayer and n-interlayer

Figure 3-1 shows XRD pattern of o-interlayer. All the diffraction peaks of the o-interlayer unequivocally corresponded to the SDC and YSZ phases. I prepared the SDC interlayer sintered at 1050°C for 2 h. Some authors reported that inter-diffusion took place between the interlayer and the electrolyte during high temperature sintering for several hours [16]. In our case, and as an important factor to be considered, the extension of the inter-diffusion, and in turn a detrimental effect on the electrolyte performance, is rather limited due to the highest sintering temperatures 1050°C for 2 h in the o-interlayer.

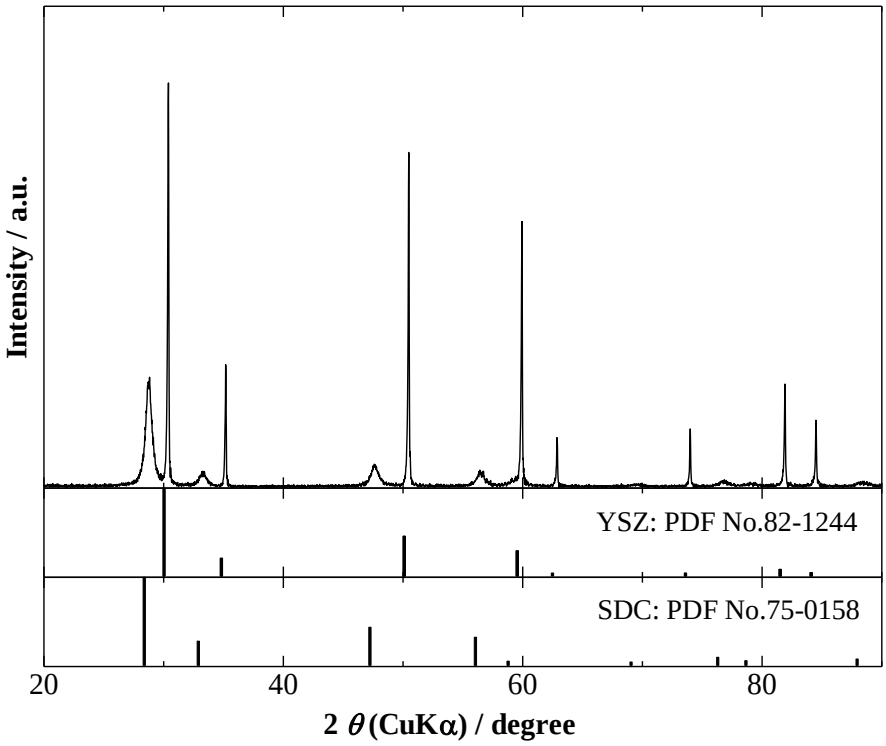

Fig. 3-1. XRD pattern of o-interlayer.

3.3.2 Microstructure of n-interlayer and o-interlayer

Figure 3-2 shows surface and cross-sectional SEM images of the n-interlayer and o-interlayer. I have found that o-interlayer and n-interlayer showed different features. From SEM images, the o-interlayer had only small cracks, and large cracks had hardly present. Moreover, the o-interlayer was observed more uniform in thickness of ca. 1.0 μm and adhered better to the YSZ electrolyte surface. In contrast, in the n-interlayer, there was a large crack, and it was observed that the lump was detached. And the thickness of n-interlayer was non-uniform at 3.0 to 6.0 μm. Other features of the n-interlayer are the presence of micro-cracks in very thin parts and partial delamination from the YSZ.

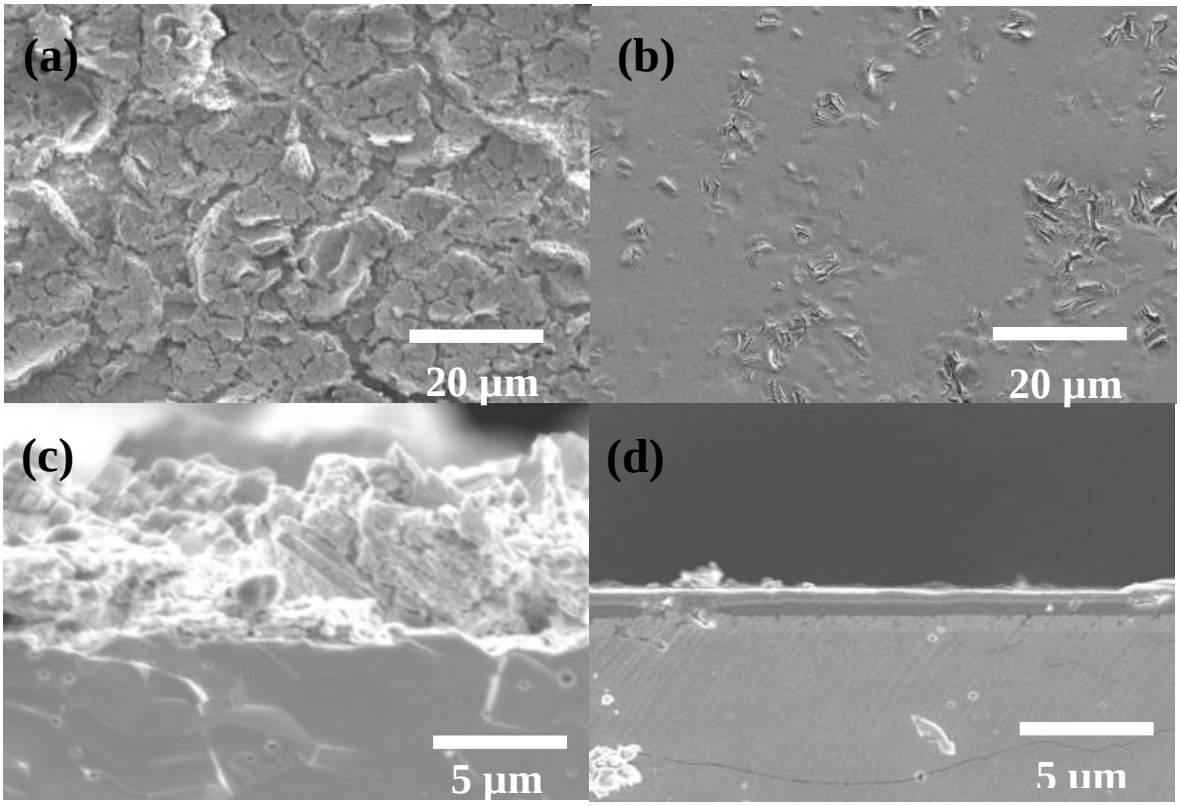

Fig.3-2. SEM surface and cross-sectional images of SDC interlayer (a) (c) n-interlayer and (b) (d) o-interlayer.

Table 1 shows a comparison between the interlayer produced in this work and interlayer reported in the literature.

Table 1 Comparison of interlayer properties

Preparation method	Material	Thickness	Structure	Reference
Screen-printing	GDC	5 μm	Porous	[11], [13]
Dip coating	GDC	3-6 μm	Porous	[12]
Magnetron sputtering	GDC	0.3, 1 μm	Dense	[13], [17]
Pulse laser deposition	GDC	1 μm	Dense	[16]
Vacuum slurry coating	GDC	2.4, 3.4, 6.0 μm	Dense	[10]
Spin-coating	SDC	1 μm	Dense	This study
Screen-printing	SDC	3-6 μm	Not dense	This study

From Table 1, in order to prepare a dense and thin interlayer, magnetron sputtering, pulsed laser deposition or vacuum slurry coating is used. On the other hand, the screen-printing or dip coating is thick and porous. Compared to other studies, in the present work, I succeeded in simply producing a dense, thin and uniform interlayer by spin-coating method.

3.4. Conclusions

I have prepared the SDC interlayer by spin-coating method from a cerium and samarium octoates. The o-interlayer was observed a dense, thin and uniform as compared with n-interlayer. Furthermore, it was possible to sufficiently suppress inter-diffusion between the SDC interlayer and the YSZ electrolyte by a sintering process at 1050°C for 2 h. I have succeeded in preparing a dense, thin and uniform SDC interlayer using by spin-coating which is an industrially scalable method.

3.5. References

[1] H. Uchida, S. Arisaka, M. Watanabe, High Performance Electrode for Medium‐Temperature Solid Oxide Fuel Cells La (Sr) CoO_3 Cathode with Ceria Interlayer on Zirconia Electrolyte, Electrochem. Solid-State Lett. 2 (1999) 428-430.

[2] Y. Tao, H. Nishino, S. Ashidate, H. Kokubo, M. Watanabe, H. Uchida, Polarization properties of $La_{0.6}Sr_{0.4}Co_{0.2}Fe_{0.8}O_3$-based double layer-type oxygen electrodes for reversible SOFCs, Electrochim. Acta, 54 (2009) 3309-3315.

[3] R. Kiebach, W. -W. Zhang, W. Zhang, M. Chen, K. Norrman, H. -J. Wang, J. R. Bowen, R. Barfod, P. V. Hendriksen, Stability of $La_{0.6}Sr_{0.4}Co_{0.2}Fe_{0.8}O_3/Ce_{0.9}Gd_{0.1}O_2$ cathodes during sintering and solid oxide fuel cell operation, J. Power Sources, 283 (2015) 151-161.

[4] F. Wang, M. E. Brito, K. Yamaji, D. -H. Cho, M. Nishi, H. Kishimoto, T. Horita, H. Yokokawa, Effect of polarization on Sr and Zr diffusion behavior in LSCF/GDC/YSZ system, Solid State Ionics, 262 (2014) 454-459.

[5] M. Shiono, K. Kobayashi, T. L. Nguyen, K. Hosoda, T. Kato, K. Ota, M. Dokiya, Effect of CeO_2 interlayer on ZrO_2 electrolyte/La(Sr)CoO_3 cathode for low-temperature SOFCs, Solid State Ionics 170 (2004) 1-7.

[6] N. Jordan, W. Assenmacher, S. Uhlenbruck, V.A.C. Haanappel, H.P. Buchkremer, D. Stöver, W. Mader, $Ce_{0.8}Gd_{0.2}O_{2-\delta}$ protecting layers manufactured by physical vapor deposition for IT-SOFC, Solid State Ionics 179 (2008) 919-923.

[7] C.M. Ronconi, D. Gonçalves, N. Suvorova, O.L. Alves, E.A. Irene, Preparation and characterization of $Cd_2Nb_2O_7$ thin films on Si substrates, J. Phys. Chem. Solids 70 (2009) 234-237.

[8] S. Morlens, L. Ortega, B. Rousseau, S. Phok, J.L. Deschanvre, P. Chaudouet, P. Odier, Use of cerium ethylhexanoate solutions for preparation of CeO_2 buffer layers by spin coating, Mater. Sci. Eng. B 104 (2003) 185-191.

[9] W. Wu, Z. Z, X. Zhang, Z. Liu, D. Cui, B. Tua, D. Ou, M. Cheng, Structure-designed gadolinia doped ceria interlayer for solid oxide fuel cell, Electrochemistry Communications, 71 (2016) 43-47.

[10] M. Z. Khan, M. T. Mehran, R. -H. Song, J. -W. Lee, S. -B. Lee, T. -H. Lim, S. -J. Park, Effect of GDC interlayer thickness on durability of solid oxide fuel cell cathode, Ceramics International, 42 (2016) 6978-6984.

Chapter 4

High durability of $La_{0.6}Sr_{0.4}Co_{0.2}Fe_{0.8}O_{3-\delta}$ (LSCF) – SDC composite oxygen electrode with SDC interlayer for reversible solid oxide cells

4.1. Introduction

At the oxygen electrode for R-SOC, high durability is required under both anodic and cathodic operation. However, it has been reported that Sr and Zr diffuse of the interlayer even in the cell into which the interlayer is inserted, and that naturally the performance decreases [1]. It is also reported that the interlayer is originally not dense or Sr and Zr are diffused from the beginning due to that it is sintered at high temperature for a long time at the preparation of the interlayer and the electrode [2, 3]. In Chapter 2, I succeeded in preparing a dense, thin and uniform SDC interlayer. Furthermore, the diffusion of Zr from YSZ electrolyte is negligible since it is lower temperature and shorter time sintering than the condition reported that Zr diffuse [2, 3].

In this chapter, using LSCF–SDC electrode with a dense, thin and uniform SDC interlayer (o-interlayer), I conducted long-term durability tests using a symmetrical cell. A symmetric cell consisting of LSCF–SDC|SDC interlayer|YSZ|SDC interlayer|LSCF–SDC as shown in the Fig. 4-1 was used for the measurement.

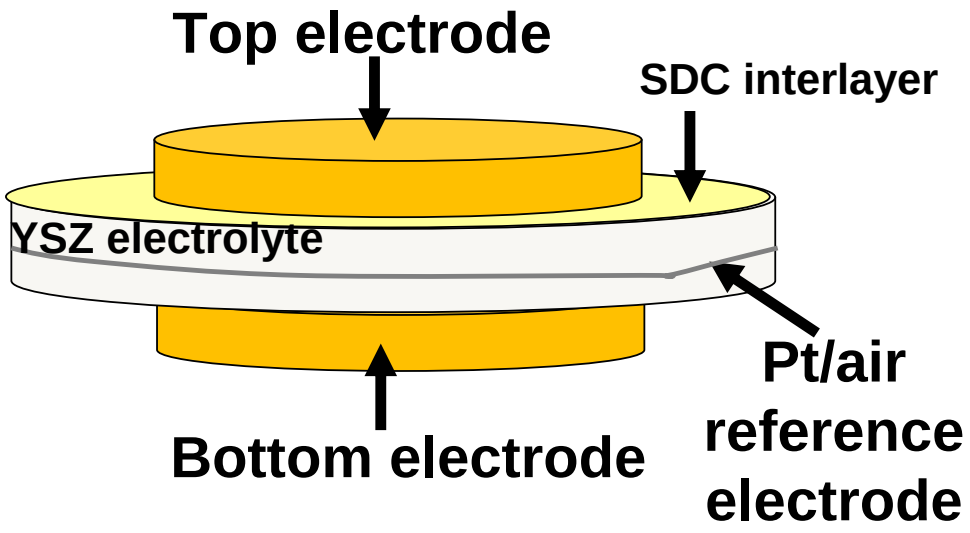

Fig. 4-1. Configuration of symmetric cell.

In the symmetric cell, the same electrode is formed on both sides of the electrolyte, oxygen is supplied to both electrodes, and an electric current is applied, whereby the anode reaction and the cathode reaction can be measured under the same conditions simultaneously. Fig. 4-2 also shows SEM image of symmetrical cell (since the electrolyte is thick, it is omitted).

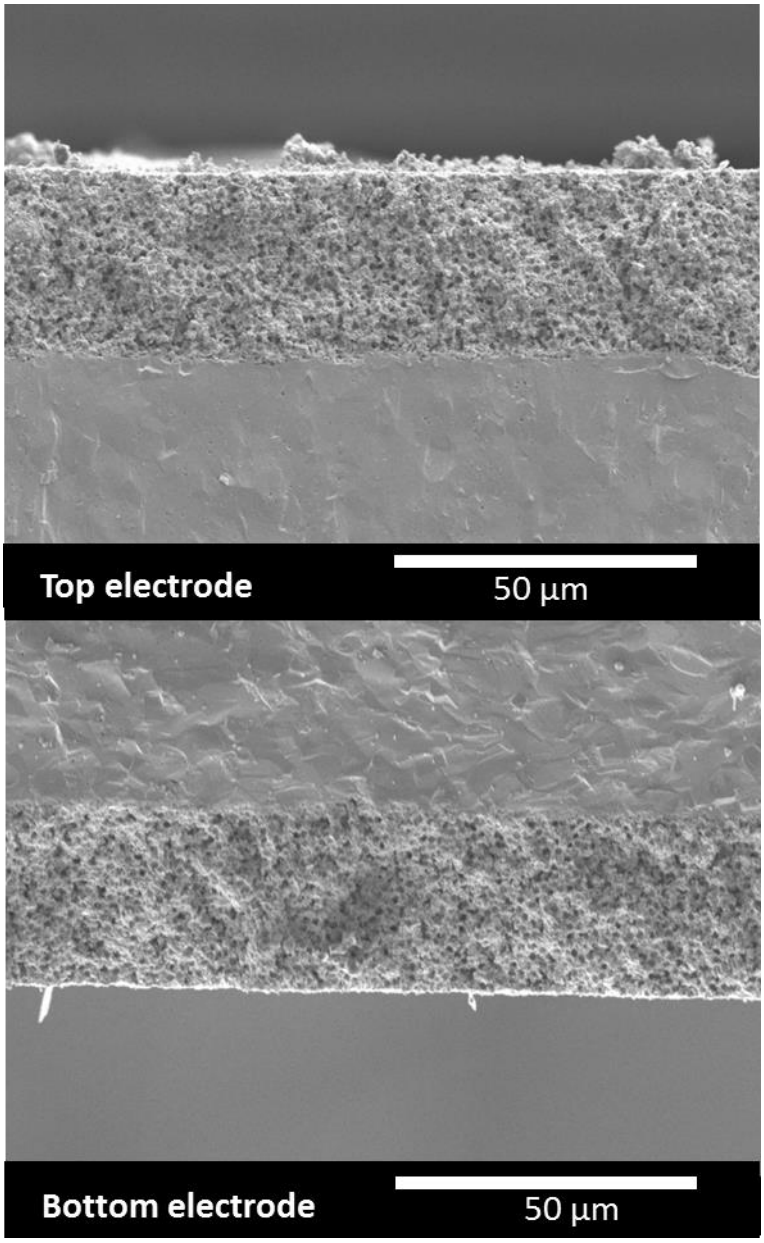

Fig. 4-2. Cross-sectional SEM images of symmetrical cell.

In this experiment, I use a symmetric cell and carried out a long-term durability test of 5500 h at 0.5 A cm^{-2} and at 900°C under anodic and cathodic operation and report an effective suppression of Sr diffusion by the SDC interlayer in particular at the anode side, leading to negligible changes in the anode overpotential and ohmic resistance. The important role of uniform and dense microstructure of the SDC interlayer on the durability is discussed.

4.2. Experimental

A symmetrical cell consisted of an 8mol% yttria-stabilized zirconia solid electrolyte disk (YSZ, 13 mm in diameter and 1 mm in thickness), $La_{0.6}Sr_{0.4}Co_{0.2}Fe_{0.8}O_{3-\delta}$ (LSCF) – SDC composite oxygen electrodes on both sides, and SDC interlayers to suppress unfavorable solid-state reactions between the LSCF and the YSZ electrolyte: LSCF–SDC|SDC interlayer|YSZ|SDC interlayer|LSCF–SDC. The SDC interlayer was prepared in the same manner of o-interlayer as described in chapter 3. Here, I briefly explain the procedure of o-interlayer. The o-interlayers were prepared on both sides of the YSZ disk by repeated spin-coating of solution of cerium and samarium octoates (Ce: Sm = 8:2, Nihon Kagaku Sangyo Co., LTD, Japan) in toluene and heat-treatment at 300°C several times. The YSZ with SDC interlayers was then heat-treated at 1050°C for 2 h. This protocol was repeated three times to form a dense, thin and uniform SDC interlayer.

The SDC powder was prepared by a solid state reaction of reagent grade oxides (CeO_2, Sm_2O_3). The powder of the raw materials were mixed and calcined at 1300°C

for 10 h. The calcined oxides were finely pulverized and pressure-molded followed by a final sintering at 1650°C for 15 h. After that, the SDC powder was pulverized to an average size of 0.5 μm.

An LSCF–SDC paste (LSCF: SDC = 60: 40vol.%) was prepared from LSCF powder (Praxair Specialty Ceramics Co.; mean diameter d = 0.4 μm), SDC powder, fine polymer beads as a pore-former (polymethyl methacrylate particles, Sekisui Plastics Co. Ltd. ; d=1.5 μm, 60vol.% in the paste) and binder consisting of α-terpineol, by mixing in a mortar and a magnetic stirrer. Onto the SDC interlayer, the composite electrode was prepared by tape-casting the LSCF–SDC paste, followed by sintering at 1050°C for 1 h.

The porosity (p) of LSCF–SDC electrode was calculated by the following equation:

$$p = \frac{V_{pore}}{V_{total}} = 1 - \left(\frac{V_{LSCF-SDC}}{V_{total}}\right) = 1 - \left(\frac{m}{\rho AL}\right) \qquad (1)$$

where V_{pore}, $V_{LSCF\text{-}SDC}$, and V_{total} are the volume of pore, (LSCF+SDC), and total one ($V_{total} = V_{pore} + V_{LSCF\text{-}SDC}$), respectively. The value of $V_{LSCF\text{-}SDC}$ was calculated as m/ρ, in which m is the mass of the electrode and ρ is the density of the LSCF-SDC (6.69 g cm^{-3} at LCSF: SDC = 60:40vol.%). The value of V_{total} was the product of the electrode area (A, 0.28 cm^2) and the thickness L (ca. 30 μm), evaluated by SEM observation of the electrode layer prepared by the same manner. Thus, we obtained the porosity of the electrode to be approximately 60%.

As a Pt/air reference electrode for the symmetrical cell, a Pt wire was wrapped around the periphery of the YSZ disk and fixed with Pt paste. Gold mesh was used as a current collector attached to each LSCF–SDC electrode. Two Au wires for current supply and potential probe were contacted to the gold mesh current collector. Pure O_2 at ambient pressure with a flow rate of 30 cm^3 min^{-1} was supplied to the both electrodes. A measurement construction is shown in Fig. 4-3. The steady-state IR-free polarization characteristics (*I–E* curves) of the LSCF–SDC electrodes were measured by the current-interruption method in a three electrode configuration at the cell temperature T_{cell} = 900°C. Long-term operation of cell was carried out at T_{cell} = 900°C and a constant current density (j) of 0.5 A cm^{-2} with the top electrode as the anode (O_2 evolution). During 5500 h of operation, *I–E* curves and ohmic resistances were measured every 1000 h. Post-test analyses were carried out by using SEM (SU-9000, Hitachi High-Technologies Co. Japan) equipped with an energy-dispersive X-ray spectrometer (EDX, Genesis 4000, CDU detector, Ametek Inc., USA) and X-ray diffraction (XRD, Rigaku Ultima IV, Japan).

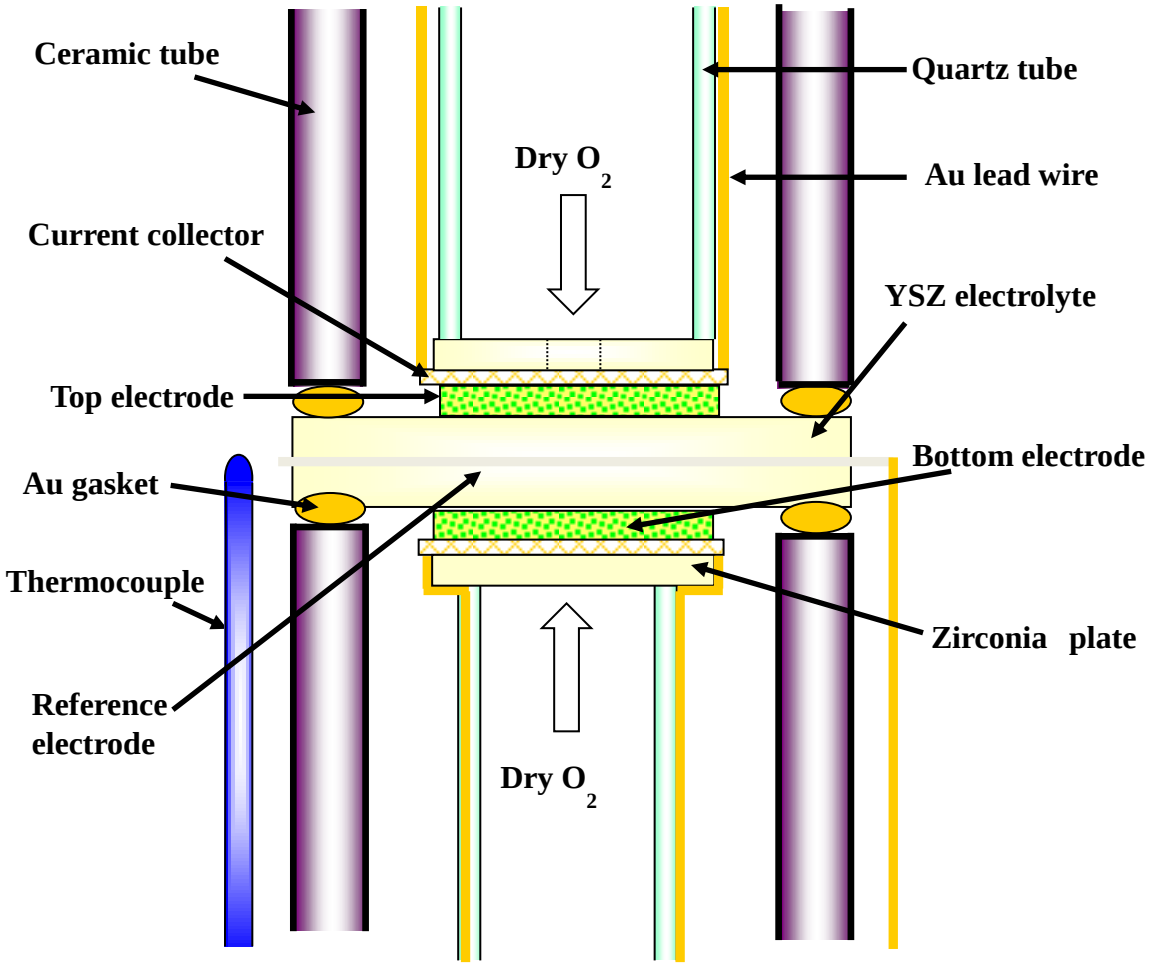

Fig. 4-3. Construction of test cell.

4.3. Results and discussion

4.3.1. Changes in performance of the LSCF–SDC electrode during a long-term operation

Figure 4-4 shows IR-free polarization curves for the pristine LSCF–SDC electrodes at T_{cell} = 900°C. The top and bottom electrodes exhibited very similar initial performances in both the anodic and cathodic reactions. For example, the values of *j* at η = 0.03 V and −0.03 V for both electrodes were −0.64 A cm^{-2} and 0.63 A cm^{-2}, respectively, indicating a good reversible performance. The ohmic resistances of the top electrode (anode) side R_A and the bottom electrode (cathode) side R_C were measured to be 0.61 Ω cm^2 and 0.57 Ω cm^2, respectively.

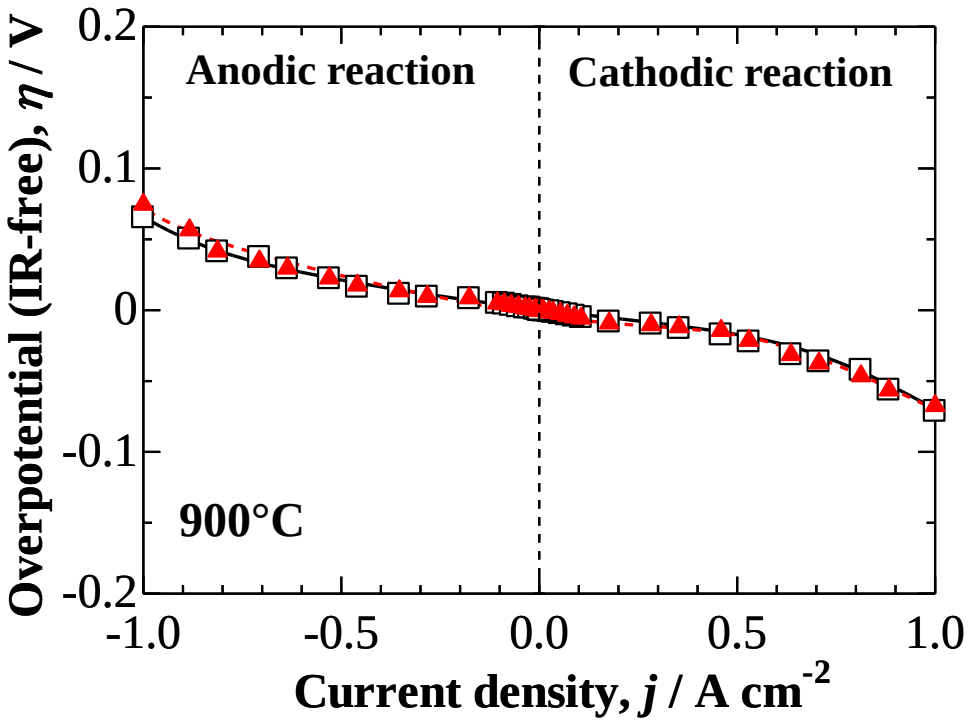

Fig. 4-4. IR-free polarization curves for the pristine LSCF–SDC top electrode (□) and bottom electrode (▲) measured in dry O_2 gas at T_{cell} = 900°C.

Figure 4-5 shows the time course of the anodic overpotential (η_A), cathodic overpotential (η_C), R_A and R_C during the operation at T_{cell} = 900 °C and a constant j = 0.5 A cm^{-2}. It was found that the values of η_A and η_C were virtually constant over the whole operation time of 5500 h. The value of R_A increased slightly, whereas the value of R_C increased somehow markedly. The degradation rate of the R_C was nearly constant (68.6 mΩ cm^2 kh^{-1}) up to 3500 h, and slowed down (30.3 mΩ cm^2 kh^{-1}) from t = 3500 to 5500 h.

In order to examine how the electrode performances changed during operation, IR-free *I–E* curves at both electrodes were measured every 1000 h. As shown in Fig. 4-6, little change in the *I–E* performance of the top electrode (operated as the anode) was observed over the whole current density range examined (from −1.0 to 1.0 A cm^{-2}). For example, the values of j at η = 0.05 V on the top electrode were −0.90 A cm^{-2} at t = 0 and −0.92 A cm^{-2} at t =5500 h, and that at η = −0.05 V little changed from 0.86 A cm^{-2} (t = 0) to 0.82 A cm^{-2} (t = 5500 h). On the other hand, the I–E performance of the bottom electrode (operated as the cathode) degraded specifically at high current densities. The value of j at η = 0.05 V on the bottom electrode decreased from −0.88 A cm^{-2} (t = 0) to −0.58 A cm^{-2} (t = 5500 h), and a similar extent of degradation was observed at η = −0.05 V (from 0.85 to 0.50 A cm^{-2}).

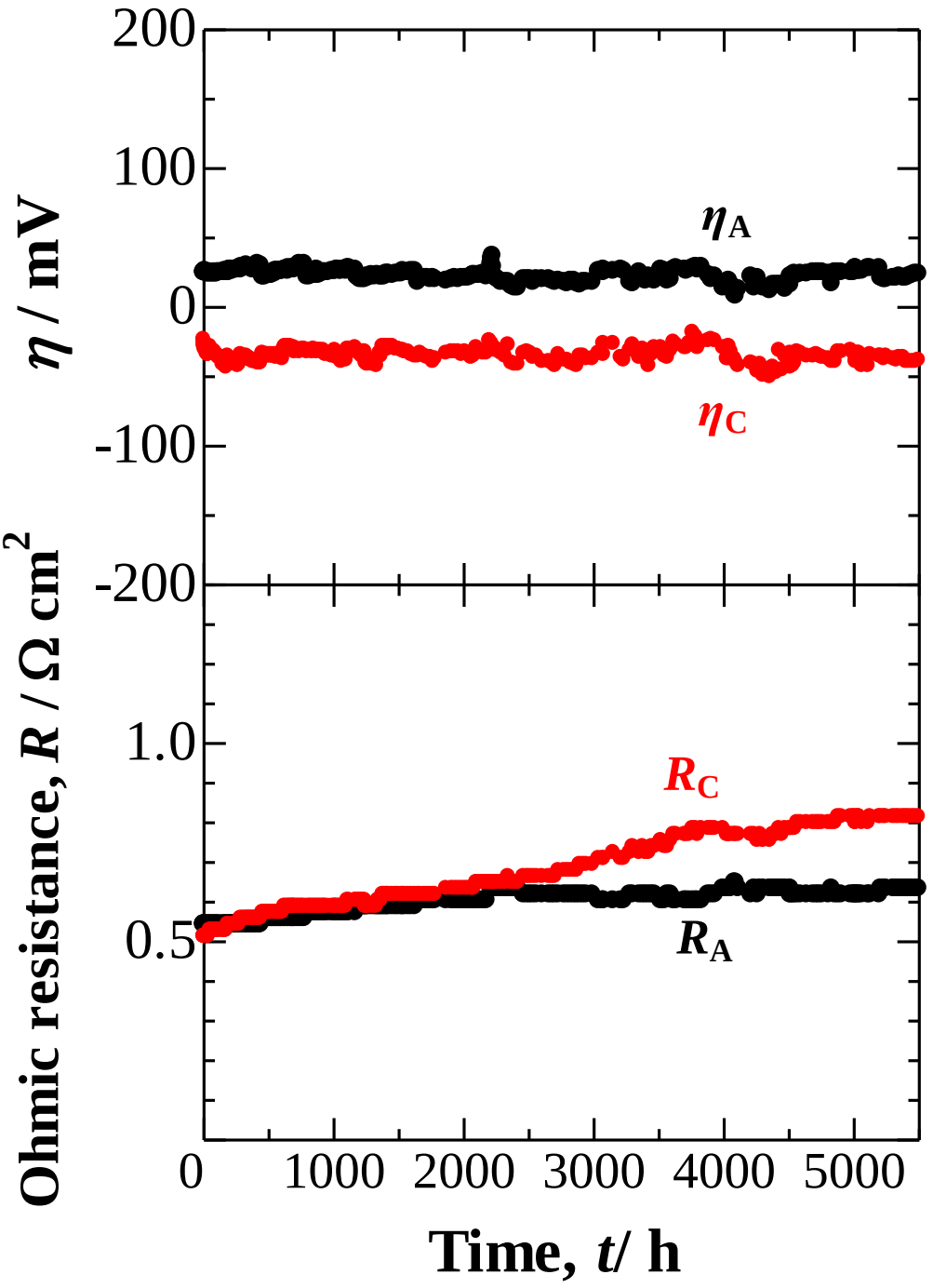

Fig. 4-5. Time course of the anodic overpotential (η_A), cathodic overpotential (η_C), R_A and R_C during the long-term operation at T_{cell} = 900°C and a constant j = 0.5 A cm^{-2}.

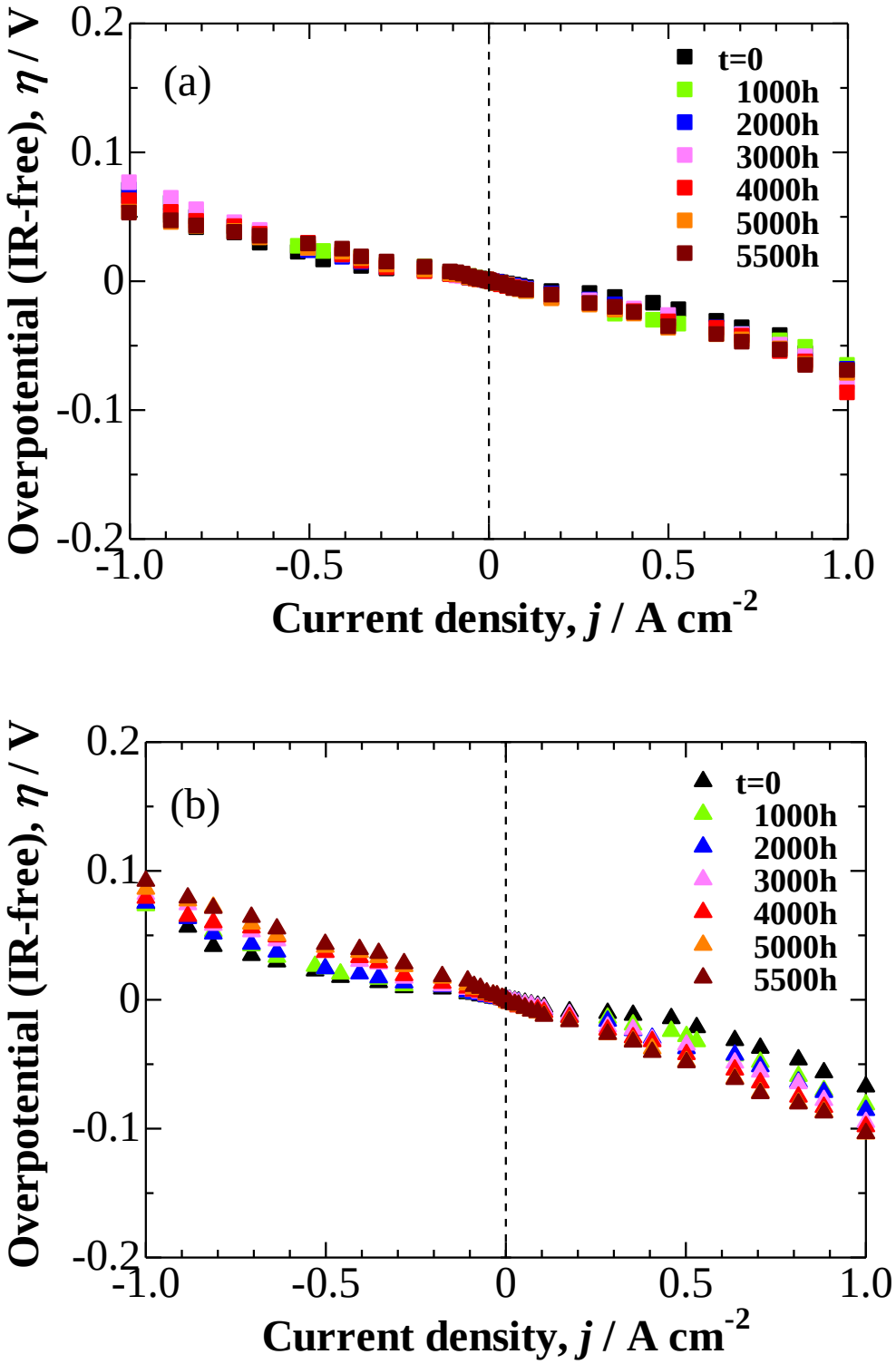

Fig. 4-6. IR-free polarization curves for the LSCF–SDC top electrode (operated as the anode) (a) and bottom electrode (operated as the cathode) (b) measured in dry O_2 gas every 1000 h at T_{cell} = 900°C.

4.3.2. Analyses of degradation of LSCF–SDC electrodes

Figure 4-7 shows XRD patterns of the pristine electrode together with the top electrode and bottom electrode after 5500 h of operation. All the diffraction peaks of the three samples unequivocally corresponded to the LSCF, SDC, and YSZ phases. It has been reported so far that $SrZrO_3$ or $La_2Zr_2O_7$ formed by solid state reaction between YSZ and LSCF after operation at high temperatures [1, 3, 4]. Considering the high temperature of operation and the length of the experiment, even by zooming up the patterns of Fig. 4-7, such a reaction phases or any other unfavorable phases were not detected by the use of XRD.

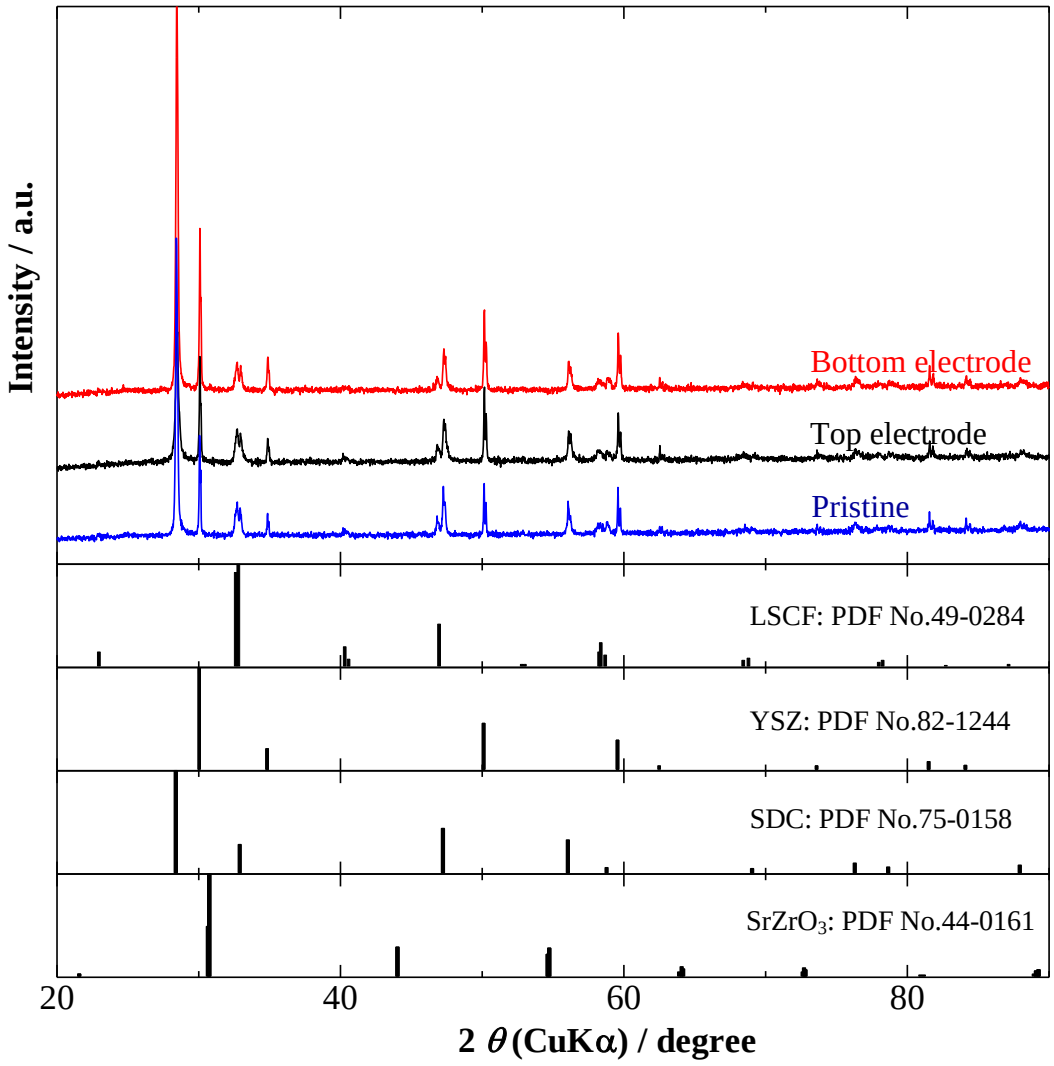

Fig. 4-7. XRD patterns LSCF–SDC electrodes; in pristine condition, top electrode, and bottom electrode after operation for 5500 h at T_{cell} = 900°C.

Next, the microstructures of these electrodes were observed by SEM. Typical images are shown in Fig. 4-8. Figure 4-8(a) corresponds to the typical microstructure of the electrode in the pristine condition while Fig. 4-8(b) and 4-8(c) correspond to the microstructure of electrodes operated for 5500 h. The thickness of all electrodes was nearly identical at ca. 30 μm, irrespective of the anodic or cathodic operations. Micropores of a few μm size were uniformly distributed in all electrodes and the average porosity (based on the mass and the volume of the layer) was calculated to be ca. 60 %. It was also observed that all samples adhered well to the SDC interlayer, i.e., no delamination was observed. Thus, the microstructures, at least in μm-scale, were unchanged in both the top and bottom electrodes at T_{cell} = 900°C operated for 5500 h.

I examined changes in the elemental distribution by EDX at the regions close to the interlayer, with special emphasis to understand mass transport across the LSCF–SDC electrode/SDC interlayer and SDC interlayer/YSZ electrolyte interfaces (Fig. 4-9 and Fig. 4-10). For the pristine electrode (sintered at 1050°C for 1 h), uniform distribution of representative elements such as Sr and Fe was observed only in the LSCF–SDC composite electrode layer, i.e., negligible diffusion of Sr and Fe components into the SDC interlayer or YSZ electrolyte during fabrication. This situation is very different from those reported so far, in which Sr component already diffused into ceria-based interlayer, probably due to higher fabrication temperatures [3].

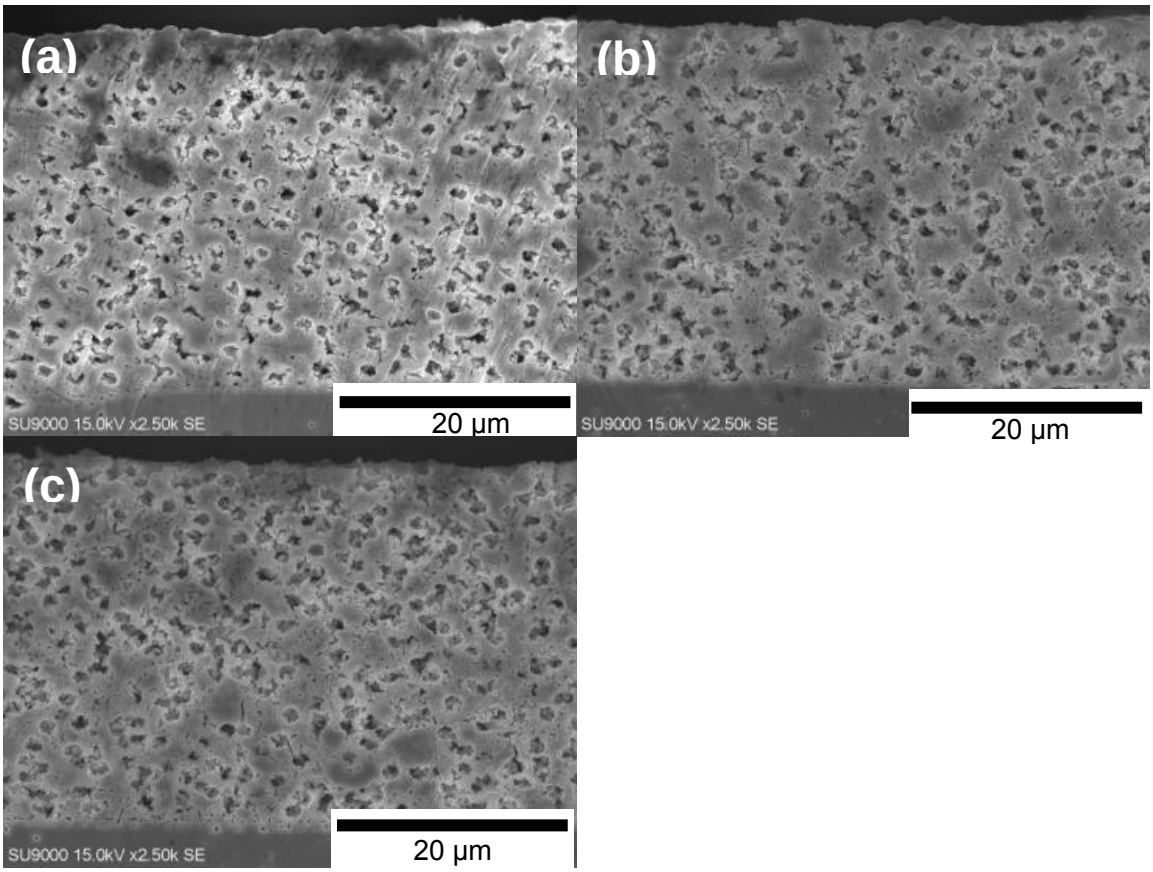

Fig. 4-7. Cross-sectional SEM images of LSCF–SDC electrode; in pristine condition (a) and after operation for 5500 h, (b) top electrode, (c) bottom electrode.

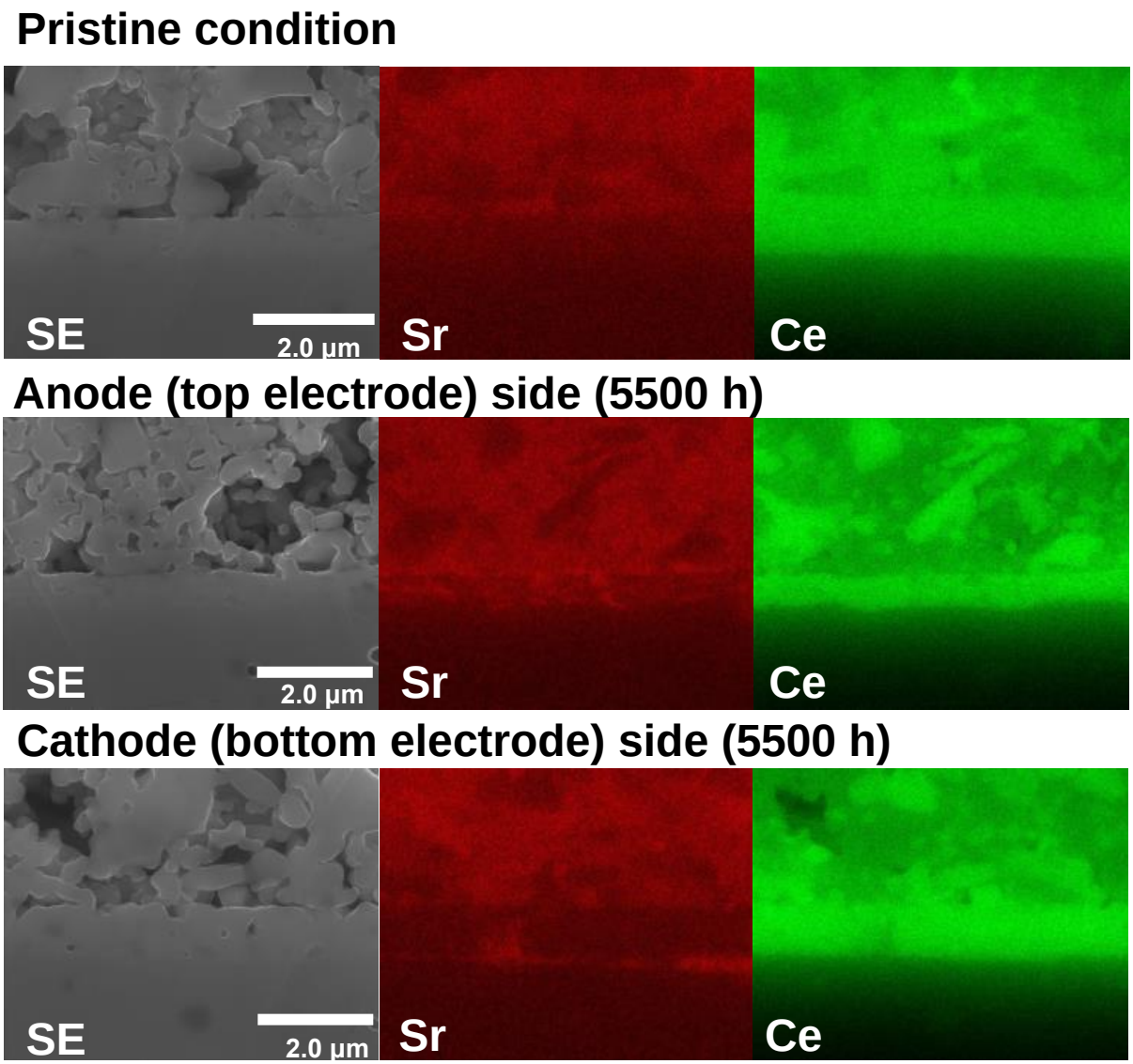

Fig. 4-9. SEM images (SE) and elemental distributions of Sr, and Ce for a cross-section of the LSCF–SDC/SDC interlayer/YSZ region.

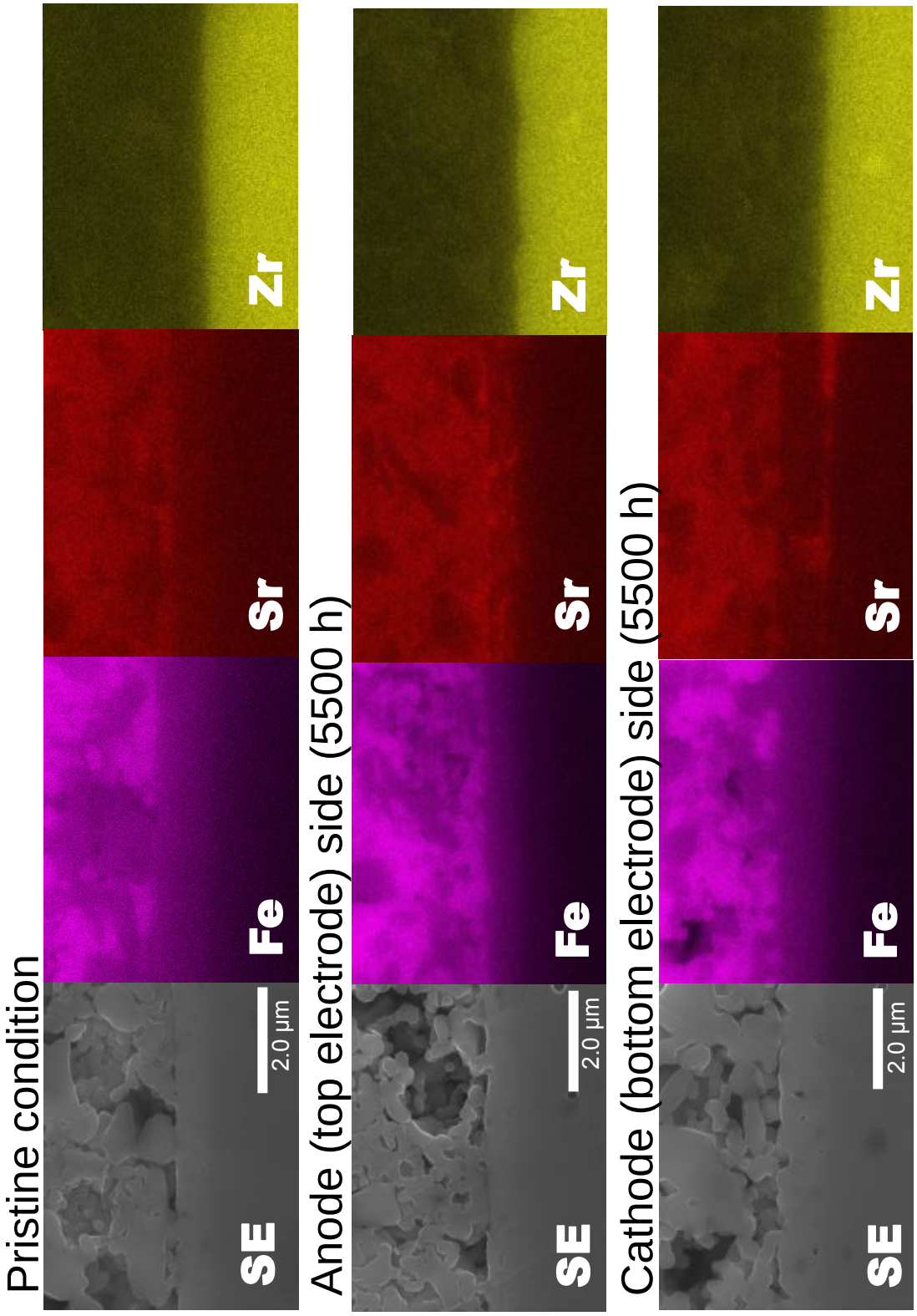

Fig. 4-10. SEM images (SE) and elemental distributions of Fe, Sr and Zr for a cross-section of the LSCF–SDC/SDC interlayer/YSZ region.

Depending upon the anodic and cathodic polarization for 5500 h, the distribution of Sr component was found to change markedly. For the anode side, the Sr component penetrated across and along the SDC interlayer. A layer-like distribution of Sr in the interlayer could be ascribed to a rapid diffusion along the sub-layer of the SDC (layer-by-layer sintering, as described in the experimental section). However, more importantly, the presence of Sr was limited within the interlayer. In contrast, for the cathode side, the Sr component reached the interface between SDC interlayer and YSZ electrolyte. Fig. 4-11 shows EDX analysis of the SDC interlayer/YSZ interface near large void. The concentration of Sr was much larger close to a large void of the SDC interlayer. This suggests that the Sr component could be enriched in the dip or void of SDC interlayer, followed by the rapid diffusion along the SDC interlayer/YSZ interface.

In order to examine the elemental distribution of Sr, Ce, and Zr at the LSCF–SDC electrode/SDC interlayer/YSZ electrolyte interface in detail, we carried out EDX line analysis. Two line profiles are shown for each electrode in Fig. 4-12, where the signal intensity of Sr is magnified by 10 times.

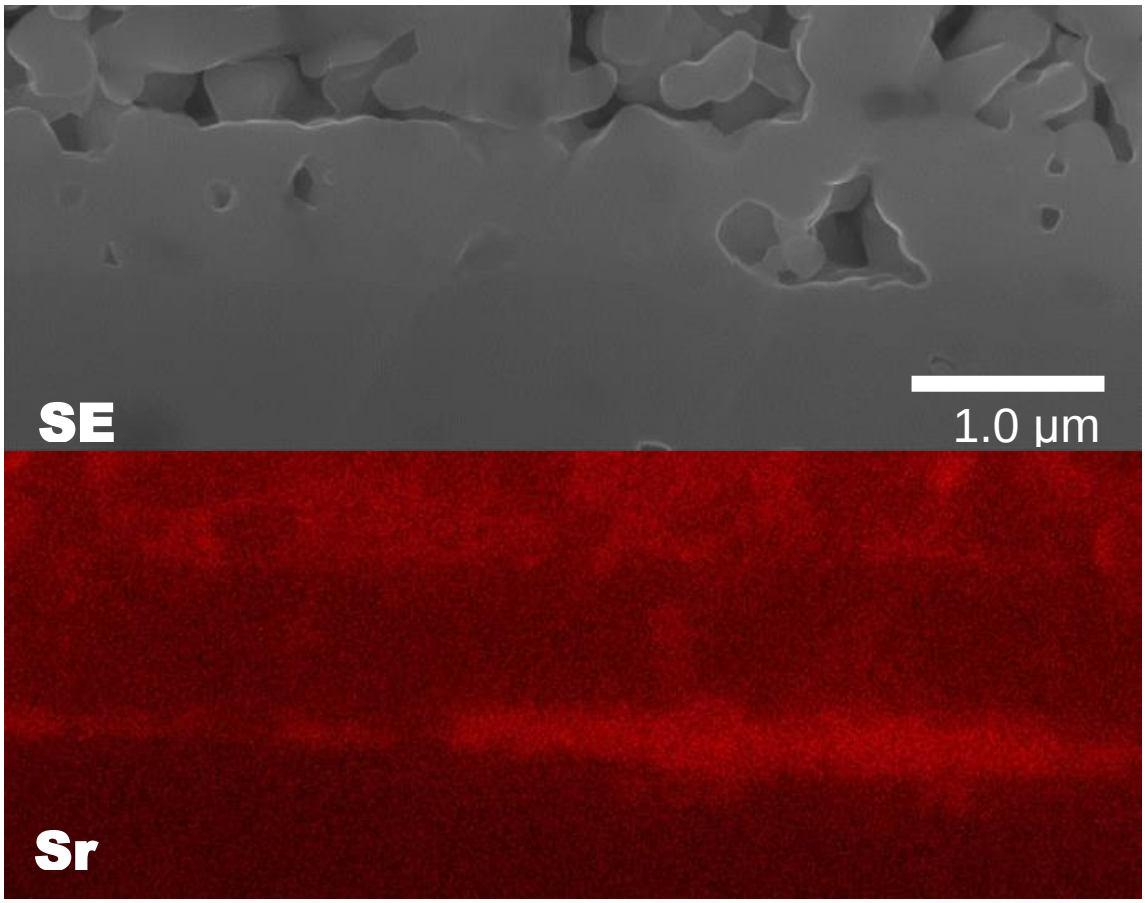

Fig. 4-11. SEM images (SE) and elemental distributions of Sr for a cross-section of the LSCF–SDC/SDC interlayer/YSZ region after the cathodic operation for 5500 h.

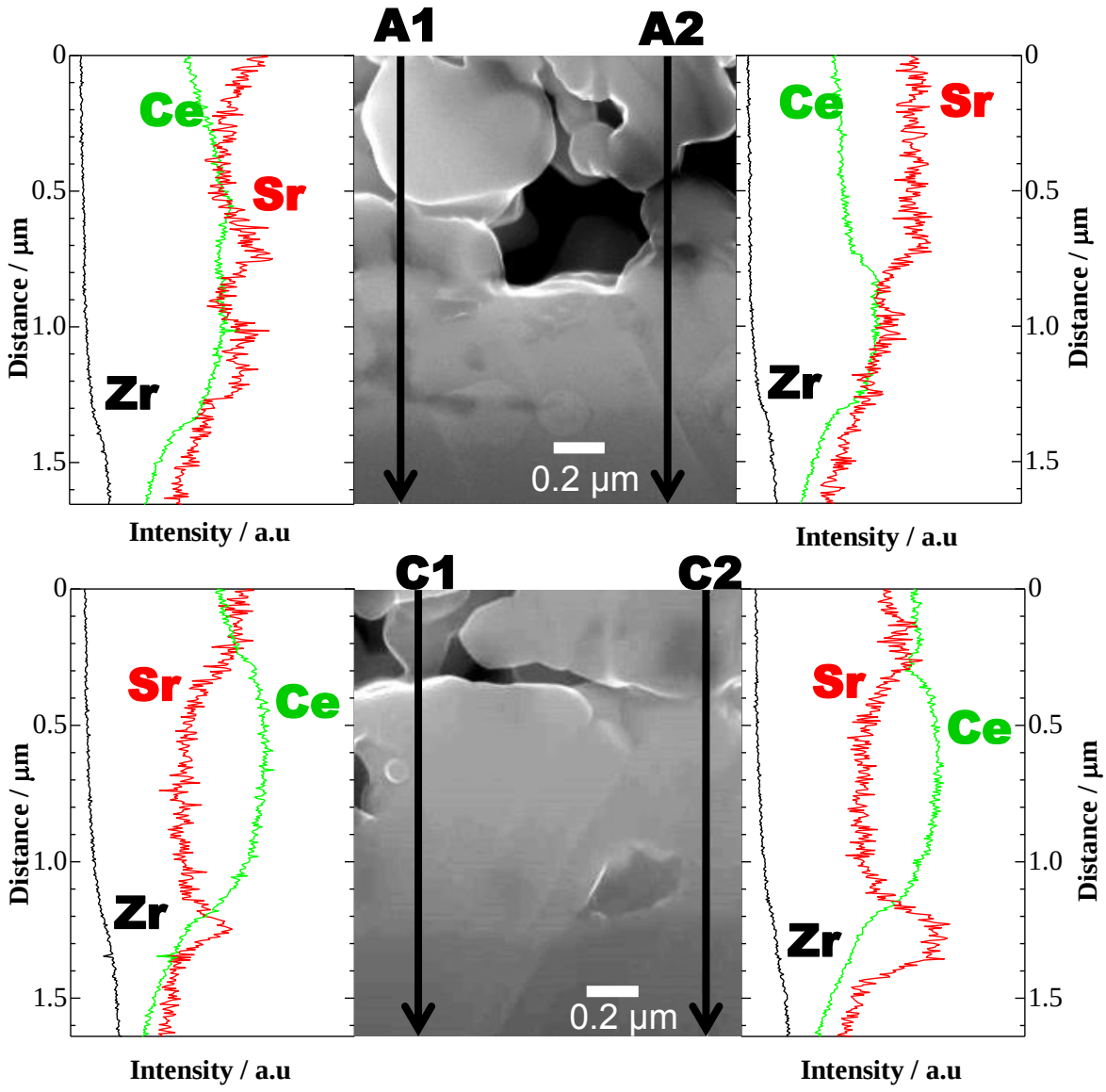

Fig. 4-12. SEM images and elemental distributions of Sr, Ce and Zr obtained by EDX line scan analysis of the LSCF–SDC/SDC interlayer/YSZ region after anodic operation and cathodic operation. The line scan was performed among A1, A2, C1, and C2.

After the anodic operation, the Sr component penetrated into the SDC interlayer, due to diffusion (by a simple concentration gradient) and an ionic migration of Sr cation moves in the direction of the applied electric field from the anode to the cathode. Along line A1, some humps in the Sr intensity were observed. Along line A2, however, the concentration of Sr decreased nearly linearly with increasing the distance from the LSCF–SDC/SDC interface. It was found that such a specific enrichment in Sr dominantly occurred at grain boundaries or voids in the SDC interlayer. This is consistent with the report that Sr component diffused dominantly via grain boundaries [2]. It has been reported for LSCF anode operated in SOEC that the performance degradation was ascribed to an increase in the ohmic resistance due to a formation of $SrZrO_3$ at YSZ interface and delamination of the electrode [5-7]. As described in the previous section, because the performance of the anode (top electrode) was nearly unchanged and the increase in the ohmic resistance R_A was very small (see Fig. 4-5), the present SDC interlayer acted as an effective barrier against the diffusion of Sr component, at least for 5500 h at 900°C.

In contrast, after the cathodic operation, the Sr enrichment was observed along the SDC interlayer/YSZ interface. The concentration of Sr was much larger close to a dip (or void) of the SDC interlayer (line C2) than that observed along line C1. This suggests that the Sr component could be enriched in the dip or void of SDC interlayer, followed by the rapid diffusion along the SDC interlayer/YSZ interface. Therefore, a significant increase in the R_C shown in Fig. 4-5 is reasonably explained by the formation of $SrZrO_3$. It has been reported that the diffusion of Sr from LSCF was

triggered by a partial decomposition of LSCF at low oxygen partial pressure caused by the cathodic polarization in an SOFC mode [8]. Wang et al. reported a segregation of Zr component to form $SrZrO_3$ at LSCF/GDC interface when the cell was prepared at high temperatures (1200°C) [2]. In the present work, however, such a diffusion of Zr component was not observed for neither the anode nor the cathode, probably due to a slower Zr diffusion at 900°C.

Here, it is recognized that the degradation of the LSCF–SDC/SDC interlayer/YSZ electrolyte in the cathode operation was more serious than in the case of the anode operation. However, as shown in Fig. 4-9 and Fig. 4-12, even for the cathode operation, the diffusion of Sr into YSZ was mitigated by dense portions of the SDC interlayer. Similar phenomenon was observed for the anode side. Hence, it is very essential to prepare uniform and dense SDC interlayer to improve the durability of the R-SOC.

4.4. Conclusions

By the use of a symmetrical cell: LSCF–SDC|SDC interlayer|YSZ |SDC interlayer|LSCF–SDC with well-defined elemental distribution (without any interdiffusion of Sr, Fe, Ce, and Zr), I have examined the durability of LSCF–SDC composite oxygen electrodes with SDC interlayers under the anodic and cathodic operation of constant j = 0.5 A cm^{-2} and 900°C. During 5500 h of operation, the most marked change was an increase in the ohmic resistance of the cathode side (R_C), while the IR-free overpotentials at the anode and cathode and the ohmic resistance of the

anode side were nearly constant. By post-test analyses, the thickness, pore size, and porosity of both electrodes, as well as their good adhesion to the interlayers, were unchanged, irrespective of the anodic and cathodic polarizations. However, changes in the distribution profile of Sr component at the LSCF–SDC/SDC interlayer/YSZ region were found to depend on the polarization. The diffusion of Sr component at the anode side was effectively suppressed within the SDC interlayer. In contrast, the Sr component from the cathode reached the YSZ surface just below the SDC interlayer, where the Sr concentration was appreciably in the vicinity of defects (dips or voids) of the SDC interlayer. It was suggested that a rapid diffusion of Sr over YSZ surface could form $SrZrO_3$, leading to the increase in R_C. However, such diffusion rates of Sr at both the anode and cathode side were found to be mitigated at dense portions of the SDC interlayer. Hence, the formation of uniform and dense SDC interlayer and the decrease in the sintering temperature of all components are very important to obtain high durability with high performance in the R–SOCs.

4.5. References

[1] T. Matsui, M. Komoto, H. Muroyama, K. Kishida, H. Inui and K. Eguchi, Degradation factors in (La, Sr)(Co, Fe)$O_{3-\delta}$ cathode/Sm_2O_3–CeO_2 interlayer/Y_2O_3–ZrO_2 electrolyte system during operation of solid oxide fuel cells, .J. Power Sources, 312 (2016) 80-85.

[2] F. Wang, M. E. Brito, K. Yamaji, D. -H. Cho, M. Nishi, H. Kishimoto, T. Horita, H. Yokokawa, Effect of polarization on Sr and Zr diffusion behavior in LSCF/GDC/YSZ system, Solid State Ionics, 262 (2014) 454-459.

[3] R. Kiebach, W. -W. Zhang, W. Zhang, M. Chen, K. Norrman, H. -J. Wang, J. R. Bowen, R. Barfod, P. V. Hendriksen, Stability of $La_{0.6}Sr_{0.4}Co_{0.2}Fe_{0.8}O_3$/$Ce_{0.9}Gd_{0.1}O_2$ cathodes during sintering and solid oxide fuel cell operation, J. Power Sources, 283 (2015) 151-161.

[4] M. Z. Khan, M. T. Mehran, R. -H. Song, J. -W. Lee, S. -B. Lee, T. -H. Lim, S. -J. Park, Effect of GDC interlayer thickness on durability of solid oxide fuel cell cathode, Ceramics International, 42 (2016) 6978-6984.

[5] A. V. Virkar, Mechanism of oxygen electrode delamination in solid oxide electrolyzer cells, Int. J. Hydrogen Energy, 35 (2010) 9527-9543.

[6] K. Chen and S. P. Jiang, Failure mechanism of (La, Sr) MnO_3 oxygen electrodes of solid oxide electrolysis cells, Int. J. Hydrogen Energy, 36 (2011) 10541-10549.

[7] F. Tietz, D. Sebold, A. Brisse and J. Schefold, Degradation phenomena in a solid oxide electrolysis cell after 9000 h of operation, J. Power Sources, 223 (2013) 129-135.

[8] S. Hashimoto, Y. Fukuda, M. Kuhn, K. Sato, K. Yashiro, J. Mizusaki, Oxygen nonstoichiometry and thermo-chemical stability of $La_{0.6}Sr_{0.4}Co_{1-y}Fe_yO_{3-\delta}$ (y= 0.2, 0.4, 0.6, 0.8), Solid State Ionics, 181 (2010) 1713-1719.

[9] K. Shimura, H. Nishino, K. Kakinuma, M. E. Brito and H. Uchida, Effect of samaria-doped ceria (SDC) interlayer on the performance of $La_{0.6}Sr_{0.4}Co_{0.2}Fe_{0.8}O_{3-\delta}$/SDC composite oxygen electrode for reversible solid oxide fuel cells, Electrochim. Acta, accepted for publication.

Chapter 5

Effect of samaria-doped ceria (SDC) interlayer on the performance of LSCF/SDC composite oxygen electrode for reversible solid oxide fuel cells

5.1. Introduction

The influence of the interlayer on performance is not well investigated. In recent research, it has been reported that the interlayer may have an effect on performance [5, 6]. However, Ramasamy et al. reported that higher performance was obtained by using Pr-doped ceria (PDC) interlayer compared with Gd-doped ceria (GDC) interlayer under both SOFC and SOEC conditions [5]. This was specifically ascribed to the use of electron-ion mixed conductor for the interlayer. On the other hand, Jordan et al. also reported a comparison of electrode performance for LSCF electrode with GDC interlayer prepared by both screen-printing method and magnetron sputtering method. The evaluation was done only for the SOFC condition and they reported an improvement in performance by the use of GDC interlayer prepared by magnetron sputtering method [6]. However, the authors did not discuss the reason beyond its effectiveness as a diffusion barrier. In addition, it is costly and difficult to industrially produce GDC interlayers by magnetron sputtering method. I succeeded in producing a dense, thin and uniform SDC interlayer using a spin-coating of Ce and Sm octoate solution, followed by sintering at relatively low temperature (1050°C), that is a readily scalable method in chapter 3 and this interlayer exhibited that long-term durability test of 5500 h at 0.5 A cm^{-2} at 900°C under anodic and cathodic operation in chapter 4.

In the previous studies, there are papers investigating the influence on the performance of the interlayer. However, there is no paper which examined the influence of the quality of the interlayer on the performance by using the interlayer having the same composition in both the anodic and the cathodic polarization.

Therefore in this chapter, I report, the effect of the SDC interlayer (with the identical composition) on the polarization performance of LSCF–SDC composite oxygen electrodes for R-SOC at 900 and 800°C. I also discuss the essential role of a dense SDC interlayer with uniform thickness in improving the performance of the oxygen electrode.

5.2. Experimental

A symmetrical cell LSCF–SDC|SDC interlayer|YSZ|SDC interlayer|LSCF–SDC was prepared in the same manner as described in chapter 3. Here, I briefly explain the procedure. The o-interlayers were prepared on both sides of the YSZ disk by repeated spin-coating of solution of cerium and samarium octoates (Ce: Sm = 8:2, Nihon Kagaku Sangyo Co., LTD, Japan) in toluene and heat-treatment at 300 °C several times. The YSZ with SDC interlayers was then heat-treated at 1050°C for 2 h. This protocol was repeated three times to form dense SDC interlayer. And the n-interlayer was prepared by screen-printing a mixed solution of cerium and samarium nitrates with a thickener, followed by heat-treatment at 400°C [7]. The screen-printing and the heat-treatment were repeated several times, and finally the interlayer was sintered at 1150°C for 4 h. Porous LSCF–SDC composite electrode (40vol% SDC) was

prepared by tape-casting an LSCF–SDC paste onto each SDC interlayer, followed by sintering at 1050°C for 1 h. The porosity (p) of LSCF–SDC electrode was calculated by the same equation in Chapter 4. The morphology of these electrodes was observed by scanning electron microscopy (SEM, S-5200 and SU-9000, Hitachi High-Technologies Co. Japan) equipped with an energy-dispersive X-ray spectrometer (EDX, Genesis 4000, CDU detector, Ametek Inc., USA). As a Pt/air reference electrode for the symmetrical cell, a Pt wire was wrapped around the periphery of the YSZ disk and fixed with Pt paste. Gold mesh was used as a current collector attached to each LSCF–SDC electrode. Two Au wires for current supply and potential probe were contacted to the gold mesh current collector. Pure O_2 at ambient pressure with a flow rate of 30 cm^3 min^{-1} was supplied to the both electrodes. The steady-state IR-free polarization characteristics of the LSCF–SDC electrodes were measured by the current-interruption method in a three electrode configuration at the cell temperature T_{cell} of 800 and 900°C.

5.3. Results and discussion

5.3.1. Electrochemical performance of LSCF–SDC electrodes with o-interlayer and n-interlayer

Figure 5-1 shows IR-free anodic and cathodic polarization curves for LSCF–SDC oxygen electrodes, prepared on the o-interlayer and n-interlayer, at T_{cell} = 800 and 900°C. The ohmic resistances of the cell with o-interlayer were 1.05 Ω cm^2 and 2.14 Ω cm^2 at 900 and 800°C, respectively. Similar values of 1.06 Ω cm^2 and 2.06 Ω cm^2 were

obtained for the cell with the n-interlayer. Thus, the ohmic resistances of the cells with o-interlayer and n-interlayer were comparable at 900 and 800°C. This result indicates a good reproducibility of the cell test procedure we have adopted. At T_{cell} = 900°C, the LSCF–SDC electrodes with the o-interlayer and n-interlayer exhibited similar performance in both the anodic and cathodic reactions. With lowering T_{cell} to 800°C, the LSCF–SDC electrode with the o-interlayer was found to exhibit a higher performance than that with the n-interlayer. For example, at the IR-free overpotential $|\eta|$ = 0.05 V and 800°C, the anodic and cathodic current densities (j) at the electrode with the o-interlayer were about two times larger than those with the n-interlayer. Then, we shall discuss the differences in performances of two electrodes in detail.

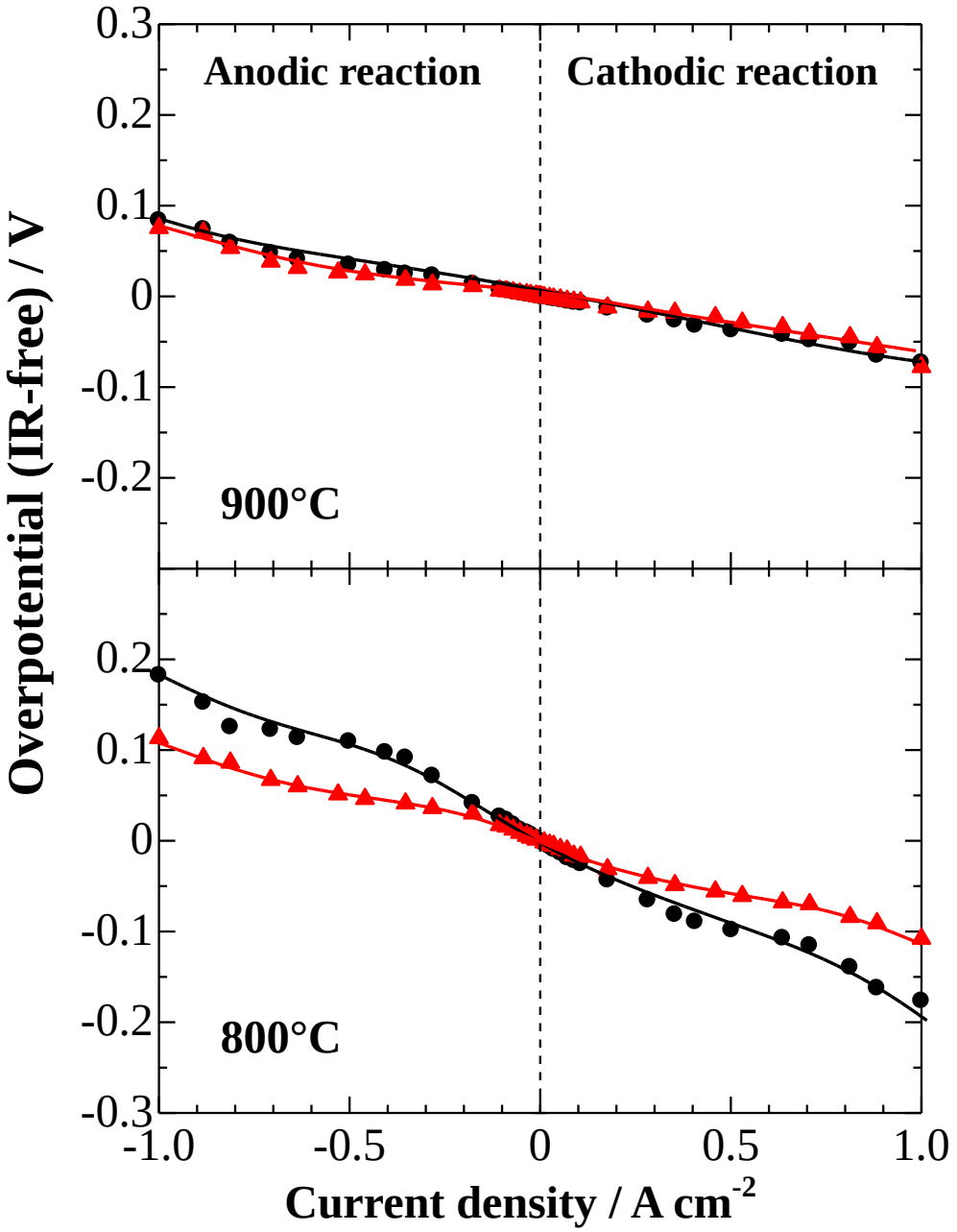

Fig. 5-1. IR-free polarization curves of LSCF–SDC electrodes on o-interlayer (▲) and n-interlayer (●) measured in dry O2 gas at T_{cell} = 900 and 800°C.

First, as a measure of the electrocatalytic activity, the exchange current density j_0 was calculated from the polarization resistance Rp (= dη/dj) at sufficiently low η. Since good linear relationships were observed between η and j for |η|< 0.01 V at T_{cell} = 800°C, we calculate the j_0 using the following equation,

$$j_0 = \left(\frac{RT}{nF}\right) \times R_p^{-1} \qquad (1)$$

where R, T, and F have their usual meanings and n is the number of electrons transferred in the reaction. Considering the electrode reaction of eq. (2), n is assumed to be 2.

$$\tfrac{1}{2}\, O_2(g) + 2\, e^- \leftrightarrows O^{2-} \qquad (2)$$

The value of j_0 thus calculated for the electrode with the o-interlayer was 0.28 A cm^{-2}, which is 1.5 times larger than that with the n-interlayer (0.17 A cm^{-2}). The reason for this will be discussed later on.

5.3.2. Microstructure of LSCF–SDC electrodes with n-interlayer and o-interlayer

Figure 5-2 shows cross-sectional SEM images of LSCF–SDC electrodes prepared on the n-interlayer and o-interlayer. Irrespective of the interlayer employed, the thickness of each LSCF–SDC electrode was nearly identical at ca. 30 μm. Micropores of a few μm in size were uniformly distributed in both electrodes and the average porosity based on the mass and the volume of the layer was calculated to be ca. 60%. As seen in the distribution maps of Fe and Ce (Fig. 5-3), fine particulates of LSCF and larger particles of SDC were uniformly distributed in both electrodes. However,

focusing at the electrode-electrolyte interface region, I have found that o-interlayer and n-interlayer showed different features.

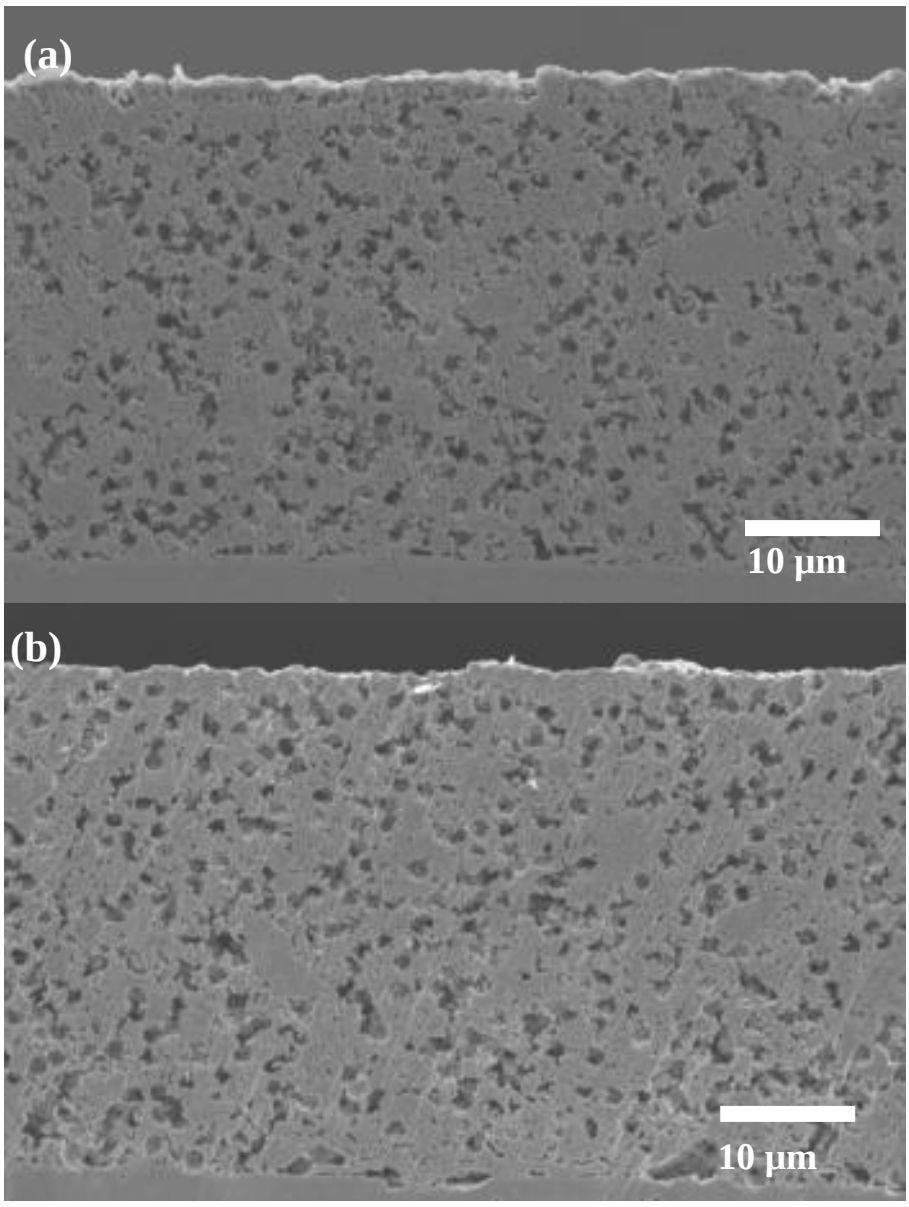

Fig. 5-2. SEM cross-section images of the LSCF–SDC electrodes prepared on (a) o-interlayer and (b) n-interlayer.

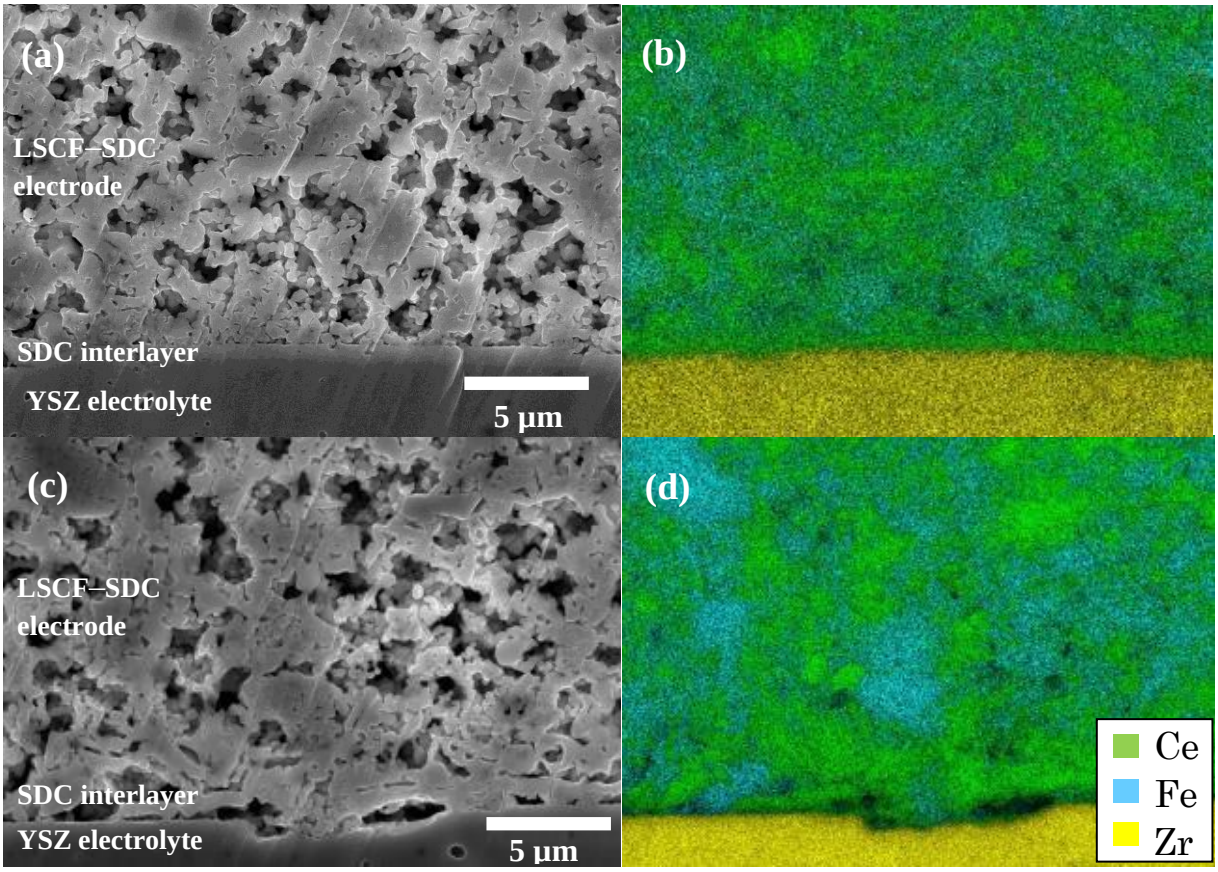

Fig. 5-3. SEM images and elemental distribution maps of Zr, Ce and Fe for a cross-section of the LSCF–SDC electrodes prepared on o-interlayer [(a) and (b)] and n-interlayer [(c) and (d)].

The SEM-EDX analysis of the electrolyte-electrode interface region is shown in Fig. 5-4. The o-interlayer was more uniform in thickness of ca. 1.0 μm and adhered better to the YSZ electrolyte surface, compared with the n-interlayer with thickness ranging from 1.0 to 3.0 μm. Other features of the n-interlayer are the presence of micro-cracks in very thin parts and partial delamination from the YSZ. I consider that the difference in the smoothness of the interlayer surface arise from the difference in the preparation method of these interlayers and from the differences in the precursors used for the SDC. I employed the screen-printing method to produce the n-interlayer. This method is inherently prone to introduce inhomogeneities and defects because, in our case, it is hand operated. On the other hand, the o-interlayer was produced by the automated spin-coating method to provide a stable and uniform coating on the substrate. In addition, as the precursor of SDC, a mixed solution of Ce and Sm octoates in toluene solvent was used because the use of metal octoates as precursors has successfully been applied to prepare dense, thin oxide films [8, 9]. Nevertheless, it has to be noted that the LSCF–SDC electrode with the SDC interlayer prepared in similar manner as n-interlayer was successfully operated for 5000 h at 0.5 A cm^{-2} at 900°C [7], suggesting a suppression of unfavorable solid-state reactions between LSCF and YSZ at that time. As for the present work, anyhow, it is evident that the microstructures of the o-interlayer and n-interlayer were quite different in terms of the uniformity and adhesion, and that I took specific interest in reproducing the microstructures of the LSCF–SDC composite electrode layers in order to evaluate the effect of the interlayer on the electrode performance.

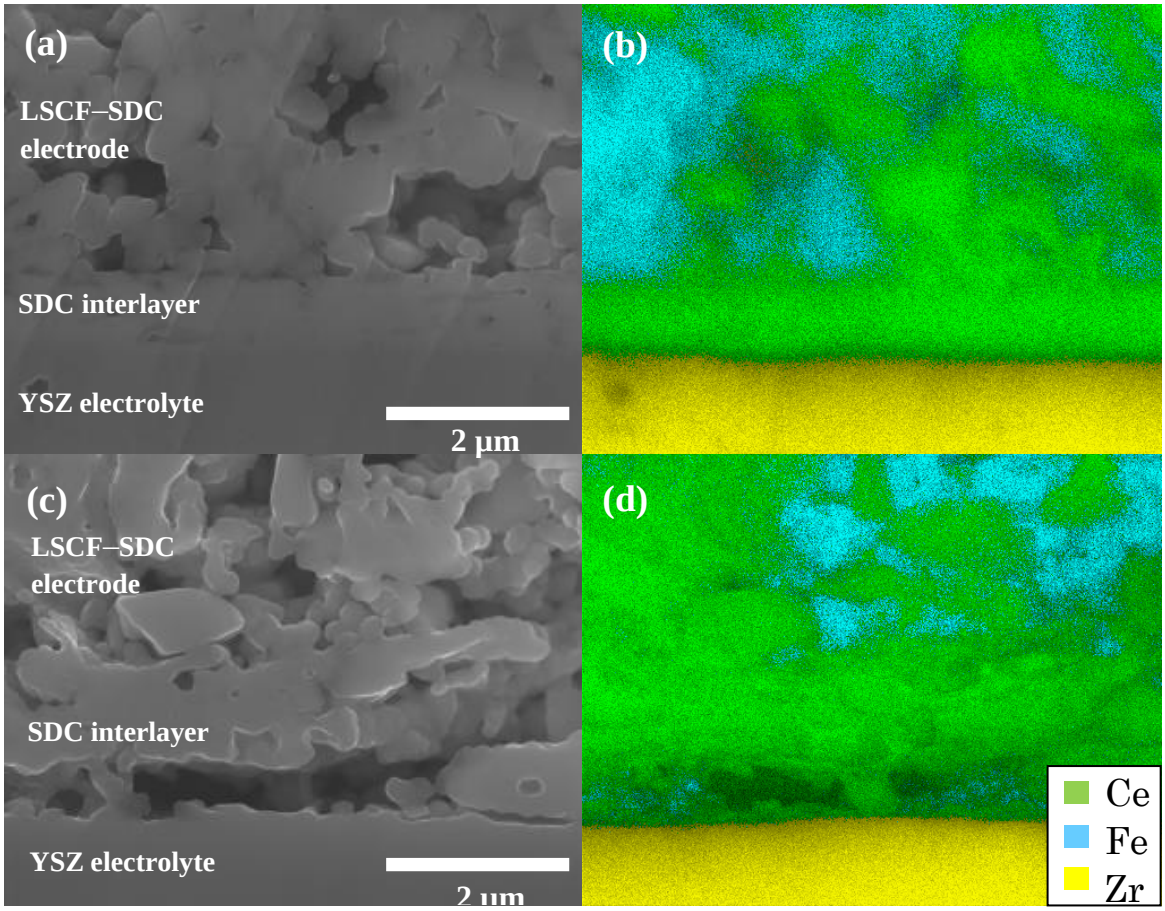

Fig. 5-4. SEM images and elemental distribution maps of Zr, Ce and Fe for a cross-section of the LSCF–SDC/ SDC interlayer/ YSZ region, o-interlayer [(a) and (b)] and n-interlayer [(c) and (d)].

5.3.3. Effect of microstructure of SDC interlayer on the electrode performance

Here, I discuss how the microstructure of SDC interlayer affected the electrode performance. Based on the morphologies observed in Figs. 5-2, 5-3 and 5-4, the oxygen evolution reaction (OER) at the LSCF–SDC electrodes with two kinds of SDC interlayers is schematically drawn in Fig. 5-5. The YSZ electrolyte surface was entirely covered by the o-interlayer of uniform thickness (Fig. 5-3, 5-4). In this case, it is expected that oxide ions would be smoothly supplied through the SDC interlayer, resulting in enlarged ERZ in the LSCF–SDC composite electrode. In contrast, as illustrated in Fig. 5-5 (b), the ionic transport rate could be slowed down at thick portions or even interrupted at detached portions of the n-interlayer, resulting in the decrease in the ERZ compared with the case of Fig. 5-5 (a).

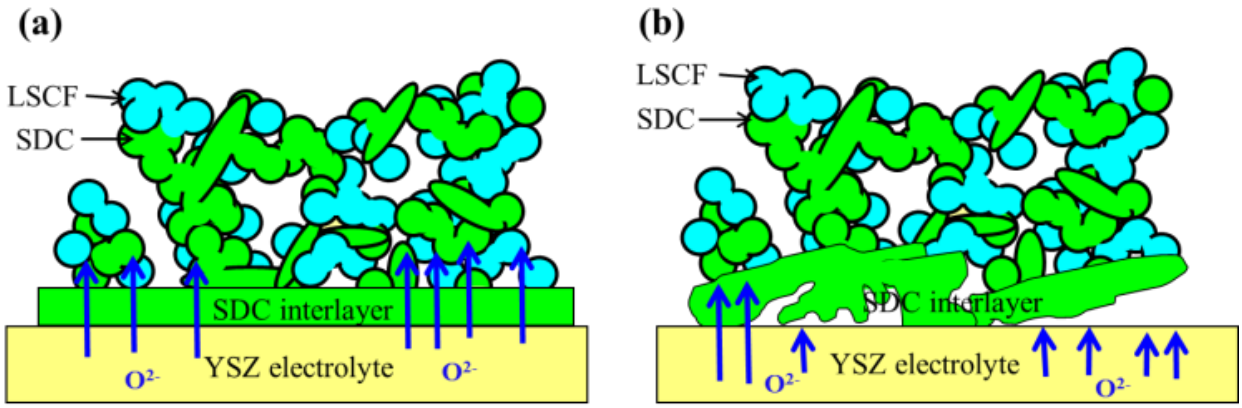

Fig. 5-5. Schematic illustration of the effects of uniformity of SDC interlayer: (a) o-interlayer, (b) n-interlayer.

A similar situation is envisioned for the oxygen reduction reaction (ORR): transport of oxide ions from the LSCF–SDC to YSZ through the interlayer could be enhanced when a high quality interlayer is used. In the high current density range, the cell performance significantly decreased due to non-uniform distribution of the current. It is noteworthy in Fig. 5-1 that the performance of both electrodes was comparable at 900°C and the electrode with the n-interlayer exhibited an inferior performance at 800°C. This is reasonably explained by the temperature-dependence of the ionic conductivity of SDC. The oxide ion conductivity of SDC was reported to be as high as 0.17 S cm^{-1} at 900°C, but it decreased to about half (0.09 S cm^{-1}) at 800°C [10]. Even if the ionic conductance of some fraction of n-interlayer were only one half of the uniform o-interlayer, such a conductance at 900°C of the n-interlayer could be comparable to that of the o-interlayer at 800°C, in which the oxide ion transport rate could not be the major factor in determining the electrode performance even at current densities as high as 1 A cm^{-2}.

As described above, the usual role of the GDC or SDC interlayer, so far, has been the suppression of unfavorable solid-state reaction between various oxide electrodes and zirconia electrolyte [3, 4, 11-13]. However, when the cell was fabricated at high temperatures (typically, ≥ 1150°C), the Sr component already diffused into ceria-based interlayer [4]. On this regard and very recently, the polarization resistance of $La_2NiO_{4+\delta}$|GDC interlayer|zirconia was found to depend on the sintering temperature of GDC, T_{GDC} [14]. An optimum T_{GDC} was defined by the authors as a balance between an increase in σ_{ion} of the GDC layer (by densification at high T_{GDC})

and a decrease in σ_{ion} by the inter-diffusion of cations at GDC/zirconia and LNO/GDC interfaces [14]. However, because the present LSCF–SDC composite electrode was sintered on the SDC interlayer at 1050°C for 1 h, the diffusion of Fe, Zr (Fig. 4), and Sr [15] was found to be negligible. Ramasamy et al. reported for Nd_2NiO_4 electrode that the use of Pr-doped ceria (PDC) interlayer decreased the polarization resistance, compared with GDC interlayer, which was ascribed to a mixed conduction in PDC to enhance the ERZ [1]. Jordan et al. reported that the microstructure of a GDC interlayer positively affected the electrochemical performance of the LSCF electrode at SOFC condition [2]. In contrast, the present work demonstrates that the microstructure (dense and uniformity in thickness), that is nearly pure ionic conductor in O_2 atmosphere and with negligible cation inter-diffusion between SDC interlayer and YSZ electrolyte, plays an important role in enhancing the electrode performance specifically at low operation temperatures for both mode operations, SOFC and SOEC.

I have carried out further experiments in order to confirm such an effect of SDC interlayer on the performance of LSCF–SDC electrode. Considering the essential factors of the uniformity and dense character of the SDC interlayer, I have prepared the LSCF–SDC electrodes directly on both faces of a sintered SDC disk electrolyte. Before coating the electrodes, the surface of the SDC electrolyte disk was polished so that the surface roughness was nearly identical with that of the o-interlayer as shown in Fig. 5-6. However, a careful SEM observation at high magnification indicated that the mechanical polishing provided better flatness in the case of the SDC disk. The thickness and the porosity of the LSCF–SDC prepared on the SDC disk electrolyte

were controlled to be identical with that prepared on the o-interlayer/YSZ electrolyte (see Fig. 5-7).

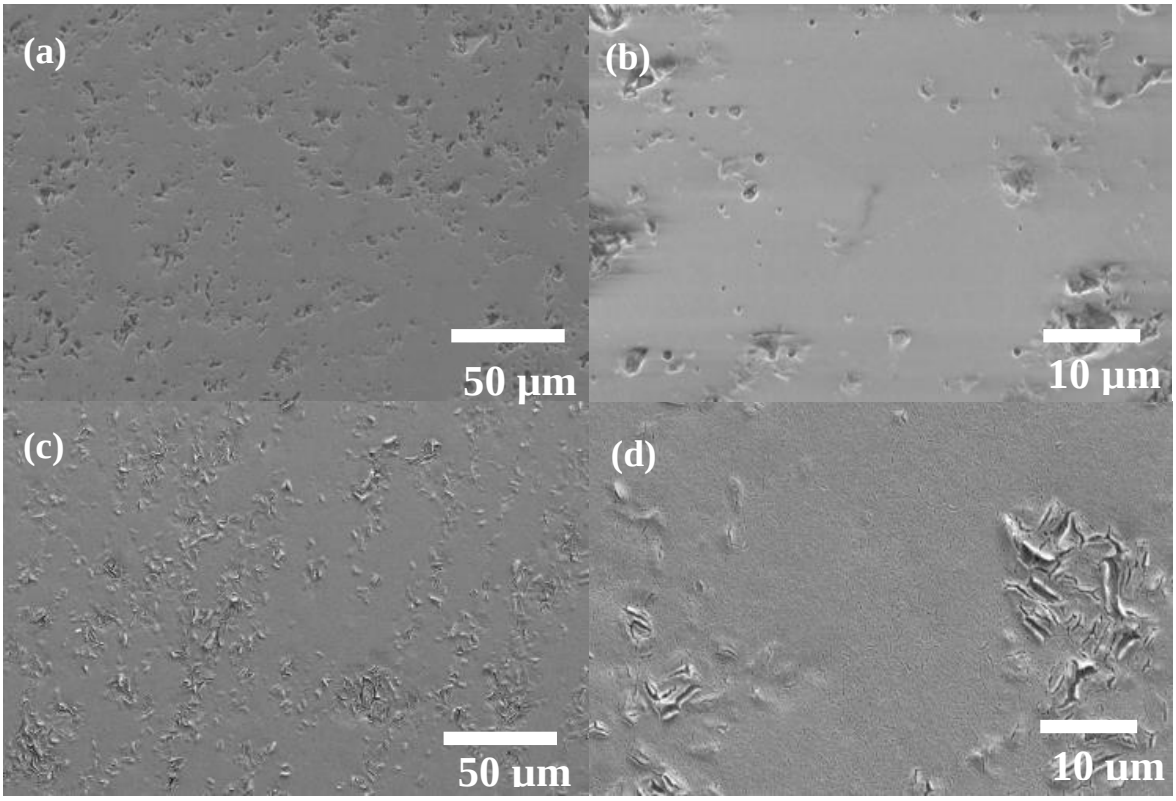

Fig. 5-6. SEM images of surfaces of SDC sintered electrolyte [(a) and (b)] and o-interlayer [(c) and (d)]. Images at high magnification are shown in (b) and (d).

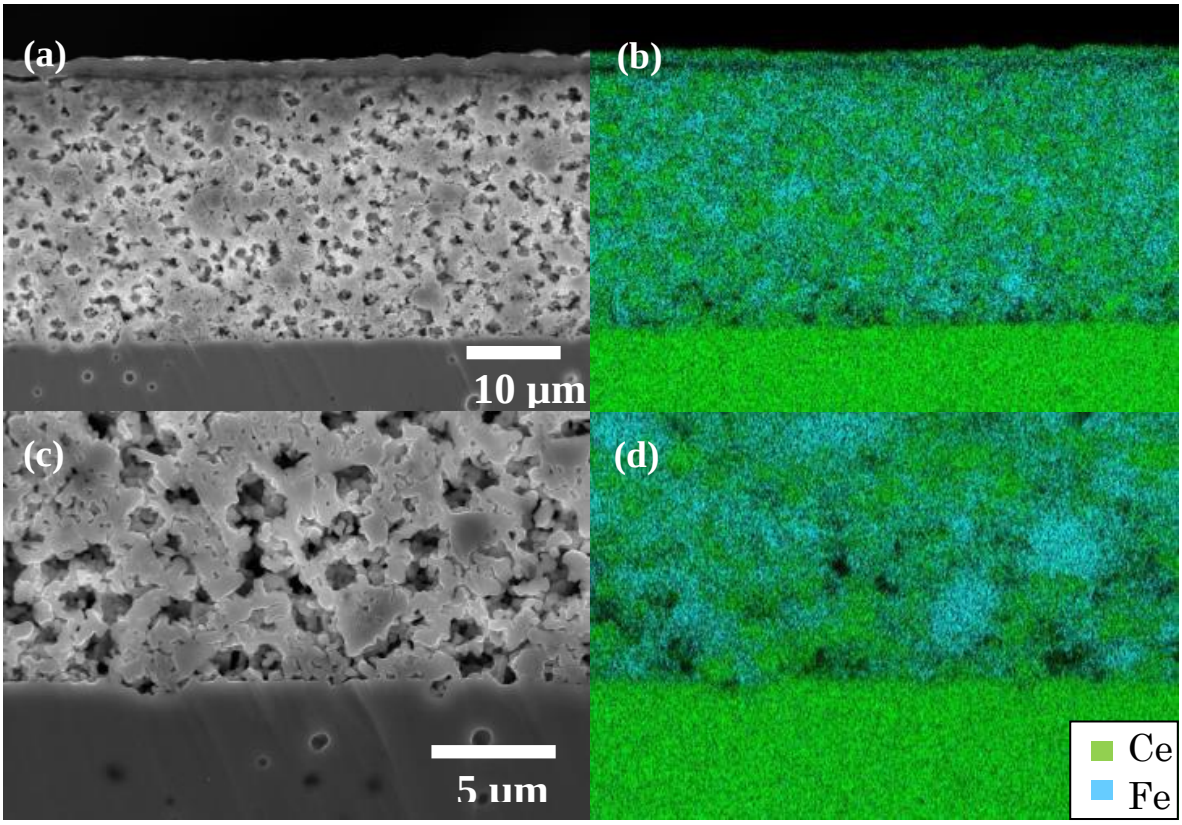

Fig. 5-7. SEM images and elemental distribution maps Ce and Fe for a cross-section of the LSCF–SDC electrodes prepared on SDC sintered electrolyte [(a) and (b)] and high magnification [(c) and (d)].

Figure 5-8 shows IR-free anodic and cathodic polarization curves for the LSCF–SDC electrodes, prepared on the SDC disk electrolyte, at T_{cell}= 800 and 900°C. It is evident that the LSCF–SDC/SDC disk electrolyte exhibited superior performances at both 800 and 900°C, compared with those of the LSCF–SDC prepared on the o-interlayer/YSZ. The values of overpotential of the LSCF–SDC prepared on SDC disk electrolyte and o-interlayer/YSZ at j = 0.5 A/cm^2 were 0.025 V and 0.049 V for the anodic reaction, respectively, while the values were –0.021 V and –0.058 V for the cathodic reaction. However, considering that the performance obtained for the LSCF–SDC/SDC disk electrolyte is the upper limit under the present conditions, the difference in the performances was fairly small, i.e., the performance of the LSCF–SDC with the o-interlayer/YSZ was extraordinarily high for R-SOC.

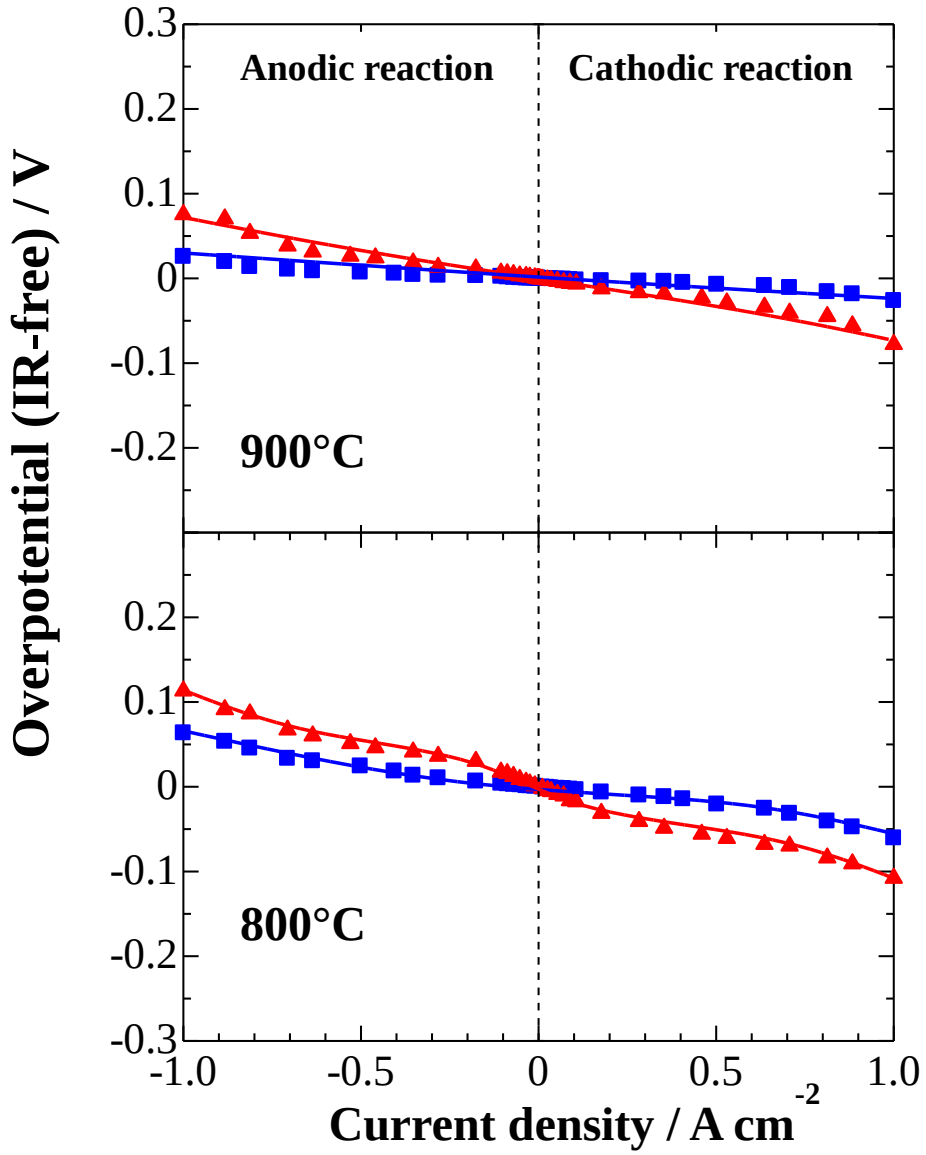

Fig. 5-8. IR-free polarization curves of LSCF–SDC electrodes prepared on o-interlayer/YSZ (▲) and sintered SDC electrolyte (■) in dry O_2 gas at T_{cell} = 900 and 800°C.

5.4. Conclusions

I have successfully prepared a uniform and dense SDC interlayer by coating a mixed solution of cerium and samarium octoates, followed by heat treatment. The performance of LSCF–SDC electrodes with the o-interlayer and n-interlayer was comparable at 900°C, while LSCF–SDC electrodes with the o-interlayer exhibited higher performance than that with the n-interlayer at 800°C. From the SEM-EDX analysis, the o-interlayer was observed to be more uniform and dense than the n-interlayer. The LSCF–SDC electrode with the o-interlayer exhibited very high performance, comparable to that prepared directly onto a dense SDC electrolyte. While thin and dense SDC or GDC interlayers so far have been used to avoid unfavorable solid-state reactions at the oxide electrode/YSZ interface, I have demonstrated for the first time that the microstructure of the SDC interlayer plays an important role in enhancing the electrode performance, specifically at reduced operation temperatures.

5.5. References

[1] H. Uchida, S. Arisaka, M. Watanabe, High Performance Electrode for Medium‐Temperature Solid Oxide Fuel Cells La (Sr) CoO_3 Cathode with Ceria Interlayer on Zirconia Electrolyte, Electrochem. Solid-State Lett. 2 (1999) 428-430.

[2] M. Shiono, K. Kobayashi, T. L. Nguyen, K. Hosoda, T. Kato, K. Ota, M. Dokiya, Effect of CeO_2 interlayer on ZrO_2 electrolyte/La(Sr)CoO_3 cathode for low-temperature SOFCs, Solid State Ionics 170 (2004) 1-7.

[3] F. Wang, M. E. Brito, K. Yamaji, D. -H. Cho, M. Nishi, H. Kishimoto, T. Horita, H. Yokokawa, Effect of polarization on Sr and Zr diffusion behavior in LSCF/GDC/YSZ system, Solid State Ionics, 262 (2014) 454-459.

[4] R. Kiebach, W. -W. Zhang, W. Zhang, M. Chen, K. Norrman, H. -J. Wang, J. R. Bowen, R. Barfod, P. V. Hendriksen, Stability of $La_{0.6}Sr_{0.4}Co_{0.2}Fe_{0.8}O_3/Ce_{0.9}Gd_{0.1}O_2$ cathodes during sintering and solid oxide fuel cell operation, J. Power Sources 283 (2015) 151-161.

[5] C.M. Ronconi, D. Gonçalves, N. Suvorova, O.L. Alves, E.A. Irene, Preparation and characterization of $Cd_2Nb_2O_7$ thin films on Si substrates, J. Phys. Chem. Solids 70 (2009) 234-237.

[6] N. Jordan, W. Assenmacher, S. Uhlenbruck, V.A.C. Haanappel, H.P. Buchkremer, D. Stöver, W. Mader, $Ce_{0.8}Gd_{0.2}O_{2-\delta}$ protecting layers manufactured by physical vapor deposition for IT-SOFC, Solid State Ionics 179 (2008) 919-923.

[7] Y. Tao, H. Nishino, S. Ashidate, H. Kokubo, M. Watanabe, H. Uchida, Polarization properties of $La_{0.6}Sr_{0.4}Co_{0.2}Fe_{0.8}O_3$-based double layer-type oxygen electrodes for reversible SOFCs, Electrochim. Acta, 54 (2009) 3309-3315.

[8] C.M. Ronconi, D. Gonçalves, N. Suvorova, O.L. Alves, E.A. Irene, Preparation and characterization of $Cd_2Nb_2O_7$ thin films on Si substrates, J. Phys. Chem. Solids 70 (2009) 234-237.

[9] S. Morlens, L. Ortega, B. Rousseau, S. Phok, J.L. Deschanvre, P. Chaudouet, P. Odier, Use of cerium ethylhexanoate solutions for preparation of CeO_2 buffer layers by spin coating, Mater. Sci. Eng. B 104 (2003) 185-191.

[10] H. Yahiro, Y. Eguchi, K. Eguchi, H. Arai, Oxygen ion conductivity of the ceria-samarium oxide system with fluorite structure, J. Appl. Electrochem. 18 (1988) 527-531.

[11] D. Tiana, B. Lin, Y. Yang, Y. Chen, X. Lu, Z. Wang, Wei Liua, E. Traversa, Enhanced performance of symmetrical solid oxide fuel cells using a doped ceria buffer layer, Electrochim. Acta 208 (2016) 318-324.

[12] T. Matsui, M. Komoto, H. Muroyama, K. Kishida, H. Inui, K. Eguchi, Degradation factors in (La,Sr)(Co,Fe)$O_{3-\delta}$cathode/Sm_2O_3–CeO_2 interlayer/Y_2O_3–ZrO_2 electrolyte system during operation of solid oxide fuel cells, J. Power Sources, 312 (2016) 80-85.

[13] M. Z. Khan, M. T. Mehran, R. -H. Song, J. -W. Lee, S. -B. Lee, T. -H. Lim, S. -J. Park, Effect of GDC interlayer thickness on durability of solid oxide fuel cell cathode, Ceramics International, 42 (2016) 6978-6984.

[14] A. Flura, C. Nicollet, V. Vibhu, B. Zeimetz, A. Rougier, J.-M. Bassat, J.-C. Grenier, Application of the Adler-Lane-Steele model to porous $La_2NiO_{4+\delta}$ SOFC cathode: influence of interfaces with gadolinia doped ceria, J. Electrochem. Soc. 163 (2016) F523-F532.

[15] K. Shimura, H. Nishino, K. Kakinuma, M. E. Brito, H. Uchida, High durability of $La_{0.6}Sr_{0.4}Co_{0.2}Fe_{0.8}O_{3-\delta}$/samaria-doped ceria (SDC) composite oxygen electrode with SDC interlayer for reversible solid oxide fuel cell/solid oxide electrolysis cell, J. Ceram. Soc. Jpn., accepted for publication.

Chapter 6

Conclusions and Future Prospects

6.1. Conclusions

In this dissertation, the oxygen electrodes with high performance and high durability have been developed for R-SOC. It was found that LSCF-SDC composite oxygen electrode with a thin, dense and uniform SDC interlayer is a very promising candidate.

The structure of the ceria-based interlayer is usually important for improving the durability of the LSCF-SDC composite oxygen electrode for both SOFC and SOEC operations. A thin (ca. 1.0 μm), dense and uniform SDC interlayer has been prepared by a scalable method, i.e., repeated spin-coating of cerium and samarium octoate and heat-treatment. The final sintering condition employed was 1050 °C for 2 h. Such a relatively low temperature process is one of the advantages of the present preparation method. For the conventional process, the sintering temperature of the ceria-based interlayer has been a very difficult choice. For example, the interlayer sintered at low temperature was not dense enough to suppress the diffusion of La, Sr, or Fe components from LSCF into the YSZ electrolyte during the operation, whereas Zr component as well as La, Sr, or Fe components already inter-diffused through the dense interlayer during the sintering process at high temperatures (> 1200 °C).

The LSCF-SDC electrode with the thin, dense and uniform SDC interlayer exhibited practically sufficient durability under both anodic and cathodic operation (in a symmetrical cell) during 5500 h at 900 °C and 0.5 A cm^{-2}. However, a small increase

in the ohmic resistance of the cathode side was observed, while the IR-free overpotentials at the anode and cathode and the ohmic resistance of the anode side were nearly constant. The Sr component from the cathode side reached the interface between SDC interlayer and YSZ electrolyte, leading to a formation of only small amount of $SrZrO_3$ at the interface. In contrast, the diffusion of Sr component from the anode was limited within the SDC interlayer. In both cases, such diffusion of Sr components were found to be mitigated at dense portions of the SDC interlayer. Hence, the formation of uniform and dense SDC interlayer as well as the decrease in the sintering temperature of all components are very important to obtain high durability with high performance in the R–SOCs.

It was found for the first time that the performance of the LSCF-SDC electrode was enhanced by the use of dense and uniform SDC interlayer specifically by lowering operation temperature. It is expected that oxide ions would be smoothly supplied through the SDC interlayer, resulting in enlarged effective reaction zone in the LSCF–SDC composite electrode.

Table 6-1 shows the comparison of the polarization resistance of various oxygen electrodes. For the cells with YSZ electrolyte, the polarization resistance R_p of the LSCF-SDC electrode in the present work is smaller than those reported so far. Compared with the R_p values measured on GDC, SDC, or LSGM electrolytes having higher conductivity than YSZ, the present performance is inferior. It has been reported that the ionic conductivity of the solid electrolyte affects the electrode performance [1]. So, the combination of the present LSCF-SDC oxygen electrode with the solid

electrolyte having higher ionic conductivity (such as ScSZ or LSGM) may improve the performance further.

Table 6-1 Comparison of polarization resistance in oxygen electrode

Electrode	Electrolyte	Temperature (ºC)	Polarization resistance (Ω cm^2)	Reference
LSM/CP82	GDC	800	0.3	[2]
LBSF-SDC	SDC	800	0.025	[3]
LSFCr	YSZ	800	0.25	[4]
BSFA-GDC	YSZ	800	0.301	[5]
PNCG-BLC	LSGM	800	0.03	[6]
LSCF	YSZ	800	0.24	[7]
LSCF-GDCS	GDCS	800	0.5	[8]
LSCF-GDC	GDC	800	0.1, 0.08	[9],[10]
LSCF-SDC	YSZ	800	0.17	This study

LSM:$La_{0.8}Sr_{0.2}MnO_3$, CP82:$Ce_{0.8}Pr_{0.2}O_{2-\delta}$, LBSF:$La_{0.4}Bi_{0.4}Sr_{0.2}FeO_{3-\delta}$, LSFCr:$La_{0.3}Sr_{0.7}Fe_{0.7}Cr_{0.3}O_{3-\delta}$, BSFA:$(Ba_{0.5}Sr_{0.5})(Fe_{0.91}Al_{0.09})O_{3-\delta}$, GDC:$Gd_{0.1}Ce_{0.9}O_2$, PNCG:$Pr_{1.91}Ni_{0.71}Cu_{0.24}Ga_{0.05}O_4$, BLC:$Ba_{0.5}La_{0.5}CoO_3$, LSCF:$La_{0.6}Sr_{0.4}Co_{0.2}Fe_{0.8}O_{3-\delta}$, GDCS:$Ce_{0.78}Gd_{0.2}Sr_{0.02}O_{2-\delta}$, $La_{0.9}Sr_{0.1}Ga_{0.8}Ma_{0.2}O_3$ (LSGM)

6.2. Future prospects

I have investigated the influence of SDC interlayer on the performance and durability of oxygen electrodes. I have clarified several important factors to improve the performance and durability of LSCF-SDC electrode formed on SDC interlayer by the use of a symmetrical cell (half cell).

It is necessary to investigate the performance and durability in a full cell: oxygen electrode | electrolyte | hydrogen electrode. Figure 6-1 shows IR-free performance of full cell NiCo/SDC|YSZ|SDC interlayer|LSCF-SDC at 800°C. The applied voltage was 1.2 V (IR-free) at the current density of 0.5 A cm^{-2}. This is a superior initial performance. However, the durability of both hydrogen electrode and the oxygen electrode has not been examined yet.

The present research has been conducted by using small-size coin cells with the electrode area of 0.283 cm^2. However, toward practical application in the future, it is necessary to increase the size of the cell. As a preliminary approach, I have just fabricated a cell with the electrode area of 19.6 cm^2, and evaluated its initial performance. However, for such large cells, it was difficult to prepare the electrodes with uniform microstructure, which is very important for the performance and durability. Development of a practical cell with a collaboration with a ceramic company will be performed in the next stage.

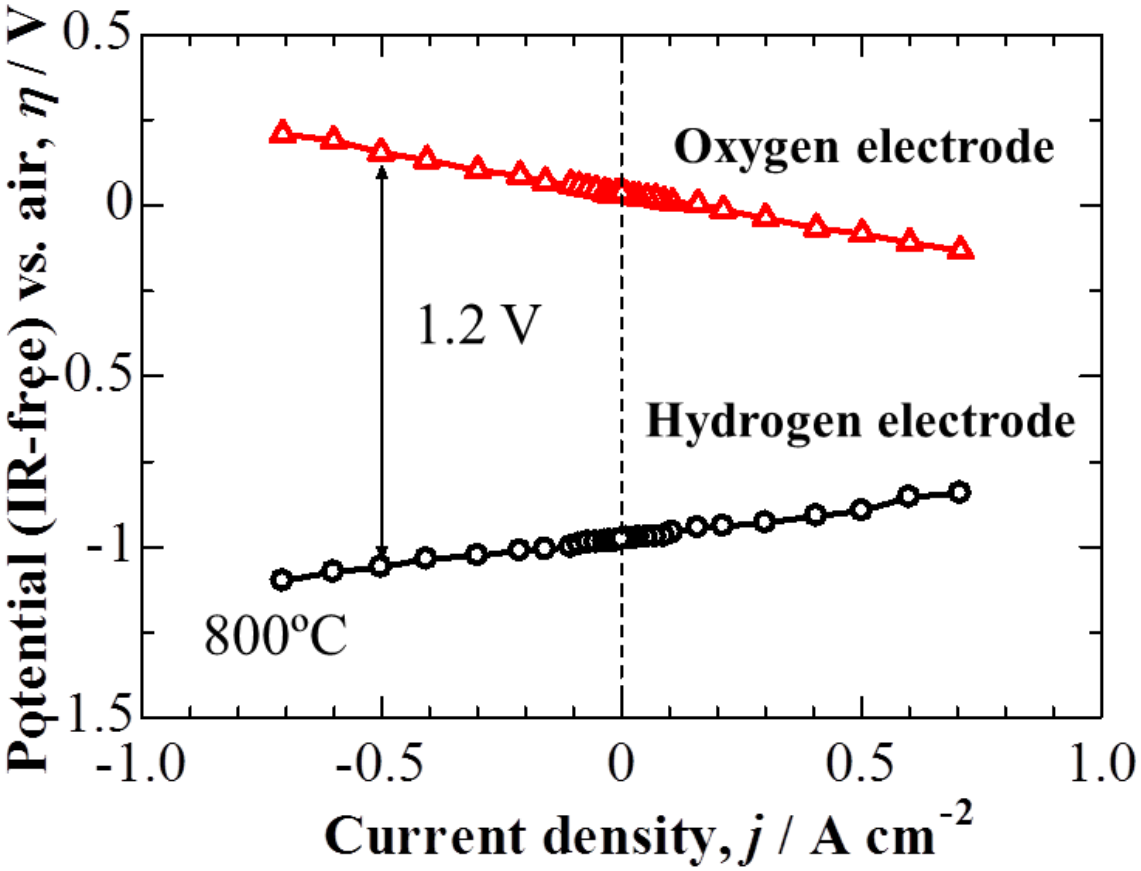

Fig. 6-1 IR-free polarization curves of NiCo/SDC hydrogen electrode ($p[H_2O]$=0.40 atm, with H_2 balance) and LSCF-SDC oxygen electrode (1 atm O_2) formed on SDC interlayer measured in the full cell with YSZ electrolyte at 800°C.

6.3. References

[1] H. Uchida, M. Yoshida, M. Watanabe, Effect of Ionic Conductivity of Zirconia Electrolytes on the Polarization Behavior of Various Cathodes in Solid Oxide Fuel Cells, J. Electrochem. Soc. 146(1) (1999) 1-7.

[2] L. Navarrete, M. Balaguer, V. B.Vert, J. M. Serra, Optimization of SOFC Composite Cathodes Based on LSM and Doped Cerias $Ce_{0.8}Ln_{0.2}O_{2-\delta}$ (Ln= Gd, Er, Tb and Pr), J. Electrochem. Soc. 163(13) (2016) F1440-F1443.

[3] M. Li, Y. Ren, Z. Zhu, S. Zhu, F. Chen, Y. Zhang, C. Xia, $La_{0.4}Bi_{0.4}Sr_{0.2}FeO_{3-\delta}$ as Cobalt-free Cathode for Intermediate-Temperature Solid Oxide Fuel Cell, Electrochim. Acta 191 (2016) 651-660.

[4] P. K. Addo, B. Molero-Sanchez, M. Chen, S. Paulson, V. Birss. CO/CO_2 Study of High Performance $La_{0.3}Sr_{0.7}Fe_{0.7}Cr_{0.3}O_{3-\delta}$ Reversible SOFC Electrodes, Fuel Cells 15(5) (2015) 689-696.

[5] T. Jiang, Z. Wang, B. Ren, J. Qiao, W. Sun, K. Sun, Compositionally continuously graded cathode layers of $(Ba_{0.5}Sr_{0.5})(Fe_{0.91}Al_{0.09})O_{3-\delta}$–$Gd_{0.1}Ce_{0.9}O_2$ by wet powder spraying technique for solid oxide fuel cells, J. Power Sources 247 (2014) 858-864.

[6] J. Xie, Y. W. Ju, M. Matsuka, S. Ida, T. Ishihara, Synergy effects of $Pr_{1.91}Ni_{0.71}Cu_{0.24}Ga_{0.05}O_4$ and $Ba_{0.5}La_{0.5}CoO_3$ composite on cathodic activity for intermediate temperature solid oxide fuel cells, J. Power Sources 228 (2013) 229-236.

[7] Z. Pan, Q. Liu, L. Zhang, X. Zhang, S. H. Chan, Study of Activation Effect of Anodic Current on $La_{0.6}Sr_{0.4}Co_{0.2}Fe_{0.8}O_{3-\delta}$ Air Electrode in Solid Oxide Electrolyzer Cell, Electrochim. Acta 209 (2016) 56-64.

[8] C. H. Hua, C. C. Chou, Preparation of nanoscale composite LSCF/GDCS cathode materials by microwave sintering for intermediate-temperature SOFC applications, Ceramics International 41 (2015) S708-S712.

[9] Y. Liu, J. Bi, B. Chi, J. Pu, L. Jian, Effects of impregnating palladium on catalytic performance of LSCF-GDC composite cathodes for intermediate temperature solid oxide fuel cells, Int. J. Hydrogen Energy 41(15) (2016) 6486-6492.

[10] X. Xi, A. Kondo, T. Kozawa, M. Naito, LSCF–GDC composite particles for solid oxide fuel cells cathodes prepared by facile mechanical method, Adv. Powder Technol. 27(2) (2016) 646-651.

List of Publications

Journal articles

1. High durability of $La_{0.6}Sr_{0.4}Co_{0.2}Fe_{0.8}O_{3-\delta}$/samaria-doped ceria (SDC) composite oxygen electrode with SDC interlayer for reversible solid oxide fuel cell/solid oxide electrolysis cell

K. Shimura, H. Nishino, K. Kakinuma, M. E. Brito, and H. Uchida, *J. Ceram. Soc. Jpn.* accepted for publication.

2. Effect of samaria-doped ceria (SDC) interlayer on the performance of $La_{0.6}Sr_{0.4}Co_{0.2}Fe_{0.8}O_{3-\delta}$/SDC composite oxygen electrode for reversible solid oxide fuel cells

K. Shimura, H. Nishino, K. Kakinuma, M. E. Brito, and H. Uchida, *Electrochem. Acta,* accepted for publication.

Meeting presentations

1. K. Shimura, H. Nishino, M. Watanabe and H. Uchida, The 6th International Fuel Cell Workshop 2012, Aug. 2012, Kofu, Japan

2. K. Shimura, H. Nishino, M. Watanabe and H. Uchida, The 2nd International Seminar for Special Doctoral Program 'Green Energy Conversion Science and Technology', Sept. 2013, Koumi, Japan

3. K. Shimura, H. Nishino, M. E. Brito, M. Watanabe and H. Uchida, 23rd Annual Meeting of MRS-J (2013), Dec. 2013, Yokohama, Japan

4. K. Shimura, H. Nishino, M. E. Brito, M. Watanabe and H. Uchida, The 22nd Symposium on Solid Oxide Fuel Cells in Japan, Dec. 2013, Tokyo, Japan

5. K. Shimura, H. Nishino, M. E. Brito, M. Watanab, and H. Uchida, 81st Annual meeting of The Electrochemical Society of Japan, Mar. 2014, Osaka, Japan

6. K. Shimura, H. Nishino, M. E. Brito, M. Watanabe and H. Uchida, The 3rd International Seminar for Special Doctoral Program 'Green Energy Conversion Science and Technology', Aug. 2014, Hokuto, Japan

7. K. Shimura, H. Nishino, M. E. Brito, M. Watanabe and H. Uchida, The 23rd Symposium on Solid Oxide Fuel Cells in Japan, Dec. 2014, Tokyo, Japan

8. K. Shimura, H. Nishino, M. E. Brito and H. Uchida, 83rd Annual meeting of The Electrochemical Society of Japan, Mar. 2016, Osaka, Japan

9. K. Shimura, H. Nishino, M. E. Brito and H. Uchida, The 5th International Seminar for Special Doctoral Program 'Green Energy Conversion Science and Technology', Aug. 2016, Koumi, Japan,

10. K. Shimura, H. Nishino, M. E. Brito, K. Chen, S. P. Jiang and H. Uchida, PRiME 2016, Oct. 2016, Honolulu, Hawaii, USA

Acknowledgements

The present thesis is the summary of work conducted at the Clean Energy Research Center, Fuel Cell Nanomaterials Research Center, and the Interdisciplinary Graduate School of Medicine and Engineering, University of Yamanashi, from 2011 to 2017.

I would like to express my deepest gratitude to Professor Hiroyuki Uchida of the University of Yamanashi for being the academic supervisor of this work, for his continuous guidance, invaluable suggestions, and warm encouragement throughout the this study.

I would like to express my sincere thanks to Professor Manuel E. Brito of the University of Yamanashi for his continuous guidance, invaluable suggestions, and warm encouragement throughout the this study.

I would like to express my sincere thanks to Professor Katsuyoshi Kakinuma and Assistant Professor Hanako Nishino of the University of Yamanashi for their helpful suggestions on this work and his pointed advice on the prepublication papers.

I would like to thank membranes of advisory committee Professor Nobuhiro Kumada of the University of Yamanashi, Professor San Ping Jiang of the Curtin University.

Sincere gratitude is expressed to, Professor Kenji Miyatake, Professor Kazutoshi Higashiyama, Professor Toshihiro Miyao, Associate Professor Mitsuru Wakisaka, Associate Professor Shinji Nohara, and Assistant Professor Jumpei Miyake of the University of Yamanashi, for their suggestions, advice and discussions, as well as continuous encouragement throughout the work.

I am grateful to Dr. Pramoto Puengjinda of the University of Yamanashi for their helpful discussion.

I also appreciate, Dr. Jun Omura, Dr. Yuichi Senoo, Dr. Masaru Sakamoto, Dr. Takayuki Hoshi, Dr. Morio Chiwata, Dr. Takashi Mochizuki, Dr. Yuji Chino for their strong assistance as my senior associates.

I also appreciate Mr. Ryousuke Nishikawa, Mr, Seiya Kosaka, Mr. Kouhei Uyama, Mr. Zyunya Yamada, and Dr. Wang Fang of “SOFC-team” in Clean Energy Research Center for their wonderful supports.

I would like to thank Mr. Yoshiyuki Ogihara, Mr. Kazuhiro Takanohashi, Mr. Hideaki Ono, Mr. Yuya Yamashita, Mr. Kento Yakahashi, Ms. Manai Shimada, Mr Zhang Yao Jian, Mr. Hideaki Ohno and all members in Clean Energy Research Center and Fuel Cell Nanomaterials Research Center for their kindly support.

I would like to thank Ms. Nozomi Toyoda, Ms. Ayako Yokouchi, Mr. Shigeki Rinno, Ms. Endo Maki, Ms. Kaori Ichinose and Ms. Yukiko Sato for their kind support.

Finally, I would like to thank my parents for their encouragement.

Kazuki Shimura

March 2017

Appendix

Table A-1 Physical Properties of Materials of Interest

	σ_{o2-} S/cm		σ_{e-} S/cm		TEC $\times 10^{-6}$/K	Reference
	900 ºC	800 ºC	900 ºC	800 ºC		
LSCF			210	280	15.3	[1]
SDC	0.17	0.09			12.8	[2],[3]
YSZ	0.06	0.02			10.92	[4]

[1] L. -W. Tai, M. M. Nasrallah, H. U. Anderson, D. M. Sparlin, S. R. Sehlin, Structure and electrical properties of $La_{1-x}Sr_xCo_{1-y}Fe_yO_3$. Part 2. The system $La_{1-x}Sr_xCo_{0.2}Fe_{0.8}O_3$, Solid State Ionics, 76 (1995) 273-283.

[2] H. Yahiro, Y. Eguchi, K. Eguchi, H. Arai, Oxygen ion conductivity of the ceria-samarium oxide system with fluorite structure, J. Appl. Electrochem. 18 (1988) 527-531.

[3] Q. Xu, D. Huang, F. Zhang, W. Chen, M. Chen, H. Liu, Structure, electrical conducting and thermal expansion properties of $La_{0.6}Sr_{0.4}Co_{0.8}Fe_{0.2}O_{3-\delta}$–$Ce_{0.8}Sm_{0.2}O_{2-\delta}$ composite cathodes, J. Alloys and Compounds 454 (2008) 460–465.

[4]D. J. L. Brett, A. Atkinson, N. P. Brandon, S. J. Skinner, Intermediate temperature solid oxide fuel cells, Chem. Soc. Rev. 37 (2008) 1568-1578.

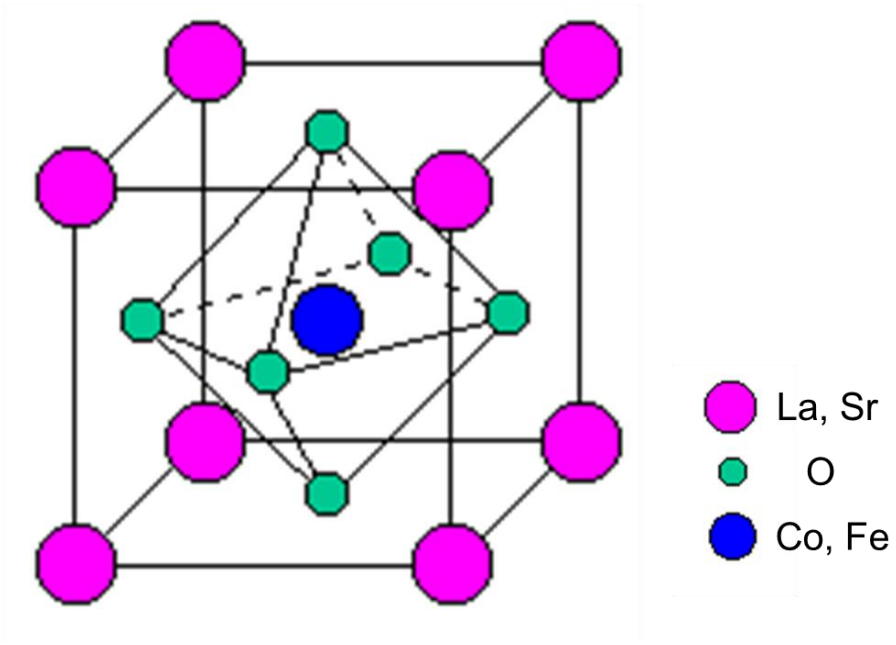

Fig. A-1 Structure of LSCF

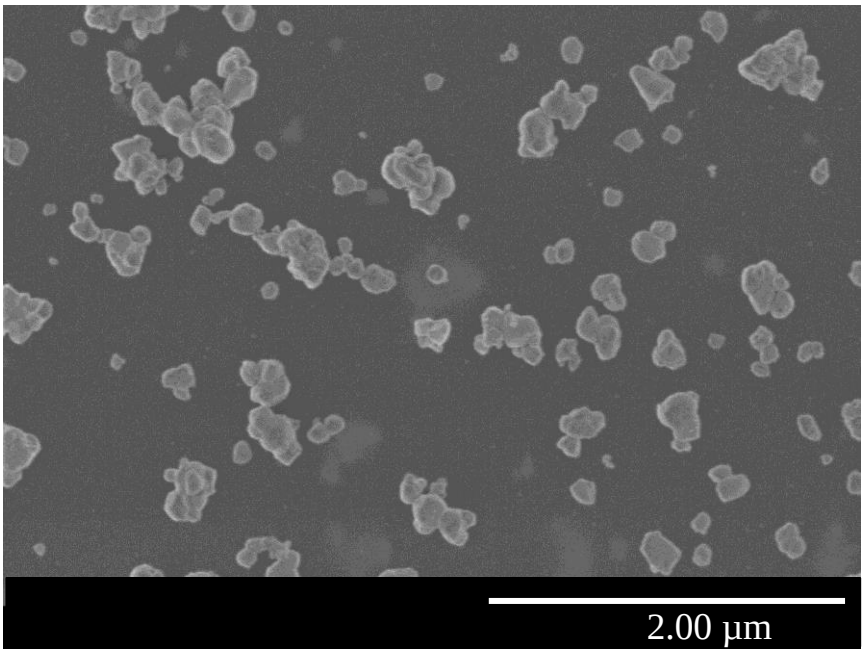

Fig. A-2 SEM image of LSCF particles

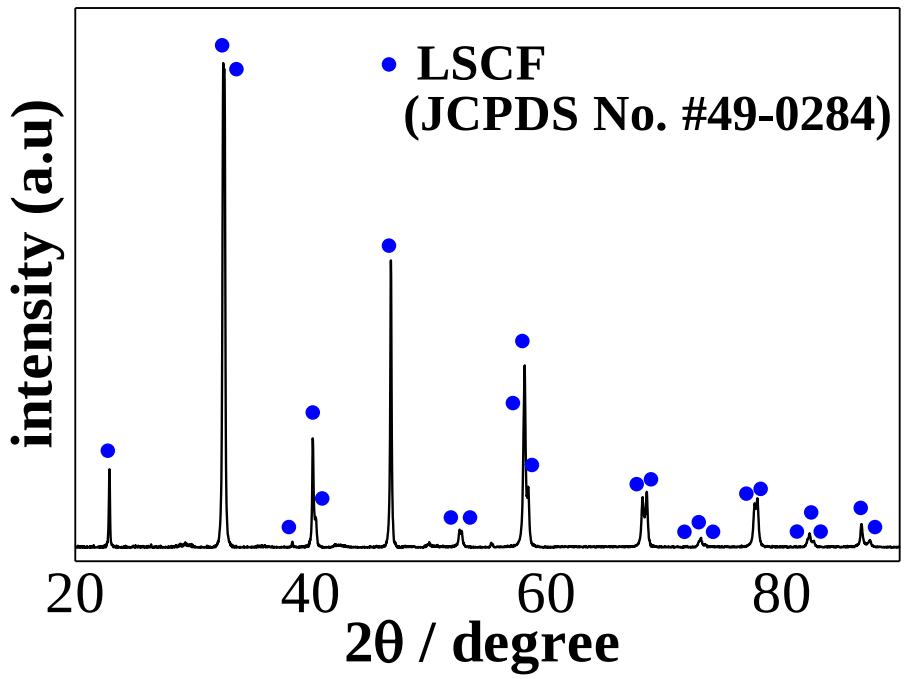

Fig. A-3 XRD pattern of LSCF

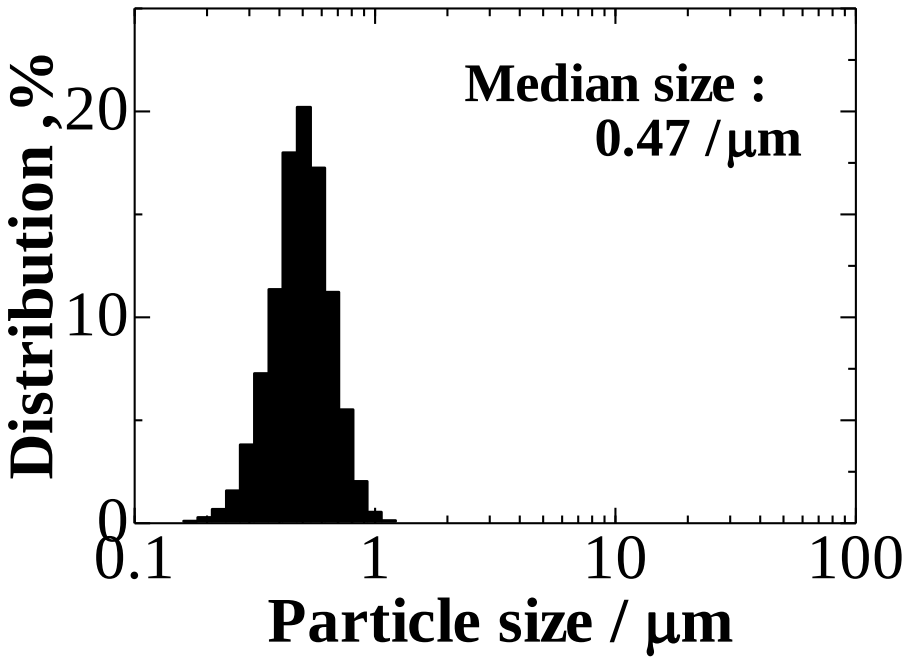

Fig. A-4 Particle distribution of LSCF

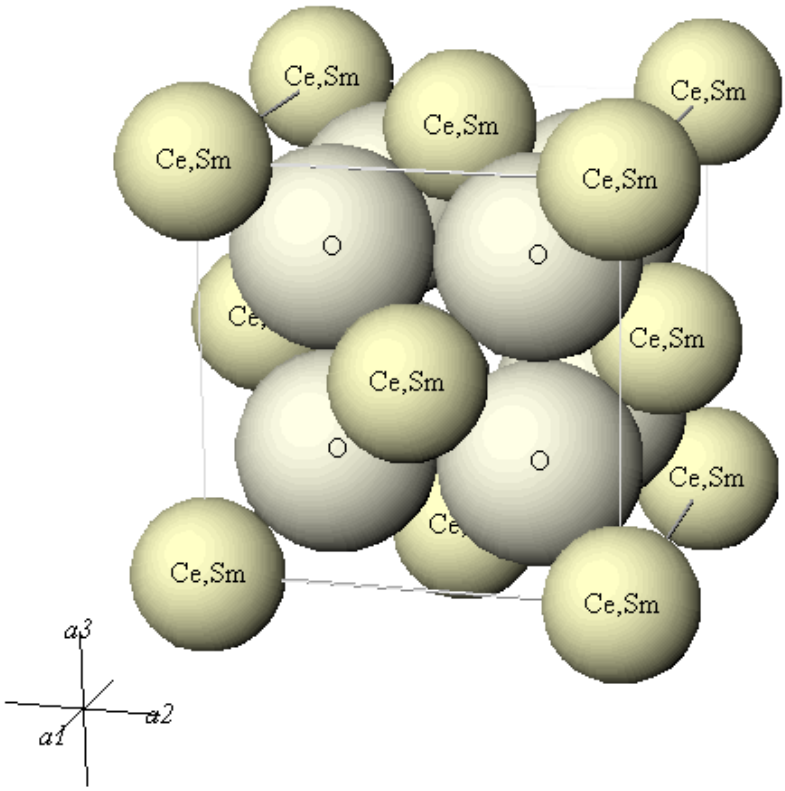

Fig. A-5 Structure of SDC

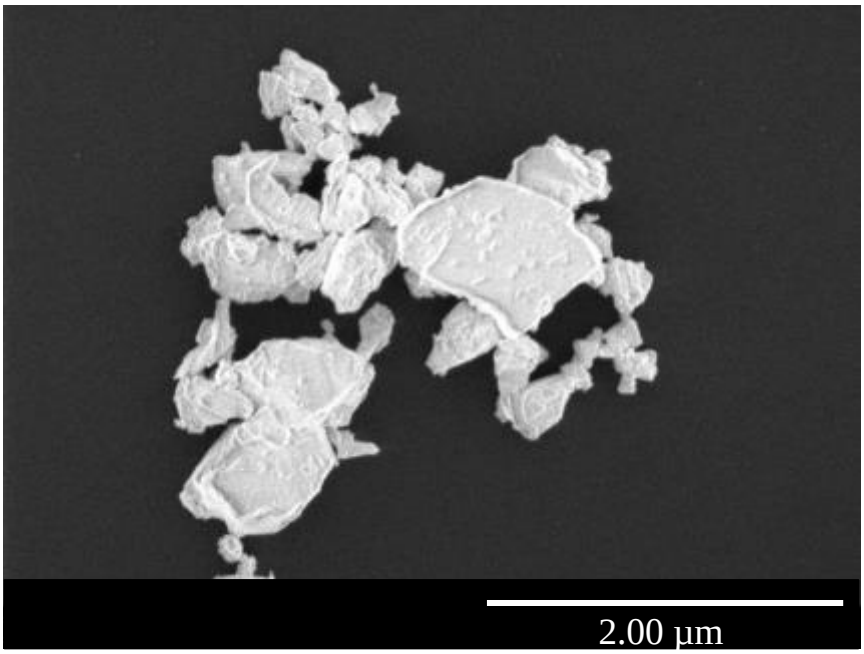

Fig. A-6 Structure of SDC

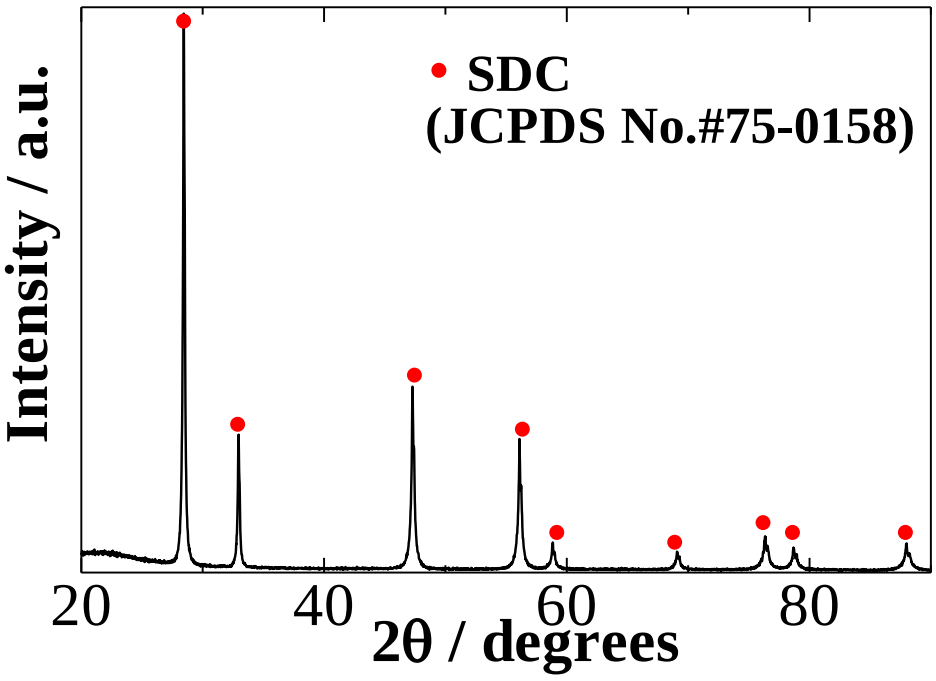

Fig. A-7 XRD patterns of SDC

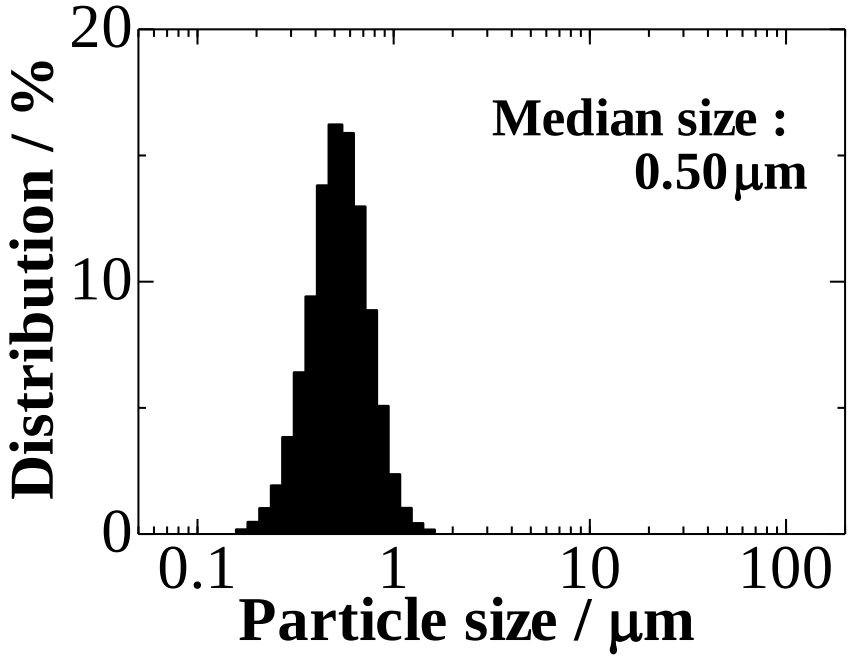

Fig. A-8 Particle distribution of SDC